



Galileo dust data from the jovian system: 2000 to 2003

H. Krüger^{a,b,*}, D. Bindschadler^c, S.F. Dermott^d, A.L. Graps^e, E. Grün^{b,f}, B.A. Gustafson^d, D.P. Hamilton^g, M.S. Hanner^h, M. Horányi^f, J. Kissel^a, D. Linkert^b, G. Linkert^b, I. Mannⁱ, J.A.M. McDonnell^j, R. Moissl^a, G.E. Morfill^k, C. Polanskey^c, M. Roy^c, G. Schwehm^l, R. Srama^{b,m}

^a Max-Planck-Institut für Sonnensystemforschung, 37191 Katlenburg-Lindau, Germany

^b Max-Planck-Institut für Kernphysik, 69029 Heidelberg, Germany

^c Jet Propulsion Laboratory, Pasadena, CA 91109, USA

^d University of Florida, 211 SSRB, Campus, Gainesville, FL 32609, USA

^e Department of Space Studies, Southwest Research Institute, 1050 Walnut Street, Suite 300, Boulder, CO 80302, USA

^f Laboratory for Atmospheric and Space Physics, University of Colorado, Boulder, CO 80309, USA

^g University of Maryland, College Park, MD 20742-2421, USA

^h Astronomy Department 619 LGRT, University of Massachusetts, Amherst, MA 01003, USA

ⁱ School of Science and Engineering, Kindai University, Kowakae 3-4-1, Higashi-Osaka, Osaka 577-8502, Japan

^j Planetary and Space Science Research Institute, The Open University, Milton Keynes, MK7 6AA, UK

^k Max-Planck-Institut für Extraterrestrische Physik, 85748 Garching, Germany

^l ESAC, PO Box 78, 28691 Villanueva de la Cañada, Spain

^m Universität Stuttgart, Institut für Raumfahrtssysteme, Pfaffenwaldring 31, 70569 Stuttgart, Germany

ARTICLE INFO

Article history:

Received 6 August 2009

Received in revised form

3 February 2010

Accepted 4 March 2010

Available online 10 March 2010

Keywords:

Circumplanetary dust

Planetary rings

Dust/magnetosphere interaction

Interplanetary dust

Dusty plasmas

ABSTRACT

The Galileo spacecraft was the first man-made satellite of Jupiter, orbiting the planet between December 1995 and September 2003. The spacecraft was equipped with a highly sensitive dust detector that monitored the jovian dust environment between approximately 2 and 370 R_J (jovian radius $R_J = 71\,492$ km). The Galileo dust detector was a twin of the one flying on board the Ulysses spacecraft. This is the tenth in a series of papers dedicated to presenting Galileo and Ulysses dust data. Here we present data from the Galileo dust instrument for the period January 2000 to September 2003 until Galileo was destroyed in a planned impact with Jupiter. The previous Galileo dust data set contains data of 2883 particles detected during Galileo's interplanetary cruise and 12978 particles detected in the jovian system between 1996 and 1999. In this paper we report on the data of additional 5389 particles measured between 2000 and the end of the mission in 2003. The majority of the 21 250 particles for which the full set of measured impact parameters (impact time, impact direction, charge rise times, charge amplitudes, etc.) was transmitted to Earth were tiny grains (about 10 nm in radius), most of them originating from Jupiter's innermost Galilean moon Io. They were detected throughout the jovian system and the impact rates frequently exceeded 10 min^{-1} . Surprisingly large impact rates up to 100 min^{-1} occurred in August/September 2000 when Galileo was far away ($\approx 280 R_J$) from Jupiter, implying dust ejection rates in excess of 100 kg s^{-1} . This peak in dust emission appears to coincide with strong changes in the release of neutral gas from the Io torus. Strong variability in the Io dust flux was measured on timescales of days to weeks, indicating large variations in the dust release from Io or the Io torus or both on such short timescales. Galileo has detected a large number of bigger micron-sized particles mostly in the region between the Galilean moons. A surprisingly large number of such bigger grains was measured in March 2003 within a four-day interval when Galileo was outside Jupiter's magnetosphere at approximately $350 R_J$ jovian distance. Two passages of Jupiter's gossamer rings in 2002 and 2003 provided the first actual comparison of in-situ dust data from a planetary ring with the results inferred from inverting optical images. Strong electronics degradation of the dust instrument due to the harsh radiation environment of Jupiter led to increased calibration uncertainties of the dust data.

© 2010 Elsevier Ltd. All rights reserved.

1. Introduction

The Galileo spacecraft was the first artificial satellite orbiting Jupiter. Galileo had a highly sensitive impact ionization dust

* Corresponding author at: Max-Planck-Institut für Sonnensystemforschung, 37191 Katlenburg-Lindau, Germany.

E-mail address: krueger@mps.mpg.de (H. Krüger).

detector on board which was identical with the dust detector of the Ulysses spacecraft (Grün et al., 1992a, 1992b, 1995c). Dust data from both spacecraft were used for the analysis of e.g. the interplanetary dust complex, dust related to asteroids and comets, interstellar dust grains sweeping through the solar system, and various dust phenomena in the environment of Jupiter. References can be found in Krüger et al. (1999a, 2010).

In Section 1.1 we summarise results that are related to dust in the Jupiter system. A more comprehensive overview of the investigation of dust in the jovian system was given by Krüger (2003) and Krüger et al. (2004).

1.1. Summary of results from the Galileo dust investigations at Jupiter

The Jupiter system was found to be a strong source of dust when in 1992 Ulysses flew by the planet and discovered streams of dust particles emanating from the giant planet's magnetosphere (Grün et al., 1993). These were later confirmed by Galileo (Grün et al., 1996a, 1996b) and measured again by Ulysses in 2003–2005 during its second flyby at the planet (Krüger et al., 2006c; Flandes and Krüger, 2007). During its two Jupiter flybys, within a distance of 3 AU from the planet, Ulysses measured 11 and 28 dust streams, respectively.

At least four dust populations were identified in the Jupiter system with Galileo (Grün et al., 1997a, 1998):

- (i) Streams of dust particles with high and variable impact rates throughout Jupiter's magnetosphere. They are the extension of the streams discovered with Ulysses outside Jupiter's magnetosphere. The particles are about 10 nm in radius (Zook et al., 1996) and they mostly originate from the innermost Galilean moon Io (Graps et al., 2000). Because of their small sizes the charged grains strongly interact with Jupiter's magnetosphere (Horányi et al., 1997; Grün et al., 1997a, 1998; Heck, 1998), and they are a natural laboratory to study dust–plasma interactions. The dust streams mostly show a dust-in-plasma behaviour, i.e. the particle motion can be described by single particle dynamics, while only some portions of those Galileo orbits displaying the highest dust stream fluxes (Galileo orbits E4, G7, G8, C21) satisfy the minimum requirements for a dusty plasma where collective effects dominate particle motion (Graps, 2006). The dust streams served as a monitor of Io's volcanic plume activity, showing that periods with high measured dust fluxes are most likely connected with heavy volcanic eruptions on Io (Krüger et al., 2003a). The dust streams measurements revealed significant dust flux variations with jovian local time (Krüger et al., 2003b) consistent with theoretical expectations (Horányi et al., 1997), demonstrating that the dust measurements probe the plasma conditions in the Io torus. Graps (2001) and Flandes (2005) investigated dust charging mechanisms in the jovian magnetosphere and in Io's plumes. The particles reach an equilibrium potential of approximately +5 V and they collect most of their charge within about 20 R_J from Jupiter. Dust measurements of the Cassini spacecraft at its Jupiter flyby in 2000 showed that the grains are mostly composed of sodium chloride (NaCl) formed by condensation in Io's volcanic plumes (Postberg et al., 2006).
- (ii) Dust clouds surrounding the Galilean moons which consist of mostly sub-micron grains (Krüger et al., 1999d, 2000, 2003c). These clouds were detected within the Hill spheres of the moons and the grains were secondary ejecta particles kicked up from the moons' surfaces by hypervelocity impacts

of interplanetary micrometeoroids (Krivov et al., 2003; Sremčević et al., 2003, 2005). The majority of the ejecta grains follows ballistic trajectories and falls back to the moons' surfaces while a small fraction can even leave the gravity field of the moons and go into orbit about Jupiter.

- (iii) Bigger micron-sized grains forming a tenuous dust ring between the Galilean moons and further beyond. The measured dust mass distribution peaks at about $2 \mu\text{m}$ (assuming spherical grains with density 1g cm^{-3} Krüger et al., 2006b). This group is composed of two sub-populations, one orbiting Jupiter on prograde orbits and a second one on retrograde orbits (Colwell et al., 1998; Thiessenhusen et al., 2000). Most of the prograde population is maintained by grains escaping from the clouds that surround the Galilean moons (Krivov et al., 2002a). Dusty motes most likely released from the surfaces of the irregular outer satellites of Jupiter were also found to about 300 R_J from Jupiter, showing both prograde and retrograde orbits (Krivov et al., 2002b).
- (iv) On 5 November 2002 and 21 September 2003—before Galileo was destroyed in a planned impact with Jupiter—the spacecraft traversed Jupiter's gossamer ring twice and provided the first in-situ measurements of a dusty planetary ring (Krüger, 2003; Moissl, 2005; Krüger et al., 2009) which is also accessible with astronomical imaging techniques. These fly-throughs revealed previously unknown structures in the gossamer rings: a drop in the dust density between the moons Amalthea and Thebe, grains orbiting Jupiter on highly inclined orbits and an increase in the number of small grains in the inner regions of the rings as compared to the regions further away from the planet. All these features can nicely be explained by electromagnetic forces on the grains that shape the gossamer rings (Hamilton and Krüger, 2008).

1.2. The Galileo and Ulysses dust data papers

This is the tenth paper in a series dedicated to presenting both raw and reduced data from the Galileo and Ulysses dust instruments. Grün et al. (1995c, hereafter Paper I) described the reduction process of Galileo and Ulysses dust data. In the even-numbered Papers II, IV, VI and VIII (Grün et al., 1995a; Krüger et al., 1999a, 2001a, 2006b) we presented the Galileo data set spanning the ten year time period from October 1989 to December 1999. The present paper extends the Galileo data set from January 2000 to September 2003, which covers the Galileo Millennium mission and two traverses of Jupiter's gossamer ring until the spacecraft impacted Jupiter on 21 September 2003. Companion odd-numbered Papers III, V, VII, IX and XI (Grün et al., 1995b; Krüger et al., 1999c, 2001b, 2006a, 2010) provide the entire dust data set measured with Ulysses between 1990 and 2007. An overview of our Galileo dust data papers and mission highlights is given in Table 1.

The main data products are a table of the number of all impacts determined from the particle accumulators and a table of both raw and reduced data of all “big” impacts received on the ground. The information presented in these papers is similar to data which we are submitting to the various data archiving centres (planetary data system, NSSDC, etc.). The only difference is that the paper version does not contain the full data set of the large number of “small” particles, and the numbers of impacts deduced from the accumulators are typically averaged over several days. Electronic access to the complete data set including the numbers of impacts deduced from the accumulators in full time resolution is also possible via the world wide web: <http://www.mpi-hd.mpg.de/dustgroup/>.

Table 1
Summary of Galileo dust data papers and significant mission events.

| Time interval | Significant mission events | Paper number |
|---------------|--|----------------------------|
| 1989–1992 | Galileo launch (18 October 1989) | II Grün et al. (1995c) |
| 1993–1995 | Jupiter orbit insertion (7 December 1995) | IV Krüger et al. (1999a) |
| 1996 | Galileo orbits G1–E4 | VI Krüger et al. (2001a) |
| 1997–1999 | Galileo orbits J5–I25 | VIII Krüger et al. (2006b) |
| 2000–2003 | Galileo orbits E26–J35, First gossamer ring passage (5 November 2002), second gossamer ring passage and Galileo Jupiter impact (21 September 2003) | X (this paper) |

This paper is organised similarly to our previous papers. Section 2 gives a brief overview of the Galileo mission with particular emphasis on the time period 2000–2003, the dust instrument operation and lists important mission events in the time interval 2000–2003 considered in this paper. A description of the new Galileo dust data set for 2000–2003 together with a discussion of the detected noise and dust impact rates is given in Section 3. Section 4 analyses and discusses various characteristics of the new data set. Finally, in Section 5 we discuss results on jovian dust achieved with this new data set, and in Section 6 we summarise our results.

2. Mission and instrument operations

2.1. Galileo mission

Galileo was launched on 18 October 1989. On 7 December 1995 the spacecraft arrived at Jupiter and was injected into a highly elliptical orbit about the planet, becoming the first spacecraft orbiting a planet of the outer solar system. Galileo performed 34 revolutions about Jupiter until 21 September 2003 when the spacecraft was destroyed in a planned impact with Jupiter.

Galileo's trajectory during its orbital tour about Jupiter from January 2000 to September 2003 is shown in Fig. 1. Galileo had regular close flybys at Jupiter's Galilean moons. Eight such encounters occurred in the 2000–2003 interval (1 at Europa, 4 at Io, 2 at Ganymede, 1 at Callisto) plus one at Amalthea (Table 2). Galileo orbits are labelled with the first letter of the Galilean moon which was the encounter target during that orbit, followed by the orbit number. For example, "G29" refers to a Ganymede flyby in orbit 29. Satellite flybys always occurred within two days of Jupiter closest approach (pericentre passage). Detailed descriptions of the Galileo mission and the spacecraft were given by Johnson et al. (1992) and D'Amario et al. (1992).

Galileo was a dual spinning spacecraft with an antenna that pointed antiparallel to the positive spin axis. During most of the initial 3 years of the mission the antenna pointed towards the Sun for thermal protection of the spacecraft (Paper II). Since 1993 the antenna was usually pointed towards Earth for data transmission. Deviations from the Earth pointing direction in 2000–2003, the time period considered in this paper, are shown in Fig. 2. Sharp spikes in the pointing deviation occurred when the spacecraft was turned away from the nominal Earth direction for dedicated imaging observations with Galileo's cameras or for orbit trim maneuvers with the spacecraft thrusters. These spikes lasted typically several hours. From January to September 2003 (Fig. 2d), the Galileo pointing deviated significantly from the Earth pointing

direction for a long time interval. Table 2 lists significant mission and dust instrument events for 2000–2003. Comprehensive lists of earlier events can be found in Papers II, IV, VI and VIII.

2.2. Dust detection geometry

The dust detector system (DDS) was mounted on the spinning section of Galileo and the sensor axis was offset by 60° from the positive spin axis (an angle of 55° was erroneously stated in publications before). A schematic view of the Galileo spacecraft and the geometry of dust detection is shown in the inset in Fig. 1.

The rotation angle measured the viewing direction of the dust sensor at the time of a dust impact. During one spin revolution of the spacecraft the rotation angle scanned through a complete circle of 360°. At rotation angles of 90° and 270° the sensor axis lay nearly in the ecliptic plane, and at 0° it was close to the ecliptic north direction. DDS rotation angles are taken positive around the negative spin axis of the spacecraft which pointed towards Earth. This is done to facilitate comparison of the Galileo spin angle data with those taken by Ulysses, which, unlike Galileo, had its positive spin axis pointed towards Earth (Grün et al., 1995c).

The nominal field-of-view (FOV) of the DDS sensor target was 140°. A smaller FOV applies to a subset of jovian dust stream particle impacts—the so-called class 3 impacts in amplitude range AR1 (Krüger et al., 1999b, cf. Papers I and IV and Section 3.1 for a definition of these parameters) while the nominal target size should be applied to class 2 jovian dust stream impacts. For all impacts which are not due to jovian dust stream particles a larger FOV of 180° should be applied because the inner sensor side wall turned out to be almost as sensitive to larger dust impacts as the target itself (Altobelli et al., 2004; Willis et al., 2004, 2005). These different sensor fields-of-view and the corresponding target sizes are summarised in Table 3.

During one spin revolution of the spacecraft the sensor axis scanned a cone with 120° opening angle towards the anti-earth direction. Dust particles that arrived from within 10° of the positive spin axis (anti-earth direction) could be detected at all rotation angles, whereas those that arrived at angles from 10° to 130° from the positive spin axis could be detected over only a limited range of rotation angles. Note that these angles refer to the nominal sensor field-of-view of 140°.

2.3. Data transmission

The Galileo dust instrument memory could store 46 instrument data frames, with each frame comprising the complete data set of an impact or noise event, consisting of 128 bits, plus ancillary and engineering data (cf. Papers I and II). Each impact event was time-tagged with an 8 bit word allowing for the identification of 256 unique steps, with a step size of 4.3 h. Hence, the total accumulation time after which the time word was reset and the time labels of older impact events became ambiguous was $256 \times 4.3 \text{ h} \approx 46 \text{ days}$.

Galileo had various data transmission modes. During a large fraction of Galileo's orbital mission about Jupiter dust detector data were transmitted to Earth in the so-called realtime science mode (RTS). In RTS mode, dust data were read out either every 7.1 or every 21.2 min—depending on the spacecraft data transmission rate—and directly transmitted to Earth. Additionally, Galileo had the so-called record mode. In this mode data read out from the dust instrument memory were recorded on Galileo's tape recorder and transmitted to Earth up to several weeks later. Recorded data were received during three satellite flybys in 2000 during short periods of $\sim \pm 1/2 \text{ h}$ around closest approach to the satellite, and for $\sim 3.8 \text{ h}$ during Galileo's gossamer ring passage on 5 November

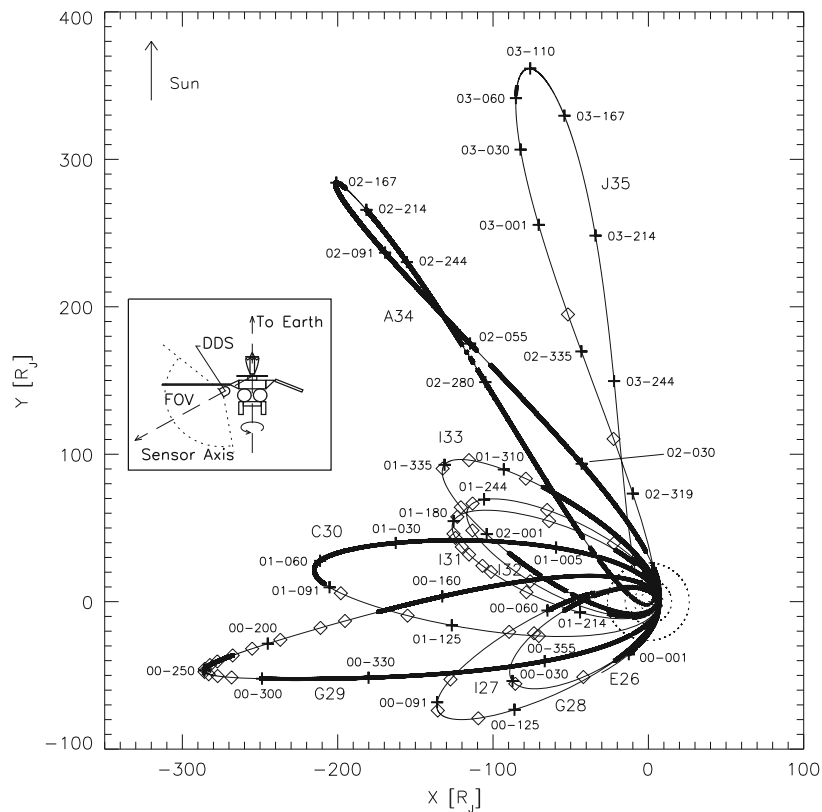


Fig. 1. Galileo's trajectory in the jovian system from 2000 to 2003 in a Jupiter-centric coordinate system (thin solid line). Crosses mark the spacecraft position at approximately 30 day intervals (days of year are indicated). Periods when RTS data were obtained are shown as thick solid lines, MROs are marked by diamonds. Galileo's orbits are labelled 'E26', 'I27', 'G28', 'G29', 'C30', 'I31', 'I32', 'I33', 'A34' and 'J35'. Sun direction is to the top and the Sun and Earth directions coincide to within 10°. The orbits of the Galilean moons are indicated (dotted lines). The sketch of the Galileo spacecraft shows the dust detector (DDS), its geometry of dust detection and its field-of-view (FOV). The spacecraft antenna usually pointed towards Earth and the spacecraft made about 3 revolutions per minute.

Table 2

Galileo mission and dust detector (DDS) configuration, tests and other events (2000–2003).

| Yr-day | Date | Time | Event |
|--------|------------------|-------|---|
| 89-291 | 18 October 1989 | 16:52 | Galileo launch |
| 95-341 | 07 December 1995 | 21:54 | Galileo Jupiter closest approach, distance: 4.0 R_J |
| 99-345 | 11 December 1999 | 02:07 | DDS configuration: HV=4, EVD=1, SSEN=0,1,1,1 |
| 00-001 | 01 January 2000 | 00:00 | DDS begin RTS data |
| 00-003 | 03 January 2000 | 17:28 | DDS end RTS data, begin record data |
| 00-003 | 03 January 2000 | 18:00 | Galileo Europa 26 (E26) closest approach , altitude 351 km |
| 00-003 | 03 January 2000 | 18:30 | DDS end record data, begin RTS data |
| 00-004 | 04 January 2000 | 03:33 | Galileo Jupiter closest approach, distance 5.8 R_J |
| 00-006 | 06 January 2000 | 02:00 | Galileo turn 5°, duration 3 h, return to nominal attitude |
| 00-007 | 07 January 2000 | 19:00 | Galileo OTM-82, size of turn 3°, duration 5 h, return to nominal attitude |
| 00-009 | 09 January 2000 | 11:49 | DDS end RTS data |
| 00-029 | 29 January 2000 | 04:00 | Galileo OTM-83, size of turn 3°, duration 3 h, return to nominal attitude |
| 00-033 | 02 February 2000 | 18:00 | Galileo turn 4°, new nominal attitude |
| 00-038 | 07 February 2000 | 23:00 | Galileo turn 7°, duration 3 h, return to nominal attitude |
| 00-049 | 18 February 2000 | 16:36 | Galileo OTM-84, no attitude change |
| 00-050 | 19 February 2000 | 12:00 | DDS begin RTS data |
| 00-053 | 22 February 2000 | 12:30 | Galileo Jupiter closest approach, distance 5.9 R_J |
| 00-053 | 22 February 2000 | 13:02 | DDS end RTS data, begin record data |
| 00-053 | 22 February 2000 | 13:47 | Galileo Io 27 (I27) closest approach , altitude 198 km |
| 00-053 | 22 February 2000 | 14:25 | DDS end record data, begin RTS data |
| 00-054 | 23 February 2000 | 19:20 | DDS last RTS data before spacecraft anomaly |
| 00-055 | 24 February 2000 | 04:00 | Galileo turn 15°, duration 30 h, return to nominal attitude |
| 00-055 | 24 February 2000 | 21:00 | Galileo spacecraft anomaly |
| 00-056 | 25 February 2000 | 04:16 | DDS begin RTS data after spacecraft anomaly |
| 00-057 | 25 February 2000 | 14:00 | Galileo OTM-85, size of turn 19°, duration 11 h, return to nominal attitude |
| 00-059 | 28 February 2000 | 23:56 | DDS end RTS data |
| 00-070 | 10 March 2000 | 10:00 | Galileo turn 8°, new nominal attitude |
| 00-088 | 28 March 2000 | 00:00 | Galileo turn 3°, duration 3 h, return to nominal attitude |
| 00-098 | 07 April 2000 | 12:00 | Galileo OTM-86, no attitude change |
| 00-116 | 25 April 2000 | 20:00 | Galileo turn 8°, new nominal attitude |
| 00-117 | 26 April 2000 | 01:11 | DDS last MRO before solar conjunction |
| 00-118 | 27 April 2000 | | Start solar conjunction period |

Table 2 (continued)

| Yr-day | Date | Time | Event |
|--------|-------------------|-------|--|
| 00-138 | 17 May 2000 | | End solar conjunction period |
| 00-138 | 17 May 2000 | 09:30 | DDS begin RTS data |
| 00-139 | 18 May 2000 | 10:00 | Galileo OTM-87, no attitude change |
| 00-141 | 20 May 2000 | 09:39 | DDS end RTS data, begin record data |
| 00-141 | 20 May 2000 | 10:10 | Galileo Ganymede 28 (G28) closest approach , altitude 808 km |
| 00-141 | 20 May 2000 | 10:40 | DDS end record data, begin RTS data |
| 00-142 | 21 May 2000 | 04:52 | Galileo Jupiter closest approach, distance 6.7 R_J |
| 00-143 | 22 May 2000 | 08:00 | Galileo turn 2°, duration 1 h, return to nominal attitude |
| 00-146 | 25 May 2000 | 08:00 | Galileo OTM-88, no attitude change |
| 00-152 | 31 May 2000 | 07:00 | Galileo turn 8°, new nominal attitude |
| 00-170 | 18 June 2000 | 23:57 | DDS end RTS data |
| 00-176 | 23 June 2000 | 03:00 | Galileo turn 7°, duration 2 h, return to nominal attitude |
| 00-189 | 07 July 2000 | 19:00 | Galileo turn 9°, new nominal attitude |
| 00-209 | 27 July 2000 | 11:11 | DDS configuration: HV=5 |
| 00-216 | 03 August 2000 | 18:31 | DDS begin RTS data |
| 00-223 | 10 August 2000 | 02:00 | Galileo turn 9°, new nominal attitude |
| 00-244 | 31 August 2000 | 16:00 | Galileo turn 2°, duration 2 h, return to nominal attitude |
| 00-252 | 08 September 2000 | 18:00 | Galileo OTM-89, size of turn 2°, duration 3 h, return to nominal attitude |
| 00-253 | 09 September 2000 | 08:11 | DDS end RTS data |
| 00-300 | 26 October 2000 | 10:01 | DDS begin RTS data |
| 00-302 | 28 October 2000 | 01:00 | Galileo OTM-90, no attitude change |
| 00-342 | 07 December 2000 | 23:00 | Galileo turn 2°, duration 1 h, return to nominal attitude |
| 00-353 | 18 December 2000 | 05:00 | Galileo turn 20°, new nominal attitude |
| 00-356 | 21 December 2000 | 20:15 | Galileo OTM-91, no attitude change |
| 00-363 | 28 December 2000 | 08:25 | Galileo Ganymede 29 (G29) closest approach , altitude 2,337 km |
| 00-364 | 29 December 2000 | 03:27 | Galileo Jupiter closest approach, distance 7.5 R_J |
| 01-002 | 02 January 2001 | 20:00 | Galileo OTM-92, no attitude change |
| 01-004 | 04 January 2001 | 03:30 | Galileo turn 10°, return to nominal attitude |
| 01-086 | 27 March 2001 | 23:00 | DDS end RTS data |
| 01-094 | 04 April 2001 | 04:00 | Galileo turn 8°, new nominal attitude |
| 01-114 | 24 April 2001 | 03:00 | Galileo turn 8°, duration 9 h, return to nominal attitude |
| 01-130 | 10 May 2001 | 16:00 | Galileo OTM-94, no attitude change |
| 01-133 | 13 May 2001 | 01:00 | Galileo turn 4°, new nominal attitude |
| 01-142 | 22 May 2001 | 23:00 | Galileo turn 6°, return to nominal attitude |
| 01-143 | 23 May 2001 | 12:01 | DDS begin RTS data |
| 01-143 | 23 May 2001 | 17:33 | Galileo Jupiter closest approach, distance 7.3 R_J |
| 01-144 | 24 May 2001 | 06:00 | DDS end RTS data |
| 01-145 | 25 May 2001 | 04:00 | DDS begin RTS data |
| 01-145 | 25 May 2001 | 11:24 | Galileo Callisto 30 (C30) closest approach , altitude 138 km |
| 01-146 | 26 May 2001 | 07:15 | DDS end RTS data |
| 01-146 | 26 May 2001 | 09:00 | Galileo turn 5°, duration 2 h, return to nominal attitude |
| 01-146 | 26 May 2001 | 22:00 | Galileo turn 12°, duration 13 h, return to nominal attitude |
| 01-148 | 28 May 2001 | 19:00 | Galileo OTM-95, size of turn 1° |
| 01-152 | 01 June 2001 | 11:00 | Galileo turn 5°, new nominal attitude |
| 01-154 | 03 June 2001 | 16:58 | DDS last MRO before solar conjunction |
| 01-155 | 04 June 2001 | | Start solar conjunction period |
| 01-174 | 23 June 2001 | | End solar conjunction period |
| 01-177 | 26 June 2001 | 22:58 | DDS fist MRO after solar conjunction |
| 01-183 | 02 July 2001 | 21:00 | Galileo turn 4°, new nominal attitude |
| 01-186 | 05 July 2001 | 05:00 | Galileo turn 5°, duration 5 h, return to nominal attitude |
| 01-194 | 13 July 2001 | 06:00 | Galileo OTM-97, size of turn 3°, duration 4 h, return to nominal attitude |
| 01-201 | 20 July 2001 | 07:00 | Galileo turn 4°, new nominal attitude |
| 01-215 | 03 August 2001 | 23:00 | Galileo OTM-98, no attitude change |
| 01-217 | 05 August 2001 | 05:12 | DDS begin RTS data |
| 01-218 | 06 August 2001 | 04:52 | Galileo Jupiter closest approach, distance 5.9 R_J |
| 01-218 | 06 August 2001 | 04:59 | Galileo Io 31 (I31) closest approach , altitude 193 km |
| 01-219 | 07 August 2001 | 16:08 | DDS end RTS data |
| 01-220 | 08 August 2001 | 03:00 | Galileo turn 7°, duration 2 h, return to nominal attitude |
| 01-222 | 10 August 2001 | 19:30 | Galileo OTM-99, no attitude change |
| 01-224 | 12 August 2001 | 08:00 | Galileo turn 3°, new nominal attitude |
| 01-236 | 24 August 2001 | 07:00 | Galileo turn 3°, duration 2 h, return to nominal attitude |
| 01-245 | 02 September 2001 | 03:00 | Galileo OTM-100, no attitude change |
| 01-246 | 03 September 2001 | 05:00 | Galileo turn 4°, new nominal attitude |
| 01-261 | 18 September 2001 | 12:00 | Galileo OTM-101, no attitude change |
| 01-270 | 27 September 2001 | 04:00 | Galileo turn 3°, new nominal attitude |
| 01-286 | 13 October 2001 | 18:00 | Galileo OTM-102, no attitude change |
| 01-287 | 14 October 2001 | 02:04 | DDS begin RTS data |
| 01-288 | 15 October 2001 | 23:56 | Galileo Jupiter closest approach, distance 5.8 R_J |
| 01-289 | 16 October 2001 | 01:23 | Galileo Io 32 (I32) closest approach , altitude 184 km |
| 01-290 | 17 October 2001 | 12:00 | Galileo turn 3°, duration 2 h, return to nominal attitude |
| 01-293 | 20 October 2001 | 04:00 | Galileo OTM-103, size of turn 1°, duration 2 h, return to nominal attitude |
| 01-301 | 28 October 2001 | 23:30 | DDS end RTS data |
| 01-324 | 20 November 2001 | 00:00 | Galileo turn 4°, duration 2 h, return to nominal attitude |
| 01-335 | 01 December 2001 | 00:00 | Galileo OTM-104, no attitude change |
| 01-340 | 06 December 2001 | 15:00 | Galileo turn 2°, new nominal attitude |
| 01-352 | 18 December 2001 | 00:00 | DDS configuration: HV=6 |

Table 2 (continued)

| Yr-day | Date | Time | Event |
|--------|-------------------|-------|--|
| 01-357 | 23 December 2001 | 16:00 | Galileo turn 2°, new nominal attitude |
| 02-004 | 04 January 2002 | 12:25 | DDS begin RTS data |
| 02-010 | 10 January 2002 | 00:00 | Galileo turn 5°, duration 2 h, new nominal attitude |
| 02-017 | 17 January 2002 | 09:15 | DDS end RTS data |
| 02-017 | 17 January 2002 | 13:40 | Galileo spacecraft anomaly |
| 02-017 | 17 January 2002 | 14:08 | Galileo Io 33 (I33) closest approach , altitude 102 km |
| 02-017 | 17 January 2002 | 16:23 | Galileo Jupiter closest approach, distance 5.5 R_J |
| 02-017 | 17 January 2002 | 23:50 | DDS begin RTS data after spacecraft anomaly |
| 02-021 | 21 January 2002 | 12:00 | Galileo OTM-106, no attitude change |
| 02-029 | 29 January 2002 | 23:00 | Galileo turn 2°, new nominal attitude |
| 02-032 | 01 February 2002 | 01:00 | Galileo turn 44°, duration 90 h, return to nominal attitude |
| 02-047 | 16 February 2002 | 19:09 | Galileo spacecraft anomaly |
| 02-051 | 20 February 2002 | 17:54 | DDS begin RTS data after spacecraft anomaly |
| 02-094 | 04 April 2002 | 00:00 | Galileo turn 3°, duration 3 h, return to nominal attitude |
| 02-102 | 12 April 2002 | 05:00 | Galileo turn 3°, new nominal attitude |
| 02-124 | 04 May 2002 | 23:00 | Galileo turn 4°, new nominal attitude |
| 02-131 | 11 May 2002 | 12:00 | Galileo turn 1°, duration 2 h, return to nominal attitude |
| 02-146 | 26 May 2002 | 02:00 | Galileo turn 4°, new nominal attitude |
| 02-157 | 06 June 2002 | 02:00 | Galileo turn 6°, duration 3 h, return to nominal attitude |
| 02-165 | 14 June 2002 | 16:00 | Galileo OTM-107, size of turn 3°, duration 3 h, return to nominal attitude |
| 02-182 | 01 July 2002 | 11:00 | Galileo turn 12°, new nominal attitude |
| 02-190 | 09 July 2002 | | Begin solar conjunction |
| 02-209 | 28 July 2002 | | End solar conjunction |
| 02-214 | 02 August 2002 | 08:00 | Galileo turn 5°, new nominal attitude |
| 02-232 | 20 August 2002 | 15:00 | Galileo turn 4°, new nominal attitude |
| 02-250 | 07 September 2002 | 12:00 | Galileo turn 4°, new nominal attitude |
| 02-274 | 01 October 2002 | 19:30 | Galileo spacecraft anomaly |
| 02-275 | 02 October 2002 | 23:54 | DDS begin RTS after spacecraft anomaly |
| 02-281 | 08 October 2002 | 02:00 | Galileo turn 6°, duration 3 h, return to nominal attitude |
| 02-285 | 12 October 2002 | 15:00 | Galileo turn 9°, new nominal attitude |
| 02-298 | 25 October 2002 | 03:00 | Galileo turn 2°, duration 2 h, return to nominal attitude |
| 02-309 | 05 November 2002 | 02:44 | DDS end RTS data |
| 02-309 | 05 November 2002 | 02:44 | DDS begin record data |
| 02-309 | 05 November 2002 | 06:19 | Galileo Amalthea 34 (A34) closest approach , 244 km distance from moon's centre |
| 02-309 | 05 November 2002 | 06:35 | Galileo spacecraft anomaly, end record data |
| 02-309 | 05 November 2002 | 07:25 | Galileo Jupiter closest approach, distance 2.0 R_J |
| 02-318 | 14 November 2002 | 08:00 | Galileo turn 9°, duration 3 h, return to nominal attitude |
| 02-322 | 18 November 2002 | 14:29 | DDS first MRO after spacecraft anomaly |
| 02-363 | 29 December 2002 | 07:53 | DDS final MRO |
| 03-003 | 03 January 2003 | 22:00 | Galileo turn 20°, duration 6 h, return to nominal attitude |
| 03-004 | 04 January 2003 | 21:00 | Galileo turn 20°, duration 5 h, return to nominal attitude |
| 03-008 | 08 January 2003 | 08:00 | Galileo turn 17°, duration 2 h, return to nominal attitude |
| 03-010 | 10 January 2003 | 22:00 | Galileo turn 22°, duration 82 h, return to nominal attitude |
| 03-015 | 15 January 2003 | 10:00 | Galileo turn 22°, new nominal attitude |
| 03-063 | 04 March 2003 | 15:00 | DDS begin RTS data |
| 03-070 | 11 March 2003 | 21:50 | DDS end RTS data |
| 03-255 | 12 September 2003 | 21:43 | DDS begin RTS data |
| 03-256 | 13 September 2003 | 18:57 | DDS end RTS data |
| 03-263 | 20 September 2003 | 13:44 | DDS begin RTS data |
| 03-263 | 20 September 2003 | 14:26 | DDS end RTS data |
| 03-264 | 21 September 2003 | 12:10 | DDS begin RTS data |
| 03-264 | 21 September 2003 | 17:59 | DDS end RTS data |
| 03-264 | 21 September 2003 | 18:57 | Galileo Jupiter impact, end of mission |

See text for details. Abbreviations used: MRO: DDS memory readout; HV: channeltron high voltage step; EVD: event definition, ion- (I), channeltron- (C), or electron-channel (E); SSEN: detection thresholds, ICP, CCP, ECP and PCP; OTM: orbit trim maneuver; RTS: Realtime science.

2002 (Table 2). Details of the various data transmission modes and corresponding data rates of Galileo are also given in Table 4.

RTS data were usually obtained when Galileo was in the inner jovian system where relatively high dust impact rates occurred. During time intervals when Galileo was in the outer jovian magnetosphere dust data were usually received as instrument memory-readouts (MROs). MROs returned event data which had accumulated in the instrument memory over time. Although the entire memory was read out during an MRO, the number of data sets of new events that could be transmitted to Earth in a given time period was much smaller than with RTS data because MROs occurred much less frequently (Table 4). For further details about Galileo dust data transmission from the jovian system the reader is referred to Papers VI and VIII.

In 2000–2003, RTS and record data were obtained during a period of 570 days (Fig. 1) which amounts to about 40% of the total almost four-year period. During the remaining times when the dust instrument was operated in neither RTS nor record mode, a total of 59 MROs occurred at approximately two to three week intervals. Until the end of 2002, MROs were frequent enough so that usually no ambiguities in the time-tagging occurred (i.e. MROs occurred at intervals smaller than 46 days).

The last MRO for the entire Galileo mission occurred at the end of 2002 on day 02-363. In 2003 we received dust data neither as MROs nor as record data. Only RTS data were received during rather short time intervals: about one week from 03-063 to 03-070 and a total time period of about two days between 03-255

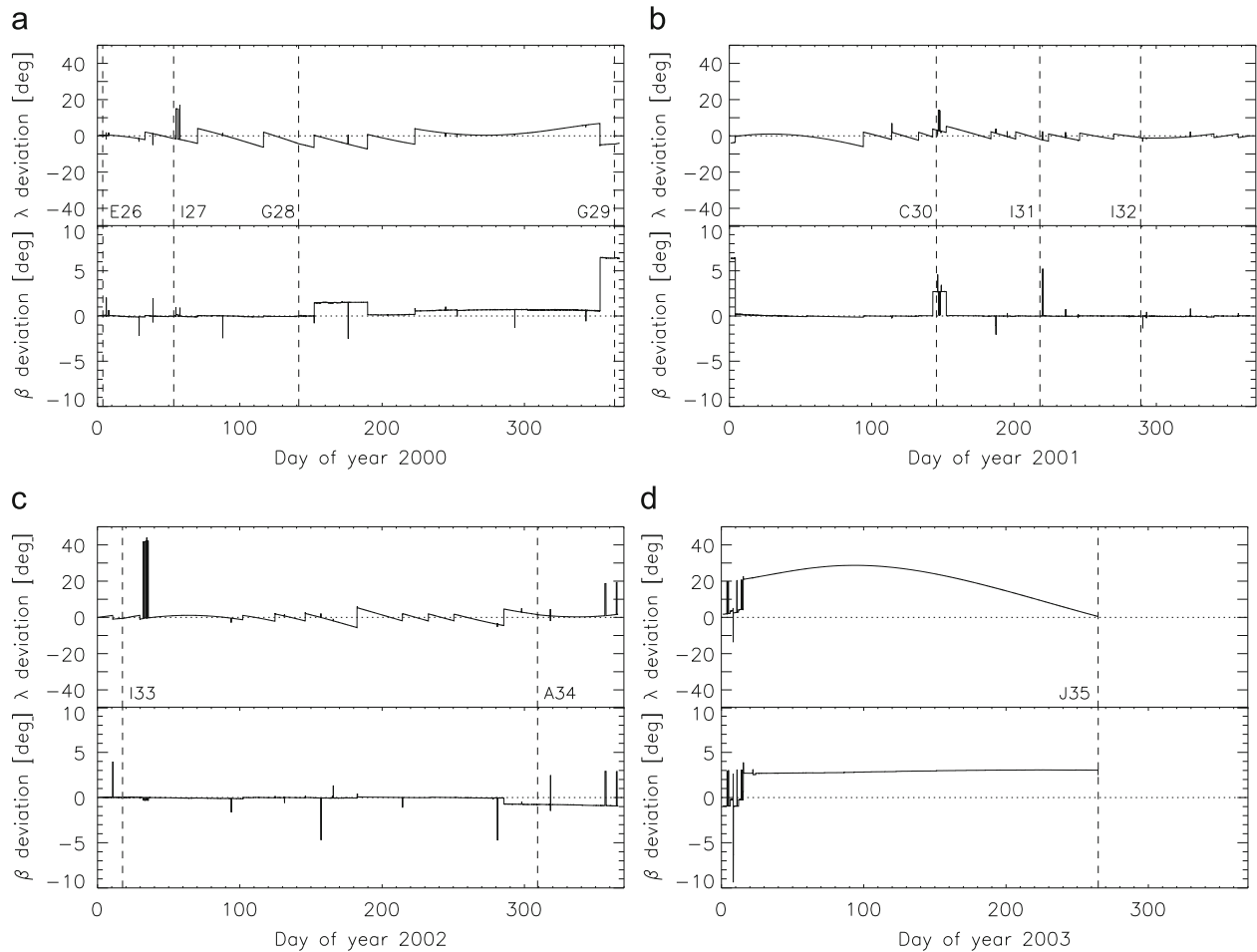


Fig. 2. Spacecraft attitude: deviation of the antenna pointing direction (i.e. negative spin axis) from the Earth direction. The angles are given in ecliptic longitude (λ) and latitude (β , equinox 1950.0). Dashed vertical lines indicate satellite flybys (E26–A34) or Galileo's Jupiter impact (J35). Sharp spikes are associated with imaging observations with Galileo's cameras or orbit trim maneuvers with the spacecraft thrusters.

and 03-264 before the spacecraft hit Jupiter (Table 2). No dust data were obtained outside these intervals in 2003.

Several resets of the dust instrument's internal clock occurred during the long periods without data transmission in 2003, leading to ambiguities in the impact time of some dust impacts. One clock reset occurred during the first data gap between 02-363 and 03-063 and four resets in the second gap between 03-070 and 03-255. Furthermore, due to data transmission problems, the time tagging was lost for the events transmitted in the interval 03-063 to 03-070. Consequently, the impact time of two events which occurred between 02-363 and 03-063 is completely unknown. We have set their impact time to 03-030 (these grains are indicated by horizontal bars in Fig. 9). For seven data sets transmitted between 03-063 and 03-070 the impact time could be determined with an accuracy of approximately one day from the time tagging of test pulses that were routinely performed by the dust instrument (see also Section 5.4).

2.4. Dust instrument operation

During Galileo's earlier orbital mission about Jupiter strong channeltron noise was usually recorded while Galileo was within about $20 R_J$ distance from Jupiter (Jupiter radius, $R_J = 71,492$ km). The details are described in Papers VI and VIII and are not repeated here. Furthermore, due to degradation of the

channeltron, the high voltage setting (HV) had to be raised two times in 1999 (Paper VIII). At the beginning of the year 2000, i.e. at the beginning of the time period considered in this paper, the dust instrument was operated in the following nominal configuration: the channeltron high voltage was set to 1250 V ($HV=4$), the event definition status was set such that only the ion-collector channel could initiate a measurement cycle ($EVD=1$) and the detection thresholds for the charges on the ion-collector, channeltron, electron-channel and entrance grid were set ($SSEN=0, 1, 1, 1$). This configuration effectively prevented dead time of the instrument due to channeltron noise (serious channeltron noise rates with $CN > 10$ occurred only during seven short time intervals in orbit A34 on day 02-309 when Galileo was inside Io's orbit and lasted only between several seconds and less than a minute. The resulting dead time is negligible because of its random occurrence and short duration). Due to degradation of the channeltron (Section 2.5) the channeltron high voltage was raised two additional times on days 00-309 and 01-352 in order to maintain a rather constant instrument sensitivity for dust impacts (Table 2).

During the Jupiter orbital tour of Galileo, orbit trim maneuvers (OTMs) were executed around perijove and apojove passages to target the spacecraft to close encounters with the Galilean moons. Many of these maneuvers required changes in the spacecraft attitude off the nominal Earth pointing direction (Fig. 2). Additionally, dedicated spacecraft turns occurred typically in the

Table 3
Dust detector sensitive area and field-of-view (FOV) for different dust data sets.

| Dust data set | FOV (°) | Sensor area (cm ²) | Comment |
|--------------------------|---------|--------------------------------|---|
| Stream particles class 2 | 140 | 1000 | Nominal target FOV Grün et al. (1992a) |
| Stream particles class 3 | 96 | 110 | Reduced target FOV Krüger et al. (1999b) |
| All other | 180 | 1000 | Target plus side wall FOV Altobelli et al. (2004) |

Table 4
Details of Galileo dust data transmission modes during the Jupiter mission.

| | Instrument channels ^a | Realtime science (RTS) | | Record | MROs |
|--|----------------------------------|------------------------|-----------------|--------|--------------------------------|
| | | Low rate | High rate | | |
| Data rate (bits s ⁻¹) | | 1.1 | 3.4 | 24 | ~ 3 × 10 ^{-3b} |
| Timing accuracy (min) | | 21.2 | 7.1 | ~ 1 | 259 |
| Data frames per readout | | 7 | 7 | 7 | 46 |
| Mission time coverage 1996 to 2003 (%) | | ~ 40 | ~ 40 | < 0.1 | ~ 60 |
| Maximum event rate recordable by accumulators (min ⁻¹) | AC21/AC31 ^c | 3000 | 9000 | 65,000 | ≈ 2 ^b |
| | All other | 12 | 36 | 256 | ≈ 0.01 ^b |
| Maximum event rate for complete data set transmission (min ⁻¹) | | $\frac{1}{21.2}$ | $\frac{1}{7.1}$ | ~ 1 | ≈ $\frac{46}{20 \text{ days}}$ |

See text for details.

^a See Section 3.1 for a definition of these parameters.

^b One MRO every 20 days assumed.

^c Since 4 December 1996; the “All other” row was valid for all data before this time.

inner jovian system within a few days around perijove passage to allow for imaging observations with Galileo’s cameras or to maintain the nominal Earth pointing direction.

In the time interval considered in this paper a total of five spacecraft anomalies (safings) occurred on days 00–055, 02–017, 02–047, 02–274, and 02–309 (Table 2). Three of these anomalies occurred in the inner jovian system in the region where the highest radiation levels were collected by the spacecraft, and recovery usually took several days. Although the dust instrument continued to measure dust impacts, the collected data could not be transmitted to Earth during the recovery and most of them were lost.

No reprogramming of the instrument’s onboard computer was necessary in the 2000–2003 time interval. In fact, the last reprogramming for the entire Galileo mission took place on 4 December 1996 when two overflow counters were added to the two channels counting events with the lowest impact charges on the ion collector grid (the so-called amplitude range AR1) and the highest quality classes (classes 2 and 3). With these overflow counters, all accumulator overflows could be recognized in these two channels in the 2000–2003 interval. It is very unlikely that unrecognized overflows occurred in the higher amplitude ranges which counted bigger events with larger impact charges. The only exception is day 02–309 when Galileo was in the gossamer ring region and the instrument continued to collect data after the spacecraft anomaly (see also Section 5.5). Here unrecognized overflows have likely occurred in amplitude range AR1, class 1 (channel AC11) and amplitude range AR2, classes 0, 1 and 2, while the higher amplitude ranges AR3 and AR4 were most likely free of overflows in all four quality classes. See Section 3.1 for a description of the amplitude ranges and quality classes of dust impacts.

2.5. Dust instrument electronics degradation

Analysis of the impact charges and rise times measured by the dust instrument revealed strong degradation of the instrument electronics which was most likely caused by the harsh radiation environment in the inner jovian magnetosphere. A detailed analysis was published by Krüger et al. (2005). Here we recall

the most significant results: (a) the sensitivity of the instrument for dust impacts and noise had dropped; (b) the amplification of the charge amplifiers had degraded, leading to reduced impact charge values measured on the detector target and the ion collector grid, Q_E and Q_i , respectively; (c) drifts in the target and ion collector rise time signals lead to prolonged rise times t_E and t_i ; (d) degradation of the channeltron required increases in the channeltron high voltage (Table 2). The degradation affects the mass and speed calibration of the dust instrument and requires a time-dependent correction when comparing dust fluxes measured early in the Galileo Jupiter mission with later measurements.

After 2000, masses and speeds derived from the instrument calibration have to be taken with caution because the electronics degradation was very severe. Only in cases where impact speeds are known from other arguments can corrected masses of particles be derived (e.g. the dust cloud measurements in the vicinity of the Galilean moons or Galileo’s gossamer ring passages). On the other hand, given the uncertainty in the impact calibration of a factor of two in speed and that of a factor of ten in mass, the increased uncertainty due to the electronics degradation was comparatively small before 2000 (it should be noted that the dust data until end 1999 published earlier—Papers II, IV, VI and VIII—remain unchanged). In particular, no corrections for dust fluxes, grain speeds and masses are necessary until end 1999 and results obtained with this data set in earlier publications remain valid. Beginning in 2000, however, the degradation became so severe that the calibrated speeds and masses have to be considered as lower and upper limits, respectively (see also Section 3.3).

3. Impact events

3.1. Event classification and noise

The dust instrument classified all events—real dust impacts and noise events—into one of 24 different categories (six amplitude ranges for the charge measured on the ion collector grid and four event classes) and counted them in 24 corresponding 8 bit

accumulators. The sensitive range of the dust instrument covered six orders in magnitude in impact charge, and the impacts were categorised according to the impact charge measured on the ion collector grid. The entire measurement range of six orders of magnitude was subdivided into six intervals, the so-called amplitude ranges, with each amplitude range covering one order of magnitude in impact charge. In addition, each event (dust impact or noise) was classified into one of four quality classes according to the quality of the impact charge and the rise time measurement of the impact signal. More detailed descriptions of the amplitude ranges and quality classes are given in Papers I and IV.

In interplanetary space most of the 24 categories were relatively free from noise and only sensitive to real dust impacts. The details of the noise behaviour in interplanetary space can be found in Papers II and IV.

In the extreme radiation environment of the jovian system, a different noise response of the instrument was recognized: especially within about $20 R_J$ from Jupiter class 1 and class 2 were contaminated with noise while class 3 was almost always noise-free (Krüger et al., 1999b). Analysis of the dust data set from Galileo's entire Jupiter mission showed that noise events could reliably be eliminated from class 2 (Krüger et al., 2005) while most class 1 events detected in the jovian environment showed signatures of being mostly noise events. For most of Galileo's Jupiter mission we therefore consider the class 3 and the noise-removed class 2 impacts as the complete set of dust data. Apart from a missing third charge signal—class 3 has three charge signals and class 2 only two—there is no physical difference between dust impacts categorized into class 2 or class 3. In particular, we usually classify all class 1 and class 0 events detected in the jovian environment as noise.

The only exceptions are the passages through Jupiter's gossamer rings in 2002 and 2003 where a somewhat different noise response of the instrument was recognized (Moissl, 2005). Here, good dust impacts could also be identified in class 1. In Table 5 we show the noise identification scheme applied to the data from the gossamer ring passages obtained while Galileo was within Io's orbit.

To summarise, noise was removed from the data set we present here with two different criteria: data obtained outside Io's orbit were processed according to the criteria derived by Krüger et al. (2005), while data obtained inside Io's orbit were noise-removed with the criteria of Moissl (2005) (Table 5). Degradation of the instrument electronics was taken into account beginning in 1997 (Paper VIII). The derivation of the noise contamination factor f_{noi} for class 2 was described in Paper VI and is not repeated here.

In this paper the terms “small” and “big” have the same meaning as in Papers IV, VI and VIII (which is different from the terminology of Paper II). Here, we call all particles in the amplitude ranges two and higher (AR2–6) “big”. Particles in the lowest amplitude range (AR1) are called “small”. This distinction

separates the small jovian dust stream particles from bigger grains which are mostly detected between the Galilean moons (see also Section 3.2). It should be noted that no impact events (neither dust impacts nor noise) were detected in amplitude ranges AR5 and AR6 in the time interval 2000 to 2003 considered in this paper. This is most likely caused by the degradation of the dust instrument electronics (cf. Section 2.5).

Table 6 lists the number of all dust impacts and noise events identified with the dust instrument in the 2000–2003 interval as deduced from the accumulators of classes 2 and 3. Depending on the event rate the numbers are given in intervals from half a day to a few weeks (the numbers with the highest time resolution are available in electronic form only and are provided to the data archiving centres). For impacts in these two classes in the lowest amplitude range AR1 the complete data sets for only 2% of all detected events were transmitted, the remaining 98% of events were only counted. About 32% of all data sets for events in the higher amplitude ranges were transmitted. We give only the number of events in classes 2 and 3 because they have been shown to contain real dust impacts during the entire Jupiter mission: class 3 is almost always noise free (although Krüger et al., 1999b found indications for a very small number of noise events in class 3, AR1, in the inner jovian system). Class 2 is strongly contaminated by noise events in the inner jovian system within about $15 R_J$ from Jupiter.

In the 2000–2003 interval Galileo had a total of eight targeted flybys at the Galilean moons plus one at Amalthea (Table 2). During the flybys at the Galilean moons no ejecta particles from the moons could be detected because of unfavourable detection geometry. During the Amalthea flyby in A34, however, the dust instrument had the right detection geometry. Taking the recently determined mass of Amalthea (Anderson et al., 2005), its Hill radius is $r_{\text{Hill}} \sim 130$ km, only slightly larger than the moon itself. Galileo's closest approach distance was 244 km from the moon's centre so that the spacecraft did not cross the Hill sphere where an increased dust density was expected. In fact, no increase in the dust impact rate could be identified, consistent with our expectations (Krüger et al., 2009).

3.2. Dust impact rates

Fig. 3 shows the dust impact rate recorded by the dust instrument in 2000–2003 as deduced from the class 2 and 3 accumulators. The impact rate measured in the lowest amplitude range (AR1) and the one measured in the higher amplitude ranges (AR2–6) are shown separately because they reflect two distinct populations of dust. Until early 2002 AR1 contains mostly stream particles which were measured throughout the jovian system. Bigger particles (AR2–6) were mostly detected in the region between the Galilean moons.

Between the perijove passages I33 and A34 in 2002 a low background rate of a few times 10^{-4} min^{-1} was measured in AR1 which is at least an order of magnitude higher than dust impact rates measured with Galileo and Ulysses in interplanetary space (Grün et al., 1997b). These impacts show a broad distribution over all rotation angles (Fig. 9) while stream particles were expected to approach from rotation angles around 90° most of the time in 2002, similar to the earlier Galileo orbits in 2000 and 2001. These grains could be stream particles approaching from a much broader range of directions as was reported from the dust measurements with Cassini during Jupiter flyby (Hsu et al., 2009).

During the gossamer ring passages impacts were measured in all amplitude ranges AR1–4 (Section 5.5). Note that the impact rate in AR1 was usually at least one to two orders of magnitude higher than that for the big particles. Diagrams showing the AR1

Table 5

Criteria for the separation of noise events in classes 1 and 2 from true dust impacts in the region within Io's orbit for Galileo orbits A34 and J35 (gossamer ring passages).

| Class, AR | EA–IA | | CA | EIC |
|----------------|----------------------|-----|----------|-----|
| Class 1, AR1 | ≤ 2 or ≥ 9 | or | ≤ 2 | – |
| Class 1, AR2–6 | ≤ 2 or ≥ 9 | and | ≤ 2 | – |
| Class 2, AR1 | – | – | – | = 0 |
| Class 2, AR2–6 | ≤ 1 or ≥ 7 | and | ≤ 2 | – |

Noise events in the lowest amplitude range (AR1) fulfill at least one of the criteria listed, whereas noise events in the higher ranges fulfill two criteria (from Moissl, 2005).

| | | | | | | | | | | | | | | | |
|---------------------------|-------|-------|-------|------|--------|-------|------|-----|----|------|-----|----|------|-----|----|
| 01-209 | 11:19 | 76.61 | 14.92 | 0.01 | 394 | 31 | 0.00 | 1 | 1 | – | – | – | – | – | – |
| 01-218 | 07:24 | 6.280 | 8.836 | 0.47 | 351 | 6 | 0.00 | 5 | 4 | 0.00 | 1 | 1 | 0.33 | 3 | 2 |
| 01-221 | 21:01 | 44.16 | 3.567 | 0.45 | 207 | 8 | 0.33 | 6 | – | – | – | – | 0.00 | 2 | – |
| 01-246 | 07:41 | 128.5 | 24.44 | 0.01 | 509 | 9 | 0.00 | 1 | – | – | – | 1 | – | – | – |
| 01-288 | 01:25 | 16.92 | 41.73 | 0.06 | 243 | 14 | – | – | – | – | – | – | – | – | – |
| 01-291 | 11:32 | 34.37 | 3.420 | 0.73 | 303 | 1 | 0.00 | 2 | 2 | 0.00 | 2 | – | 0.50 | 2 | – |
| 01-314 | 06:23 | 137.8 | 22.78 | 0.33 | 51 | – | – | – | – | – | – | – | – | – | – |
| 01-348 | 23:00 | 152.6 | 34.69 | 0.33 | 19 | 1 | 0.00 | 2 | – | – | – | – | – | – | – |
| 02-017 | 02:52 | 12.09 | 33.16 | 0.57 | 36 | – | 0.00 | 1 | – | – | – | 1 | 0.00 | 2 | 1 |
| 02-018 | 00:32 | 8.820 | 0.902 | 0.86 | 341 | – | 0.00 | 1 | 2 | – | – | – | 0.00 | 2 | 2 |
| 02-032 | 03:41 | 118.4 | 14.13 | 0.51 | 80 | 3 | 0.20 | 5 | 2 | 0.00 | 1 | – | – | – | – |
| 02-069 | 12:20 | 247.7 | 37.36 | 0.30 | 47 | 1 | – | – | – | – | – | – | – | – | – |
| 02-106 | 03:02 | 312.8 | 36.61 | 0.48 | 23 | – | – | – | – | – | – | – | – | – | – |
| 02-151 | 13:43 | 346.5 | 45.44 | 0.17 | 29 | 1 | 0.00 | 1 | – | – | – | – | – | – | – |
| 02-184 | 10:32 | 343.9 | 32.86 | 0.27 | 22 | – | – | – | – | – | – | – | – | – | – |
| 02-222 | 06:37 | 312.7 | 37.83 | 0.88 | 24 | 1 | – | – | – | – | – | – | – | – | – |
| 02-265 | 21:04 | 228.9 | 43.60 | 0.51 | 19 | 3 | – | – | 1 | – | – | – | – | – | – |
| 02-306 | 10:19 | 42.73 | 40.55 | 0.06 | 18 | – | 0.00 | 1 | – | – | – | 1 | – | – | – |
| 02-308 | 21:03 | 11.18 | 2.447 | 0.52 | 55 | 3 | – | – | 2 | – | – | 1 | – | – | – |
| 02-309 | 04:21 | 4.540 | 0.304 | 0.80 | 17 | – | 0.00 | 2 | 2 | 0.00 | 3 | 1 | – | – | 2 |
| 02-309 | 05:32 | 3.320 | 0.048 | 0.83 | 77 | – | – | – | – | 0.00 | 2 | – | – | – | – |
| 02-309 | 06:34 | 2.410 | 0.043 | 0.83 | 512 | 5 | 0.14 | 21 | 1 | 0.00 | 21 | 1 | 0.00 | 15 | 5 |
| 02-323 | 16:36 | 121.7 | 14.41 | 0.67 | 9841 | 80 | 0.00 | 191 | 2 | 0.00 | 46 | – | 0.00 | 62 | 2 |
| 02-357 | 20:16 | 245.2 | 34.15 | 0.04 | 92 | 6 | – | – | – | – | – | – | – | – | 1 |
| 03-066 | 18:08 | 357.0 | 73.91 | 0.86 | 11 | 1 | – | – | – | – | – | – | – | – | 2 |
| 03-262 | 11:23 | 38.06 | 195.7 | 0.00 | 28 | 1 | 0.00 | 2 | 5 | 0.00 | 1 | – | – | – | 1 |
| 03-264 | 14:11 | 7.190 | 2.117 | 0.00 | 36 | – | 0.00 | 14 | 1 | – | – | – | 0.00 | 1 | 1 |
| 03-264 | 15:43 | 5.500 | 0.063 | 0.53 | 41 | – | – | – | 1 | 0.00 | 1 | 2 | – | – | 1 |
| 03-264 | 17:59 | 2.540 | 0.094 | 0.53 | 124 | – | 0.00 | 45 | 8 | 0.42 | 26 | 10 | 0.12 | 68 | 36 |
| Events (counted) | | | | – | 284545 | 20976 | – | 372 | 45 | – | 107 | 23 | – | 163 | 59 |
| Impacts (complete data) | | | | – | 3291 | 1865 | – | 68 | 38 | – | 36 | 16 | – | 26 | 28 |
| All events(complete data) | | | | 0.22 | 4229 | 1865 | 0.28 | 95 | 41 | 0.05 | 38 | 16 | 0.07 | 28 | 28 |

The jovicentric distance D_{Jup} , the length of the time interval Δt (days) from the previous table entry, and the corresponding numbers of impacts are given for the class 2 and 3 accumulators. The accumulators are arranged with increasing signal amplitude ranges (AR), e.g. AC31 means counter for CLN=3 and AR=1. The determination of the noise contamination f_{noi} in class 2 is described in Paper VI. The Δt in the first line (day 00-002) is the time interval counted from the last entry in Table 2 in Paper VIII. The totals of counted impacts, of impacts with complete data, and of all events (noise plus impact events) for the entire period are given as well. f_{noi} has been estimated from the data sets transmitted.

^a AC21 and AC31: Overflows of the 8 bit accumulators were counted with overflow counters so that no unrecognized overflows occurred in these two channels.

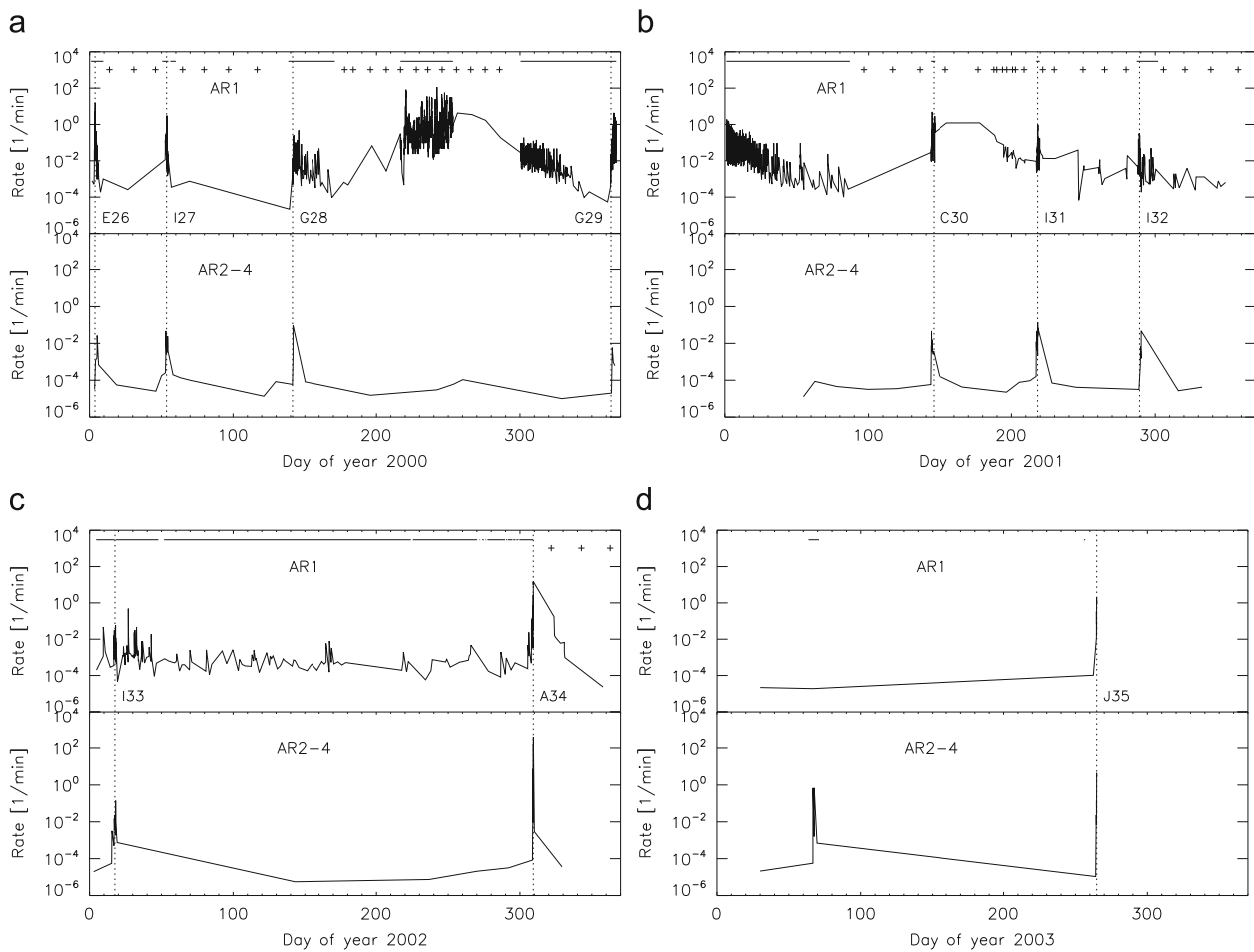


Fig. 3. Dust impact rate detected in 2000–2003. For each year the top panel shows the impact rate in AR1 and the bottom panel that for the higher amplitude ranges AR2–4 (no impacts were detected in AR5 and AR6 in the time interval considered in this paper). Only data for classes 2 and 3 are shown. Dotted lines indicate satellite flybys (E26–A34) or Galileo’s Jupiter impact (J35). Perijove passages occurred within two days of the moon closest approaches. These curves are plotted from the number of impacts with the highest time resolution which is available only in electronic form. No smoothing was applied to the data. In the top panels (AR1), time intervals with continuous RTS coverage are indicated by horizontal bars, memory readouts (MROs) are marked by crosses.

impact rate with a much higher time resolution in the inner jovian system are given in Fig. 4, and Galileo’s gossamer ring passages are discussed in detail by Krüger et al. (2009).

In the inner jovian system the impact rates of AR1 particles frequently exceeded 10 min^{-1} . An exceptionally large dust impact rate was recorded during the orbit G28 in the outer jovian system when Galileo was approximately $280 R_J$ away from Jupiter (Section 5.2 and Fig. 12). This represents one of the highest dust ejection rates of Io recorded during the entire Galileo Jupiter mission and is likely connected with a single strong volcanic eruption on Io (Krüger et al., 2003a; Geissler et al., 2004).

3.3. Event tables

Table 7 lists the data sets for all 224 big particles detected between 1 January 2000 and 21 September 2003 for which the complete information exists. Class 1 and class 2 particles were separated from noise by applying the criteria developed by Krüger et al. (1999b, 2005) and Moissl (2005) (Section 3.1). We do not list the small stream particles (AR1) in Table 7 because their masses and velocities are outside the calibrated range of the dust instrument and they are by far too numerous to be listed here. The complete information of a total of 5165 small (AR1) dust particles was transmitted in 2000–2003. These are mostly stream particles which are believed to be about 10 nm in size and their

velocities exceed 200 km s^{-1} (Zook et al., 1996). Any masses and velocities derived for these particles with existing calibration algorithms would be unreliable. The full data set for all 5389 particles is submitted to the data archiving centres and is available in electronic form. A total number of 7566 events (dust plus noise in all amplitude ranges and classes) were transmitted in 2000–2003, each with a complete data set.

In Table 7 dust particles are identified by their sequence number and their impact time. Gaps in the sequence number are due to the omission of the small particles. The time error value (TEV) which was introduced for the data set from the Jupiter mission because of the large differences in the timing accuracy of the dust instrument in the various data readout modes is listed next (see Table 4 and Paper VI for details). Then the event category—class (CLN) and amplitude range (AR)—are given. Raw data as transmitted to Earth are displayed in the next columns: sector value (SEC) which is the spacecraft spin orientation at the time of impact, impact charge numbers (IA, EA, CA) and rise times (IT, ET), time difference and coincidence of electron and ion signals (EIT, EIC), coincidence of ion and channeltron signal (IIC), charge reading at the entrance grid (PA) and time (PET) between this signal and the impact. Then the instrument configuration is given: event definition (EVD), charge sensing thresholds (ICP, ECP, CCP, PCP) and channeltron high voltage step (HV). See Paper I for further explanation of the instrument parameters, except TEV which was introduced in Paper VI.

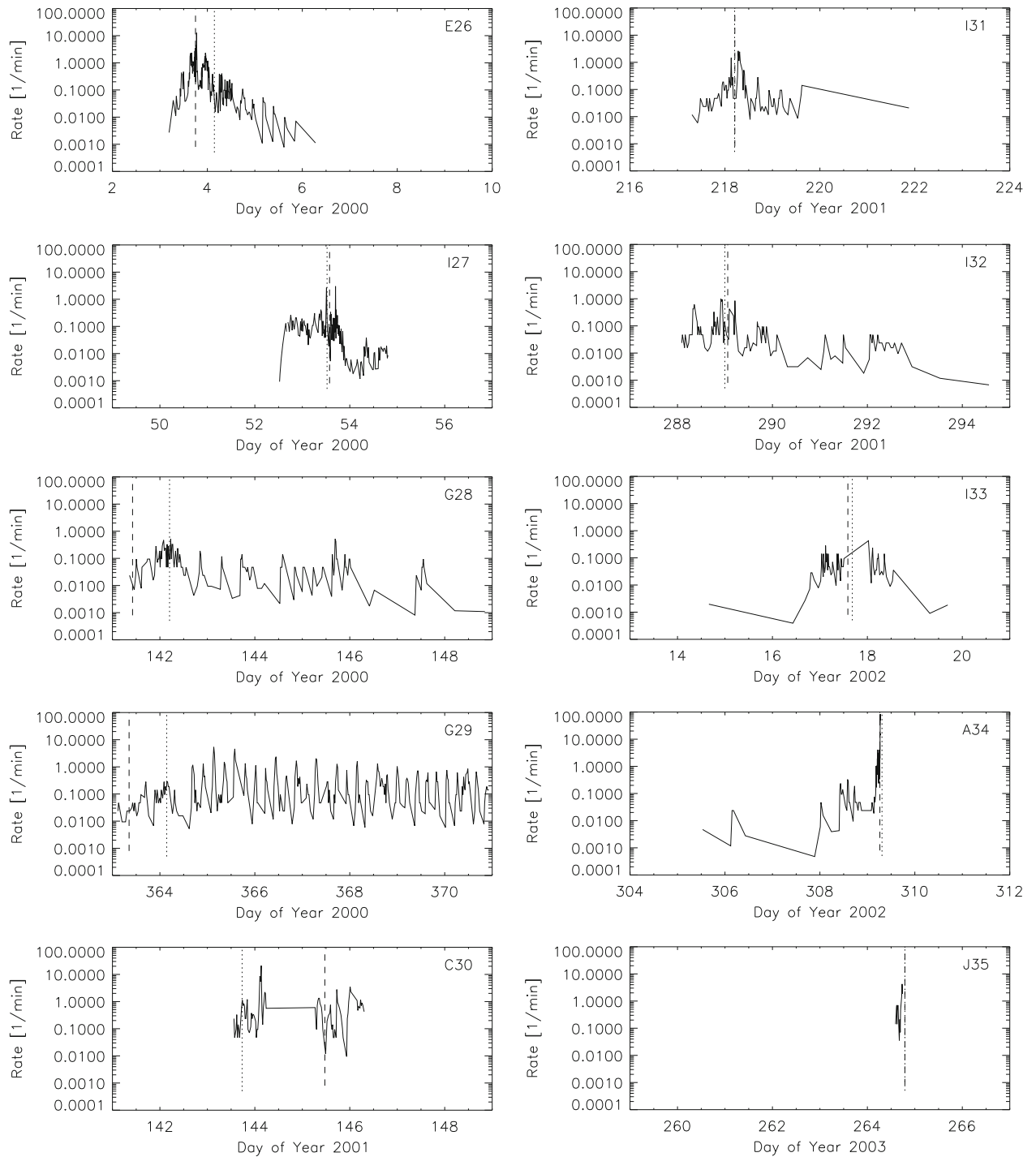


Fig. 4. Dust impact rate detected in the inner jovian system in higher time resolution. An eight-day interval is shown in each panel. Only data for AR1 (classes 2 and 3) are shown. Dotted lines indicate perijove passages of Galileo, dashed lines satellite closest approaches (E26–A34) or Jupiter impact (J35).

The next four columns in Table 7 give information about Galileo's orbit: ecliptic longitude and latitude (LON, LAT) and distance from Jupiter (D_{Jup} , in R_J). The next column gives the rotation angle (ROT) as described in Section 2. Whenever this value is unknown, ROT is arbitrarily set to 999. This occurs 71 times in the full data set that includes the small particles. Then follows the pointing direction of the instrument at the time of particle impact in ecliptic longitude and latitude (S_{LON} , S_{LAT}). When ROT is not valid, S_{LON} and S_{LAT} are also useless and set to 999. Mean impact velocity (v) and velocity error factor (VEF, i.e. multiply or divide stated velocity by VEF to obtain upper or lower

limits) as well as mean particle mass (m) and mass error factor (MEF) are given in the last columns. For VEF > 6, both velocity and mass estimates are invalid and should be discarded.

Beginning in 2000 the degradation of the dust instrument electronics became very severe, leading to artificially too long rise times and reduced charge amplitudes. The calibrated mass and speed values for VEF < 6 listed in Table 7 should thus be considered as lower limits for the impact velocity and upper limits for the particle mass throughout the 2000–2003 interval.

No intrinsic dust charge values are given (Svestka et al., 1996). Even though the charge carried by the dust grains is expected to

Table 7
 Number, impact time, TEV (in minutes) CLN, AR, SEC, IA, EA, CA, IT, ET, EIT, EIC, ICC, PA, PET, EVD, ICP, ECP, CCP, PCP, HV and evaluated data: LON, LAT, D_{Jup} (in R_{J}), rotation angle (ROT), instr. pointing (S_{LON} , S_{LAT}), speed v (in km s^{-1}), speed error factor (VEF), mass m (in g) and mass error factor (MEF). Velocity and mass should be considered as lower and upper limits for the true values, respectively, because of the strong degradation of the dust instrument electronics (see text for details).

| No. | IMP. DATE | TEV | CLN | AR | SEC | IA | EA | CA | IT | ET | EIT | EIC | ICC | PA | PET | EVD | ICP | ECP | CCP | PCP | HV | LON | LAT | D_{Jup} | ROT | S_{LON} | S_{LAT} | V | VEF | M | MEF |
|-------|-----------------|-----|-----|----|-----|----|----|----|----|----|-----|-----|-----|----|-----|-----|-----|-----|-----|-----|----|------|------|------------------|-----|------------------|------------------|------|-----|-----------------------|-------|
| 15881 | 00-003 12:24:10 | 8 | 2 | 2 | 188 | 9 | 4 | 3 | 15 | 11 | 11 | 0 | 0 | 8 | 0 | 5 | 0 | 1 | 1 | 1 | 4 | 35.8 | -1.2 | 12.631 | 186 | 17 | -55 | 2.0 | 1.9 | 3.9×10^{-11} | 10.5 |
| 16010 | 00-004 02:52:43 | 8 | 3 | 3 | 133 | 20 | 23 | 22 | 11 | 10 | 8 | 0 | 1 | 41 | 0 | 5 | 0 | 1 | 1 | 1 | 4 | 35.9 | -1.2 | 5.808 | 263 | 330 | -5 | 5.2 | 1.9 | 8.3×10^{-11} | 10.3 |
| 16038 | 00-005 01:17:30 | 22 | 2 | 3 | 117 | 22 | 14 | 8 | 9 | 14 | 0 | 1 | 1 | 38 | 12 | 5 | 0 | 1 | 1 | 1 | 4 | 35.8 | -1.2 | 16.274 | 285 | 331 | 12 | 7.2 | 1.9 | 1.4×10^{-11} | 10.5 |
| 16041 | 00-005 05:11:04 | 22 | 3 | 3 | 174 | 20 | 9 | 15 | 13 | 1 | 8 | 0 | 1 | 41 | 0 | 5 | 0 | 1 | 1 | 1 | 4 | 35.8 | -1.2 | 18.306 | 205 | 353 | -48 | 2.0 | 1.9 | 3.8×10^{-10} | 10.5 |
| 16042 | 00-005 05:48:29 | 259 | 3 | 2 | 111 | 8 | 27 | 9 | 14 | 15 | 8 | 0 | 1 | 47 | 1 | 5 | 0 | 1 | 1 | 1 | 4 | 35.8 | -1.2 | 18.623 | 294 | 333 | 19 | 2.0 | 1.9 | 9.6×10^{-10} | 10.5 |
| 16047 | 00-006 06:18:37 | 22 | 3 | 2 | 153 | 13 | 21 | 19 | 12 | 11 | 8 | 0 | 1 | 38 | 0 | 5 | 0 | 1 | 1 | 1 | 4 | 35.9 | -1.2 | 29.696 | 235 | 335 | -28 | 4.5 | 1.9 | 4.2×10^{-11} | 10.5 |
| 16051 | 00-046 02:20:57 | 259 | 2 | 4 | 219 | 27 | 31 | 22 | 12 | 12 | 4 | 1 | 1 | 14 | 9 | 5 | 0 | 1 | 1 | 1 | 4 | 39.4 | -1.1 | 65.806 | 142 | 71 | -40 | 2.0 | 1.9 | 2.6×10^{-08} | 10.5 |
| 16052 | 00-050 01:15:31 | 259 | 3 | 4 | 21 | 30 | 50 | 4 | 13 | 12 | 9 | 0 | 1 | 27 | 0 | 5 | 0 | 1 | 1 | 1 | 4 | 39.9 | -1.1 | 41.387 | 60 | 80 | 23 | 2.0 | 1.9 | 8.6×10^{-08} | 10.5 |
| 16066 | 00-052 19:13:01 | 22 | 3 | 2 | 196 | 10 | 49 | 4 | 12 | 12 | 7 | 0 | 1 | 25 | 1 | 5 | 0 | 1 | 1 | 1 | 4 | 40.3 | -1.1 | 13.836 | 174 | 37 | -55 | 4.5 | 1.9 | 1.8×10^{-10} | 10.5 |
| 16080 | 00-053 01:35:12 | 22 | 2 | 2 | 225 | 8 | 4 | 3 | 15 | 14 | 11 | 0 | 0 | 4 | 23 | 5 | 0 | 1 | 1 | 1 | 4 | 40.3 | -1.1 | 10.244 | 134 | 76 | -34 | 2.0 | 1.9 | 3.3×10^{-11} | 10.5 |
| 16082 | 00-053 01:56:26 | 22 | 2 | 2 | 236 | 9 | 21 | 5 | 15 | 15 | 12 | 0 | 0 | 9 | 28 | 5 | 0 | 1 | 1 | 1 | 4 | 40.3 | -1.1 | 10.044 | 118 | 81 | -22 | 2.0 | 1.9 | 4.2×10^{-10} | 10.5 |
| 16085 | 00-053 03:42:37 | 22 | 2 | 2 | 249 | 9 | 4 | 3 | 15 | 14 | 11 | 0 | 0 | 6 | 0 | 5 | 0 | 1 | 1 | 1 | 4 | 40.3 | -1.1 | 9.055 | 100 | 84 | -8 | 2.0 | 1.9 | 3.9×10^{-11} | 10.5 |
| 16103 | 00-053 17:01:24 | 8 | 2 | 2 | 149 | 9 | 11 | 5 | 14 | 15 | 0 | 1 | 1 | 47 | 31 | 5 | 0 | 1 | 1 | 1 | 4 | 40.4 | -1.1 | 6.844 | 240 | 338 | -23 | 2.1 | 1.6 | 9.1×10^{-11} | 6.0 |
| 16105 | 00-053 17:50:57 | 8 | 2 | 4 | 255 | 30 | 59 | 24 | 12 | 12 | 4 | 1 | 1 | 28 | 1 | 5 | 0 | 1 | 1 | 1 | 4 | 40.4 | -1.1 | 7.202 | 91 | 84 | -1 | 2.0 | 1.9 | 5.0×10^{-07} | 10.5 |
| 16107 | 00-053 18:33:25 | 8 | 3 | 4 | 143 | 30 | 30 | 28 | 12 | 10 | 5 | 0 | 1 | 46 | 0 | 5 | 0 | 1 | 1 | 1 | 4 | 40.4 | -1.1 | 7.536 | 249 | 336 | -17 | 2.0 | 1.9 | 3.7×10^{-08} | 10.5 |
| 16111 | 00-053 23:30:40 | 22 | 2 | 2 | 74 | 11 | 13 | 4 | 14 | 15 | 0 | 1 | 1 | 43 | 14 | 5 | 0 | 1 | 1 | 1 | 4 | 40.3 | -1.1 | 10.247 | 346 | 10 | 52 | 2.1 | 1.6 | 1.7×10^{-10} | 6.0 |
| 16113 | 00-054 06:56:34 | 22 | 3 | 2 | 24 | 11 | 50 | 12 | 13 | 13 | 7 | 0 | 1 | 26 | 1 | 5 | 0 | 1 | 1 | 1 | 4 | 40.3 | -1.1 | 14.540 | 56 | 79 | 26 | 2.3 | 1.9 | 3.0×10^{-09} | 10.5 |
| 16114 | 00-054 08:21:30 | 22 | 3 | 2 | 50 | 13 | 51 | 12 | 12 | 12 | 6 | 0 | 1 | 26 | 1 | 5 | 0 | 1 | 1 | 1 | 4 | 40.3 | -1.1 | 15.337 | 20 | 54 | 49 | 4.5 | 1.9 | 4.5×10^{-10} | 10.5 |
| 16116 | 00-054 11:53:49 | 22 | 2 | 2 | 211 | 8 | 10 | 0 | 12 | 13 | 10 | 0 | 0 | 3 | 26 | 5 | 0 | 1 | 1 | 1 | 4 | 40.3 | -1.1 | 17.284 | 153 | 62 | -47 | 5.9 | 1.6 | 2.0×10^{-12} | 6.0 |
| 16117 | 00-054 13:18:45 | 22 | 3 | 4 | 157 | 30 | 54 | 25 | 13 | 12 | 5 | 0 | 1 | 46 | 0 | 5 | 0 | 1 | 1 | 1 | 4 | 40.3 | -1.1 | 18.046 | 229 | 341 | -32 | 2.0 | 1.9 | 1.4×10^{-07} | 10.5 |
| 16118 | 00-054 15:26:10 | 22 | 2 | 2 | 66 | 8 | 10 | 0 | 12 | 7 | 10 | 0 | 0 | 4 | 27 | 5 | 0 | 1 | 1 | 1 | 4 | 40.3 | -1.1 | 19.167 | 357 | 25 | 54 | 15.9 | 3.7 | 1.3×10^{-13} | 106.8 |
| 16119 | 00-055 02:04:11 | 259 | 2 | 2 | 228 | 9 | 12 | 0 | 12 | 10 | 10 | 0 | 0 | 4 | 26 | 5 | 0 | 1 | 1 | 1 | 4 | 40.3 | -1.1 | 24.470 | 129 | 79 | -30 | 10.9 | 2.1 | 5.5×10^{-13} | 14.2 |
| 16121 | 00-058 01:55:34 | 22 | 3 | 2 | 45 | 11 | 15 | 15 | 14 | 15 | 6 | 0 | 1 | 42 | 8 | 5 | 0 | 1 | 1 | 1 | 4 | 40.5 | -1.1 | 51.750 | 27 | 61 | 46 | 2.1 | 1.6 | 2.3×10^{-10} | 6.0 |
| 16123 | 00-063 04:11:32 | 259 | 2 | 2 | 167 | 8 | 10 | 0 | 12 | 11 | 11 | 0 | 0 | 2 | 22 | 5 | 0 | 1 | 1 | 1 | 4 | 40.8 | -1.1 | 83.010 | 215 | 349 | -42 | 9.5 | 1.7 | 4.7×10^{-13} | 7.6 |
| 16124 | 00-070 04:27:03 | 259 | 2 | 3 | 138 | 21 | 14 | 7 | 10 | 15 | 0 | 1 | 1 | 45 | 31 | 5 | 0 | 1 | 1 | 1 | 4 | 41.3 | -1.1 | 112.177 | 256 | 335 | -11 | 4.5 | 1.9 | 5.1×10^{-11} | 10.5 |
| 16125 | 00-109 08:54:08 | 259 | 2 | 2 | 68 | 8 | 14 | 0 | 13 | 14 | 7 | 0 | 0 | 38 | 1 | 5 | 0 | 1 | 1 | 1 | 4 | 44.7 | -1.1 | 147.606 | 354 | 30 | 54 | 2.7 | 1.6 | 4.8×10^{-11} | 6.0 |
| 16127 | 00-121 09:56:42 | 259 | 2 | 2 | 178 | 13 | 22 | 14 | 14 | 15 | 15 | 0 | 1 | 17 | 1 | 5 | 0 | 1 | 1 | 1 | 4 | 46.0 | -1.0 | 124.594 | 200 | 20 | -50 | 2.0 | 1.9 | 9.5×10^{-10} | 10.5 |
| 16129 | 00-129 16:23:32 | 259 | 2 | 2 | 16 | 10 | 13 | 11 | 12 | 10 | 15 | 0 | 1 | 11 | 2 | 5 | 0 | 1 | 1 | 1 | 4 | 46.9 | -1.0 | 96.258 | 68 | 98 | 18 | 10.9 | 2.1 | 7.6×10^{-13} | 14.2 |
| 16133 | 00-141 08:59:32 | 22 | 2 | 2 | 98 | 11 | 50 | 4 | 12 | 12 | 7 | 0 | 0 | 26 | 1 | 5 | 0 | 1 | 1 | 1 | 4 | 48.3 | -1.0 | 15.647 | 312 | 360 | 33 | 4.5 | 1.9 | 2.9×10^{-10} | 10.5 |
| 16134 | 00-141 18:17:11 | 22 | 2 | 2 | 59 | 9 | 20 | 6 | 15 | 14 | 11 | 0 | 0 | 19 | 0 | 5 | 0 | 1 | 1 | 1 | 4 | 48.4 | -1.0 | 10.473 | 7 | 56 | 54 | 2.0 | 1.9 | 3.5×10^{-10} | 10.5 |
| 16135 | 00-141 18:27:48 | 22 | 2 | 2 | 141 | 9 | 15 | 4 | 15 | 0 | 8 | 0 | 0 | 37 | 31 | 5 | 0 | 1 | 1 | 1 | 4 | 48.4 | -1.0 | 10.377 | 252 | 352 | -14 | 2.0 | 1.9 | 2.3×10^{-10} | 10.5 |
| 16283 | 00-195 19:58:14 | 259 | 3 | 3 | 69 | 20 | 21 | 11 | 10 | 11 | 6 | 0 | 1 | 13 | 1 | 5 | 0 | 1 | 1 | 1 | 5 | 51.9 | -1.0 | 238.002 | 353 | 51 | 54 | 4.5 | 1.9 | 9.3×10^{-11} | 10.5 |
| 16366 | 00-219 15:53:18 | 22 | 2 | 2 | 194 | 8 | 4 | 10 | 13 | 14 | 11 | 0 | 0 | 6 | 31 | 5 | 0 | 1 | 1 | 1 | 5 | 53.9 | -0.9 | 272.964 | 177 | 65 | -55 | 2.3 | 1.9 | 1.8×10^{-11} | 10.5 |
| 18055 | 00-242 05:00:03 | 259 | 2 | 2 | 43 | 10 | 12 | 13 | 12 | 14 | 2 | 1 | 1 | 0 | 0 | 5 | 0 | 1 | 1 | 1 | 5 | 55.8 | -0.9 | 288.137 | 30 | 104 | 45 | 3.8 | 1.6 | 1.5×10^{-11} | 6.0 |
| 18056 | 00-242 05:01:04 | 259 | 2 | 2 | 214 | 8 | 10 | 18 | 12 | 14 | 1 | 1 | 1 | 5 | 31 | 5 | 0 | 1 | 1 | 1 | 5 | 55.8 | -0.9 | 288.137 | 149 | 106 | -44 | 3.8 | 1.6 | 7.9×10^{-12} | 6.0 |
| 18880 | 00-253 17:06:45 | 259 | 2 | 2 | 39 | 8 | 3 | 14 | 12 | 10 | 0 | 1 | 1 | 3 | 31 | 5 | 0 | 1 | 1 | 1 | 5 | 56.8 | -0.9 | 289.854 | 35 | 108 | 42 | 4.5 | 1.9 | 1.5×10^{-12} | 10.5 |
| 18897 | 00-260 04:24:34 | 259 | 3 | 2 | 75 | 8 | 14 | 7 | 13 | 14 | 6 | 0 | 1 | 37 | 0 | 5 | 0 | 1 | 1 | 1 | 5 | 57.4 | -0.9 | 289.088 | 345 | 48 | 52 | 2.7 | 1.6 | 4.8×10^{-11} | 6.0 |
| 19332 | 00-363 15:50:50 | 22 | 3 | 2 | 61 | 10 | 49 | 7 | 13 | 13 | 7 | 0 | 1 | 26 | 1 | 5 | 0 | 1 | 1 | 1 | 5 | 68.2 | -0.7 | 11.175 | 4 | 64 | 60 | 2.3 | 1.9 | 1.8×10^{-09} | 10.5 |
| 19344 | 00-364 01:45:21 | 22 | 2 | 2 | 166 | 9 | 12 | 3 | 15 | 14 | 13 | 0 | 0 | 8 | 7 | 5 | 0 | 1 | 1 | 1 | 5 | 68.2 | -0.7 | 7.596 | 217 | 20 | -36 | 2.5 | 1.6 | 5.4×10^{-11} | 6.0 |
| 19349 | 00-364 04:35:14 | 22 | 2 | 2 | 60 | 11 | 25 | 3 | 13 | 15 | 5 | 0 | 0 | 20 | 1 | 5 | 0 | 1 | 1 | 1 | 5 | 68.2 | -0.7 | 7.539 | 6 | 67 | 60 | 2.3 | 1.9 | 6.2×10^{-10} | 10.5 |

| | | | | | | | | | | | | | | | | | | | | | | | | | | | | | | | |
|-------|-----------------|-----|---|---|-----|----|----|----|----|----|----|---|---|----|----|---|---|---|---|---|---|------|------|---------|-----|-----|-----|------|------|-----------------------|--------|
| 19368 | 00-364 22:16:54 | 22 | 2 | 2 | 66 | 8 | 13 | 8 | 13 | 14 | 11 | 0 | 0 | 9 | 3 | 5 | 0 | 1 | 1 | 1 | 5 | 68.3 | -0.7 | 14.891 | 357 | 53 | 60 | 2.7 | 1.6 | 4.1×10^{-11} | 6.0 |
| 19414 | 00-366 01:23:46 | 259 | 2 | 3 | 115 | 20 | 13 | 3 | 12 | 15 | 0 | 1 | 1 | 10 | 31 | 5 | 0 | 1 | 1 | 1 | 5 | 68.3 | -0.7 | 28.040 | 288 | 2 | 18 | 2.0 | 1.9 | 7.2×10^{-10} | 10.5 |
| 20394 | 01-054 15:37:37 | 22 | 2 | 2 | 55 | 15 | 20 | 0 | 14 | 14 | 13 | 0 | 0 | 11 | 0 | 5 | 0 | 1 | 1 | 1 | 5 | 72.0 | -0.6 | 209.299 | 13 | 78 | 52 | 2.5 | 1.6 | 3.3×10^{-10} | 6.0 |
| 20408 | 01-077 21:42:34 | 22 | 3 | 3 | 165 | 21 | 26 | 12 | 15 | 9 | 7 | 0 | 1 | 43 | 0 | 5 | 0 | 1 | 1 | 1 | 5 | 74.0 | -0.5 | 215.070 | 218 | 19 | -40 | 6.4 | 3.1 | 8.2×10^{-11} | 58.7 |
| 20415 | 01-092 19:28:24 | 259 | 2 | 2 | 242 | 8 | 4 | 4 | 10 | 14 | 11 | 0 | 0 | 3 | 31 | 5 | 0 | 1 | 1 | 1 | 5 | 75.4 | -0.5 | 203.645 | 110 | 114 | -15 | 9.7 | 1.9 | 1.6×10^{-13} | 10.5 |
| 20435 | 01-119 14:15:13 | 259 | 3 | 2 | 240 | 10 | 19 | 19 | 15 | 15 | 9 | 0 | 1 | 3 | 31 | 5 | 0 | 1 | 1 | 1 | 5 | 78.0 | -0.5 | 147.493 | 113 | 125 | -18 | 2.0 | 1.9 | 3.4×10^{-10} | 10.5 |
| 20451 | 01-143 07:42:40 | 259 | 3 | 2 | 132 | 11 | 49 | 3 | 12 | 13 | 7 | 0 | 1 | 26 | 1 | 5 | 0 | 1 | 1 | 1 | 5 | 80.9 | -0.4 | 10.240 | 264 | 27 | -2 | 4.5 | 1.9 | 2.1×10^{-10} | 10.5 |
| 20453 | 01-143 15:12:36 | 22 | 2 | 2 | 182 | 11 | 13 | 3 | 15 | 11 | 14 | 0 | 0 | 13 | 3 | 5 | 0 | 1 | 1 | 1 | 5 | 80.9 | -0.4 | 7.491 | 194 | 63 | -49 | 6.4 | 3.1 | 4.1×10^{-12} | 58.7 |
| 20455 | 01-143 16:58:47 | 64 | 2 | 2 | 238 | 10 | 30 | 5 | 12 | 11 | 7 | 0 | 1 | 26 | 1 | 5 | 0 | 1 | 1 | 1 | 5 | 81.0 | -0.4 | 7.291 | 115 | 133 | -18 | 4.5 | 1.9 | 1.1×10^{-10} | 10.5 |
| 20456 | 01-143 18:02:29 | 22 | 2 | 4 | 131 | 26 | 30 | 12 | 6 | 11 | 4 | 1 | 1 | 11 | 0 | 5 | 0 | 1 | 1 | 1 | 5 | 81.0 | -0.4 | 7.287 | 266 | 27 | -1 | 12.1 | 1.6 | 5.9×10^{-11} | 6.0 |
| 20458 | 01-143 18:23:43 | 22 | 2 | 2 | 136 | 8 | 21 | 3 | 13 | 11 | 6 | 0 | 0 | 10 | 1 | 5 | 0 | 1 | 1 | 1 | 5 | 81.0 | -0.4 | 7.306 | 259 | 27 | -7 | 2.3 | 1.9 | 1.9×10^{-10} | 10.5 |
| 20461 | 01-143 23:20:58 | 22 | 2 | 4 | 83 | 30 | 9 | 24 | 13 | 0 | 4 | 1 | 1 | 28 | 1 | 5 | 0 | 1 | 1 | 1 | 5 | 81.0 | -0.4 | 8.473 | 333 | 47 | 49 | 2.0 | 1.9 | 1.9×10^{-09} | 10.5 |
| 20467 | 01-144 02:53:19 | 22 | 2 | 2 | 55 | 11 | 5 | 3 | 12 | 15 | 15 | 0 | 1 | 26 | 0 | 5 | 0 | 1 | 1 | 1 | 5 | 81.0 | -0.4 | 9.998 | 13 | 100 | 55 | 4.5 | 1.9 | 3.2×10^{-12} | 10.5 |
| 20472 | 01-144 04:18:15 | 22 | 2 | 2 | 76 | 11 | 30 | 5 | 12 | 11 | 7 | 0 | 0 | 26 | 1 | 5 | 0 | 1 | 1 | 1 | 5 | 81.0 | -0.4 | 10.687 | 343 | 58 | 54 | 4.5 | 1.9 | 1.3×10^{-10} | 10.5 |
| 20475 | 01-144 05:21:57 | 22 | 2 | 2 | 25 | 12 | 31 | 13 | 12 | 13 | 7 | 0 | 1 | 26 | 1 | 5 | 0 | 1 | 1 | 1 | 5 | 81.0 | -0.4 | 11.220 | 55 | 132 | 30 | 4.5 | 1.9 | 1.7×10^{-10} | 10.5 |
| 20478 | 01-144 09:35:57 | 259 | 2 | 2 | 235 | 8 | 51 | 3 | 13 | 13 | 8 | 0 | 0 | 26 | 1 | 5 | 0 | 1 | 1 | 1 | 5 | 81.0 | -0.4 | 13.423 | 120 | 132 | -21 | 2.3 | 1.9 | 2.1×10^{-09} | 10.5 |
| 20482 | 01-144 22:32:29 | 259 | 3 | 2 | 55 | 10 | 22 | 3 | 12 | 15 | 5 | 0 | 1 | 5 | 0 | 5 | 0 | 1 | 1 | 1 | 5 | 81.0 | -0.4 | 20.129 | 13 | 100 | 55 | 4.5 | 1.9 | 3.0×10^{-11} | 10.5 |
| 20487 | 01-145 07:11:10 | 22 | 2 | 2 | 187 | 8 | 30 | 3 | 13 | 12 | 7 | 0 | 0 | 25 | 8 | 5 | 0 | 1 | 1 | 1 | 5 | 81.0 | -0.4 | 24.328 | 187 | 72 | -51 | 2.3 | 1.9 | 8.0×10^{-10} | 10.5 |
| 20540 | 01-149 10:24:05 | 259 | 2 | 2 | 27 | 15 | 7 | 8 | 0 | 15 | 13 | 0 | 0 | 5 | 31 | 5 | 0 | 1 | 1 | 1 | 5 | 81.2 | -0.4 | 58.949 | 52 | 131 | 32 | 11.8 | 11.8 | 5.2×10^{-13} | 5858.3 |
| 20624 | 01-196 12:40:34 | 259 | 3 | 2 | 252 | 13 | 22 | 18 | 13 | 11 | 8 | 0 | 1 | 40 | 0 | 5 | 0 | 1 | 1 | 1 | 5 | 84.9 | -0.3 | 120.888 | 96 | 144 | -4 | 2.3 | 1.9 | 5.1×10^{-10} | 10.5 |
| 20671 | 01-205 12:23:30 | 259 | 2 | 2 | 229 | 8 | 4 | 3 | 13 | 14 | 11 | 0 | 0 | 4 | 31 | 5 | 0 | 1 | 1 | 1 | 5 | 85.8 | -0.3 | 94.336 | 128 | 141 | -29 | 2.3 | 1.9 | 1.8×10^{-11} | 10.5 |
| 20688 | 01-212 21:15:24 | 259 | 3 | 3 | 212 | 23 | 10 | 5 | 14 | 3 | 10 | 0 | 1 | 26 | 3 | 5 | 0 | 1 | 1 | 1 | 5 | 86.6 | -0.3 | 56.506 | 152 | 127 | -45 | 2.0 | 1.9 | 7.5×10^{-10} | 10.5 |
| 20691 | 01-217 04:47:40 | 259 | 3 | 4 | 218 | 27 | 30 | 27 | 8 | 12 | 6 | 0 | 1 | 59 | 0 | 5 | 0 | 1 | 1 | 1 | 5 | 87.2 | -0.3 | 17.719 | 143 | 133 | -40 | 5.6 | 1.6 | 6.1×10^{-10} | 6.0 |
| 20692 | 01-217 06:09:54 | 259 | 3 | 2 | 208 | 8 | 26 | 12 | 14 | 15 | 7 | 0 | 1 | 47 | 1 | 5 | 0 | 1 | 1 | 1 | 5 | 87.2 | -0.3 | 16.987 | 158 | 121 | -48 | 2.0 | 1.9 | 8.2×10^{-10} | 10.5 |
| 20693 | 01-217 08:45:16 | 22 | 2 | 2 | 14 | 9 | 13 | 0 | 15 | 1 | 10 | 0 | 0 | 39 | 0 | 5 | 0 | 1 | 1 | 1 | 5 | 87.2 | -0.3 | 15.577 | 70 | 146 | 16 | 11.8 | 9.5 | 5.4×10^{-13} | 2690.1 |
| 20694 | 01-217 13:21:19 | 22 | 3 | 4 | 228 | 27 | 30 | 24 | 8 | 11 | 5 | 0 | 1 | 47 | 0 | 5 | 0 | 1 | 1 | 1 | 5 | 87.2 | -0.3 | 12.994 | 129 | 141 | -30 | 8.6 | 1.6 | 1.6×10^{-10} | 6.0 |
| 20695 | 01-217 14:25:01 | 22 | 3 | 2 | 230 | 12 | 20 | 5 | 15 | 13 | 5 | 0 | 1 | 47 | 11 | 5 | 0 | 1 | 1 | 1 | 5 | 87.3 | -0.3 | 12.386 | 127 | 142 | -28 | 2.0 | 1.9 | 5.7×10^{-10} | 10.5 |
| 20696 | 01-217 15:28:43 | 22 | 2 | 2 | 40 | 8 | 31 | 4 | 13 | 14 | 8 | 0 | 0 | 26 | 1 | 5 | 0 | 1 | 1 | 1 | 5 | 87.3 | -0.3 | 11.775 | 34 | 131 | 43 | 2.3 | 1.9 | 9.2×10^{-10} | 10.5 |
| 20697 | 01-217 17:57:20 | 22 | 2 | 3 | 130 | 22 | 25 | 14 | 15 | 15 | 0 | 1 | 1 | 17 | 29 | 5 | 0 | 1 | 1 | 1 | 5 | 87.3 | -0.3 | 10.349 | 267 | 38 | -1 | 2.5 | 1.6 | 1.8×10^{-09} | 6.0 |
| 20698 | 01-217 22:12:09 | 22 | 3 | 2 | 214 | 11 | 30 | 4 | 12 | 11 | 7 | 0 | 1 | 26 | 1 | 5 | 0 | 1 | 1 | 1 | 5 | 87.3 | -0.3 | 8.007 | 149 | 129 | -44 | 4.5 | 1.9 | 1.3×10^{-10} | 10.5 |
| 20701 | 01-217 22:54:37 | 22 | 3 | 2 | 63 | 11 | 22 | 4 | 12 | 15 | 6 | 0 | 1 | 7 | 0 | 5 | 0 | 1 | 1 | 1 | 5 | 87.3 | -0.3 | 7.652 | 1 | 95 | 55 | 4.5 | 1.9 | 3.5×10^{-11} | 10.5 |
| 20714 | 01-218 06:41:45 | 22 | 2 | 4 | 143 | 30 | 60 | 24 | 13 | 13 | 4 | 1 | 1 | 28 | 1 | 5 | 0 | 1 | 1 | 1 | 5 | 87.4 | -0.3 | 6.111 | 249 | 39 | -16 | 2.0 | 1.9 | 6.8×10^{-07} | 10.5 |
| 20715 | 01-218 07:02:59 | 22 | 2 | 2 | 225 | 8 | 21 | 3 | 13 | 11 | 6 | 0 | 0 | 10 | 1 | 5 | 0 | 1 | 1 | 1 | 5 | 87.4 | -0.3 | 6.187 | 134 | 139 | -34 | 2.3 | 1.9 | 1.9×10^{-10} | 10.5 |
| 20716 | 01-218 07:24:13 | 22 | 2 | 4 | 215 | 30 | 4 | 24 | 13 | 15 | 15 | 0 | 1 | 27 | 0 | 5 | 0 | 1 | 1 | 1 | 5 | 87.4 | -0.3 | 6.276 | 148 | 130 | -43 | 2.0 | 1.9 | 8.2×10^{-10} | 10.5 |
| 20717 | 01-218 07:45:27 | 22 | 2 | 2 | 221 | 15 | 21 | 4 | 0 | 11 | 14 | 0 | 0 | 10 | 1 | 5 | 0 | 1 | 1 | 1 | 5 | 87.4 | -0.3 | 6.377 | 139 | 136 | -38 | 7.7 | 2.0 | 1.0×10^{-11} | 12.5 |
| 20727 | 01-219 00:02:10 | 22 | 2 | 2 | 248 | 8 | 6 | 3 | 15 | 12 | 10 | 0 | 0 | 3 | 0 | 5 | 0 | 1 | 1 | 1 | 5 | 87.4 | -0.3 | 15.000 | 101 | 147 | -8 | 2.0 | 1.9 | 4.6×10^{-11} | 10.5 |
| 20752 | 01-228 03:57:12 | 259 | 2 | 2 | 24 | 8 | 14 | 10 | 14 | 14 | 12 | 0 | 0 | 39 | 0 | 5 | 0 | 1 | 1 | 1 | 5 | 87.9 | -0.3 | 82.021 | 56 | 146 | 27 | 2.5 | 1.6 | 6.3×10^{-11} | 6.0 |
| 20764 | 01-244 21:09:41 | 259 | 3 | 3 | 54 | 22 | 28 | 10 | 15 | 7 | 5 | 0 | 1 | 46 | 1 | 5 | 0 | 1 | 1 | 1 | 5 | 89.1 | -0.2 | 126.938 | 14 | 116 | 52 | 7.9 | 4.6 | 7.0×10^{-11} | 211.2 |
| 20807 | 01-288 14:31:31 | 22 | 2 | 4 | 176 | 29 | 28 | 24 | 13 | 11 | 0 | 1 | 1 | 1 | 14 | 5 | 0 | 1 | 1 | 1 | 5 | 93.3 | -0.1 | 9.456 | 203 | 75 | -48 | 2.0 | 1.9 | 2.4×10^{-08} | 10.5 |
| 20808 | 01-288 15:56:27 | 22 | 2 | 3 | 28 | 23 | 24 | 23 | 15 | 12 | 0 | 1 | 1 | 43 | 10 | 5 | 0 | 1 | 1 | 1 | 5 | 93.3 | -0.1 | 8.655 | 51 | 151 | 31 | 2.0 | 1.9 | 4.9×10^{-09} | 10.5 |
| 20809 | 01-288 15:56:27 | 22 | 2 | 4 | 47 | 30 | 29 | 24 | 13 | 10 | 0 | 1 | 1 | 11 | 10 | 5 | 0 | 1 | 1 | 1 | 5 | 93.3 | -0.1 | 8.655 | 24 | 133 | 48 | 2.0 | 1.9 | 3.3×10^{-08} | 10.5 |
| 20821 | 01-289 15:39:06 | 22 | 3 | 2 | 167 | 9 | 49 | 7 | 14 | 13 | 9 | 0 | 1 | 26 | 1 | 5 | 0 | 1 | 1 | 1 | 5 | 93.5 | -0.2 | 13.175 | 215 | 64 | -41 | 2.0 | 1.9 | 2.9×10^{-09} | 10.5 |
| 20823 | 01-289 18:07:43 | 22 | 2 | 2 | 71 | 8 | 12 | 10 | 15 | 15 | 12 | 0 | 0 | 15 | 28 | 5 | 0 | 1 | 1 | 1 | 5 | 93.5 | -0.2 | 14.603 | 350 | 90 | 54 | 2.1 | 1.6 | 9.0×10^{-11} | 6.0 |
| 20824 | 01-290 05:05:57 | 22 | 2 | 3 | 32 | 21 | 22 | 7 | 14 | 11 | 0 | 1 | 1 | 46 | 30 | 5 | 0 | 1 | 1 | 1 | 5 | 93.5 | -0.2 | 20.551 | 45 | 149 | 35 | 2.0 | 1.9 | 2.4×10^{-09} | 10.5 |
| 20825 | 01-290 05:27:11 | 22 | 3 | 2 | 146 | 8 | 50 | 10 | 14 | 14 | 9 | 0 | 1 | 26 | 1 | 5 | 0 | 1 | 1 | 1 | 5 | 93.5 | -0.2 | 20.733 | 245 | 51 | -20 | 2.0 | 1.9 | 3.4×10^{-09} | 10.5 |

Table 7 (continued)

| No. | IMP. DATE | TEV | CLN | AR | SEC | IA | EA | CA | IT | ET | EIT | EIC | ICC | PA | PET | EVD | ICP | ECP | CCP | PCP | HV | LON | LAT | D _{Jup} | ROT | S _{LON} | S _{LAT} | V | VEF | M | MEF |
|-------|-----------------|-----|-----|----|-----|----|----|----|----|----|-----|-----|-----|----|-----|-----|-----|-----|-----|-----|----|-------|------|------------------|-----|------------------|------------------|------|-----|-----------------------|-------|
| 20826 | 01-290 05:48:25 | 22 | 2 | 2 | 183 | 8 | 12 | 2 | 13 | 14 | 9 | 0 | 0 | 11 | 4 | 5 | 0 | 1 | 1 | 1 | 5 | 93.5 | -0.2 | 20.914 | 193 | 86 | -52 | 2.7 | 1.6 | 3.4×10^{-11} | 6.0 |
| 20863 | 01-316 01:32:08 | 259 | 2 | 2 | 21 | 8 | 6 | 6 | 13 | 15 | 11 | 0 | 0 | 4 | 31 | 5 | 0 | 1 | 1 | 1 | 5 | 95.1 | -0.1 | 141.637 | 60 | 155 | 24 | 2.3 | 1.9 | 2.5×10^{-11} | 10.5 |
| 20867 | 01-332 14:25:42 | 259 | 2 | 2 | 238 | 14 | 22 | 14 | 14 | 9 | 0 | 1 | 1 | 59 | 27 | 5 | 0 | 1 | 1 | 1 | 6 | 96.4 | -0.1 | 160.228 | 115 | 156 | -20 | 2.0 | 1.9 | 1.1×10^{-09} | 10.5 |
| 20877 | 02-002 19:59:10 | 259 | 2 | 4 | 107 | 24 | 22 | 14 | 15 | 6 | 0 | 1 | 1 | 19 | 19 | 5 | 0 | 1 | 1 | 1 | 6 | 99.5 | 0.0 | 107.169 | 300 | 48 | 24 | 2.0 | 1.9 | 4.1×10^{-09} | 10.5 |
| 20890 | 02-015 08:17:10 | 8 | 2 | 4 | 20 | 30 | 53 | 26 | 14 | 13 | 0 | 1 | 1 | 11 | 4 | 5 | 0 | 1 | 1 | 1 | 6 | 100.9 | 0.0 | 33.272 | 62 | 149 | 23 | 2.0 | 1.9 | 1.2×10^{-07} | 10.5 |
| 20891 | 02-015 13:28:34 | 8 | 3 | 3 | 45 | 22 | 25 | 12 | 11 | 11 | 9 | 0 | 1 | 42 | 0 | 5 | 0 | 1 | 1 | 1 | 6 | 100.9 | 0.0 | 31.075 | 27 | 130 | 47 | 4.2 | 1.6 | 3.2×10^{-10} | 6.0 |
| 20892 | 02-016 22:44:31 | 8 | 2 | 2 | 234 | 11 | 4 | 12 | 14 | 13 | 0 | 1 | 1 | 45 | 28 | 5 | 0 | 1 | 1 | 1 | 6 | 101.2 | 0.0 | 14.523 | 121 | 148 | -24 | 2.0 | 1.9 | 5.3×10^{-11} | 10.5 |
| 20893 | 02-017 02:38:04 | 8 | 3 | 4 | 0 | 24 | 29 | 21 | 15 | 9 | 5 | 0 | 1 | 46 | 1 | 5 | 0 | 1 | 1 | 1 | 6 | 101.2 | 0.0 | 12.217 | 999 | 999 | 999 | 6.4 | 3.1 | 2.2×10^{-10} | 58.7 |
| 20897 | 02-017 07:56:35 | 8 | 3 | 4 | 236 | 29 | 19 | 11 | 11 | 11 | 5 | 0 | 1 | 46 | 0 | 5 | 0 | 1 | 1 | 1 | 6 | 101.2 | 0.0 | 9.006 | 118 | 149 | -22 | 2.3 | 1.9 | 1.5×10^{-08} | 10.5 |
| 20899 | 02-017 08:39:03 | 8 | 3 | 4 | 227 | 24 | 27 | 25 | 15 | 11 | 9 | 0 | 1 | 9 | 0 | 5 | 0 | 1 | 1 | 1 | 6 | 101.2 | 0.0 | 8.586 | 131 | 144 | -31 | 3.9 | 1.6 | 7.6×10^{-10} | 6.0 |
| 20900 | 02-017 10:46:26 | 22 | 3 | 2 | 125 | 9 | 29 | 5 | 12 | 10 | 7 | 0 | 1 | 26 | 1 | 5 | 0 | 1 | 1 | 1 | 6 | 101.3 | 0.0 | 7.384 | 274 | 42 | 3 | 4.5 | 1.9 | 8.1×10^{-11} | 10.5 |
| 20902 | 02-017 18:03:14 | 259 | 2 | 4 | 78 | 26 | 4 | 9 | 6 | 15 | 15 | 0 | 1 | 25 | 0 | 5 | 0 | 1 | 1 | 1 | 6 | 101.3 | 0.0 | 5.741 | 340 | 71 | 50 | 19.0 | 1.9 | 3.3×10^{-13} | 10.5 |
| 20903 | 02-018 03:22:22 | 22 | 2 | 2 | 224 | 11 | 11 | 6 | 12 | 13 | 10 | 0 | 0 | 5 | 31 | 5 | 0 | 1 | 1 | 1 | 6 | 101.4 | 0.0 | 10.567 | 135 | 142 | -34 | 4.5 | 1.9 | 8.8×10^{-12} | 10.5 |
| 20904 | 02-018 03:43:36 | 22 | 3 | 2 | 178 | 8 | 49 | 4 | 13 | 14 | 8 | 0 | 1 | 26 | 1 | 5 | 0 | 1 | 1 | 1 | 6 | 101.4 | 0.0 | 10.787 | 200 | 72 | -49 | 2.3 | 1.9 | 1.3×10^{-09} | 10.5 |
| 20905 | 02-018 05:29:46 | 8 | 2 | 2 | 185 | 8 | 14 | 5 | 13 | 14 | 5 | 0 | 0 | 43 | 1 | 5 | 0 | 1 | 1 | 1 | 6 | 101.4 | 0.0 | 11.885 | 190 | 83 | -53 | 2.7 | 1.6 | 4.8×10^{-11} | 6.0 |
| 20907 | 02-019 03:40:25 | 8 | 2 | 3 | 40 | 17 | 15 | 13 | 12 | 0 | 13 | 0 | 1 | 26 | 1 | 5 | 0 | 1 | 1 | 1 | 6 | 101.4 | 0.0 | 24.398 | 34 | 136 | 43 | 2.0 | 1.9 | 6.6×10^{-10} | 10.5 |
| 20997 | 02-143 00:49:36 | 22 | 2 | 2 | 185 | 9 | 5 | 10 | 12 | 15 | 11 | 0 | 0 | 5 | 31 | 5 | 0 | 1 | 1 | 1 | 6 | 110.6 | 0.3 | 343.589 | 190 | 88 | -53 | 4.5 | 1.9 | 2.3×10^{-12} | 10.5 |
| 21041 | 02-270 02:38:21 | 22 | 2 | 2 | 15 | 12 | 8 | 12 | 13 | 15 | 0 | 1 | 1 | 14 | 31 | 5 | 0 | 1 | 1 | 1 | 6 | 121.4 | 0.5 | 216.955 | 69 | 182 | 17 | 2.3 | 1.9 | 6.7×10^{-11} | 10.5 |
| 21046 | 02-292 00:55:21 | 22 | 3 | 3 | 13 | 22 | 29 | 12 | 15 | 9 | 6 | 0 | 1 | 46 | 1 | 5 | 0 | 1 | 1 | 1 | 6 | 123.4 | 0.5 | 135.606 | 72 | 191 | 15 | 2.0 | 1.9 | 9.2×10^{-09} | 10.5 |
| 21075 | 02-308 16:48:59 | 22 | 3 | 3 | 13 | 23 | 27 | 25 | 15 | 9 | 8 | 0 | 1 | 35 | 31 | 5 | 0 | 1 | 1 | 1 | 6 | 125.1 | 0.6 | 14.372 | 72 | 191 | 15 | 6.4 | 3.1 | 1.4×10^{-10} | 58.7 |
| 21076 | 02-308 16:48:59 | 22 | 3 | 2 | 107 | 9 | 50 | 4 | 14 | 14 | 8 | 0 | 1 | 26 | 1 | 5 | 0 | 1 | 1 | 1 | 6 | 125.1 | 0.6 | 14.372 | 300 | 86 | 24 | 2.0 | 1.9 | 4.1×10^{-09} | 10.5 |
| 21078 | 02-308 20:00:06 | 22 | 3 | 2 | 244 | 9 | 14 | 12 | 13 | 14 | 7 | 0 | 1 | 4 | 12 | 5 | 0 | 1 | 1 | 1 | 6 | 125.1 | 0.6 | 12.002 | 107 | 191 | -13 | 2.7 | 1.6 | 5.7×10^{-11} | 6.0 |
| 21079 | 02-308 22:28:43 | 259 | 3 | 2 | 239 | 12 | 21 | 14 | 13 | 12 | 9 | 0 | 1 | 38 | 0 | 5 | 0 | 1 | 1 | 1 | 6 | 125.2 | 0.6 | 10.014 | 114 | 190 | -19 | 2.3 | 1.9 | 3.7×10^{-10} | 10.5 |
| 21080 | 02-308 22:51:23 | 259 | 2 | 3 | 98 | 23 | 15 | 26 | 15 | 15 | 0 | 1 | 1 | 40 | 31 | 5 | 0 | 1 | 1 | 1 | 6 | 125.2 | 0.6 | 9.698 | 312 | 91 | 33 | 2.0 | 1.9 | 1.6×10^{-09} | 10.5 |
| 21081 | 02-308 22:51:52 | 259 | 3 | 4 | 27 | 29 | 30 | 27 | 12 | 12 | 5 | 0 | 1 | 46 | 1 | 5 | 0 | 1 | 1 | 1 | 6 | 125.2 | 0.6 | 9.691 | 52 | 186 | 30 | 2.0 | 1.9 | 3.1×10^{-08} | 10.5 |
| 21082 | 02-308 22:52:53 | 259 | 3 | 4 | 240 | 29 | 30 | 25 | 12 | 12 | 9 | 0 | 1 | 46 | 1 | 5 | 0 | 1 | 1 | 1 | 6 | 125.2 | 0.6 | 9.676 | 113 | 190 | -17 | 2.0 | 1.9 | 3.1×10^{-08} | 10.5 |
| 21085 | 02-309 02:22:17 | 22 | 3 | 2 | 235 | 11 | 21 | 18 | 13 | 12 | 8 | 0 | 1 | 40 | 0 | 5 | 0 | 1 | 1 | 1 | 6 | 125.2 | 0.6 | 6.530 | 120 | 189 | -23 | 2.3 | 1.9 | 3.1×10^{-10} | 10.5 |
| 21087 | 02-309 02:44:49 | 2 | 2 | 3 | 52 | 22 | 27 | 8 | 13 | 15 | 15 | 0 | 1 | 23 | 3 | 5 | 0 | 1 | 1 | 1 | 6 | 125.2 | 0.6 | 6.164 | 17 | 160 | 51 | 2.5 | 1.6 | 2.5×10^{-09} | 6.0 |
| 21088 | 02-309 03:10:28 | 2 | 2 | 2 | 245 | 11 | 13 | 9 | 6 | 15 | 15 | 0 | 1 | 8 | 5 | 5 | 0 | 1 | 1 | 1 | 6 | 125.2 | 0.6 | 5.740 | 105 | 191 | -12 | 9.5 | 5.0 | 1.2×10^{-12} | 282.4 |
| 21089 | 02-309 03:21:48 | 2 | 3 | 3 | 234 | 21 | 25 | 22 | 15 | 15 | 7 | 0 | 1 | 44 | 0 | 5 | 0 | 1 | 1 | 1 | 6 | 125.2 | 0.6 | 5.550 | 121 | 188 | -24 | 2.5 | 1.6 | 1.5×10^{-09} | 6.0 |
| 21090 | 02-309 04:13:33 | 104 | 2 | 3 | 232 | 22 | 25 | 22 | 15 | 15 | 0 | 1 | 1 | 42 | 9 | 5 | 0 | 1 | 1 | 1 | 6 | 125.2 | 0.6 | 4.665 | 124 | 187 | -26 | 2.5 | 1.6 | 1.8×10^{-09} | 6.0 |
| 21091 | 02-309 04:30:41 | 2 | 1 | 2 | 66 | 9 | 9 | 22 | 15 | 4 | 0 | 1 | 0 | 44 | 27 | 5 | 0 | 1 | 1 | 1 | 6 | 125.2 | 0.6 | 4.366 | 357 | 133 | 55 | 2.0 | 1.9 | 9.0×10^{-11} | 10.5 |
| 21093 | 02-309 05:05:18 | 2 | 2 | 3 | 82 | 21 | 22 | 20 | 14 | 10 | 0 | 1 | 1 | 46 | 27 | 5 | 0 | 1 | 1 | 1 | 6 | 125.2 | 0.6 | 3.759 | 335 | 106 | 48 | 2.0 | 1.9 | 2.4×10^{-09} | 10.5 |
| 21095 | 02-309 05:19:00 | 2 | 2 | 3 | 25 | 22 | 23 | 3 | 11 | 13 | 12 | 0 | 0 | 46 | 4 | 5 | 0 | 1 | 1 | 1 | 6 | 125.2 | 0.6 | 3.519 | 55 | 187 | 28 | 2.3 | 1.9 | 1.9×10^{-09} | 10.5 |
| 21097 | 02-309 05:29:23 | 2 | 1 | 2 | 26 | 8 | 14 | 2 | 15 | 15 | 0 | 1 | 0 | 44 | 14 | 5 | 0 | 1 | 1 | 1 | 6 | 125.2 | 0.6 | 3.339 | 53 | 186 | 29 | 2.1 | 1.6 | 1.3×10^{-10} | 6.0 |
| 21098 | 02-309 05:34:43 | 2 | 3 | 4 | 24 | 24 | 3 | 12 | 15 | 15 | 10 | 0 | 1 | 6 | 3 | 5 | 0 | 1 | 1 | 1 | 6 | 125.2 | 0.6 | 3.247 | 56 | 187 | 27 | 2.0 | 1.9 | 2.8×10^{-10} | 10.5 |
| 21099 | 02-309 05:36:36 | 2 | 2 | 2 | 221 | 9 | 21 | 7 | 11 | 12 | 15 | 0 | 1 | 17 | 2 | 5 | 0 | 1 | 1 | 1 | 6 | 125.2 | 0.6 | 3.215 | 139 | 181 | -38 | 7.2 | 1.9 | 5.0×10^{-12} | 10.5 |
| 21100 | 02-309 05:37:35 | 2 | 2 | 4 | 234 | 28 | 30 | 25 | 12 | 11 | 0 | 1 | 1 | 22 | 11 | 5 | 0 | 1 | 1 | 1 | 6 | 125.2 | 0.6 | 3.198 | 121 | 188 | -24 | 3.9 | 1.6 | 2.1×10^{-09} | 6.0 |
| 21102 | 02-309 05:39:32 | 2 | 1 | 2 | 237 | 9 | 13 | 20 | 14 | 15 | 15 | 0 | 0 | 11 | 6 | 5 | 0 | 1 | 1 | 1 | 6 | 125.2 | 0.6 | 3.165 | 117 | 189 | -21 | 2.1 | 1.6 | 1.3×10^{-10} | 6.0 |
| 21104 | 02-309 05:39:32 | 2 | 2 | 3 | 217 | 22 | 10 | 3 | 15 | 15 | 15 | 0 | 1 | 17 | 5 | 5 | 0 | 1 | 1 | 1 | 6 | 125.2 | 0.6 | 3.165 | 145 | 177 | -41 | 2.0 | 1.9 | 6.3×10^{-10} | 10.5 |

| | | | | | | | | | | | | | | | | | | | | | | | | | | | | | | | |
|-------|-----------------|---|---|---|-----|----|----|----|----|----|----|---|---|----|----|---|---|---|---|---|---|-------|-----|-------|-----|-----|-----|-----|-----|-----------------------|------|
| 21107 | 02-309 05:42:19 | 2 | 1 | 2 | 212 | 8 | 6 | 18 | 13 | 6 | 15 | 0 | 0 | 7 | 6 | 5 | 0 | 1 | 1 | 1 | 6 | 125.2 | 0.6 | 3.117 | 152 | 172 | -45 | 2.3 | 1.9 | 2.5×10^{-11} | 10.5 |
| 21108 | 02-309 05:43:01 | 2 | 2 | 4 | 30 | 24 | 21 | 24 | 13 | 14 | 0 | 1 | 1 | 49 | 31 | 5 | 0 | 1 | 1 | 1 | 6 | 125.2 | 0.6 | 3.106 | 48 | 184 | 33 | 2.0 | 1.9 | 3.5×10^{-09} | 10.5 |
| 21109 | 02-309 05:43:01 | 2 | 2 | 3 | 190 | 21 | 13 | 5 | 15 | 13 | 0 | 1 | 1 | 42 | 31 | 5 | 0 | 1 | 1 | 1 | 6 | 125.2 | 0.6 | 3.106 | 183 | 133 | -54 | 2.0 | 1.9 | 8.2×10^{-10} | 10.5 |
| 21110 | 02-309 05:45:57 | 2 | 3 | 4 | 244 | 30 | 57 | 24 | 13 | 15 | 5 | 0 | 1 | 46 | 0 | 5 | 0 | 1 | 1 | 1 | 6 | 125.2 | 0.6 | 3.056 | 107 | 191 | -13 | 2.0 | 1.9 | 2.4×10^{-07} | 10.5 |
| 21112 | 02-309 05:49:51 | 2 | 2 | 3 | 26 | 19 | 9 | 4 | 15 | 14 | 0 | 1 | 1 | 46 | 27 | 5 | 0 | 1 | 1 | 1 | 6 | 125.2 | 0.6 | 2.991 | 53 | 186 | 29 | 2.0 | 1.9 | 3.4×10^{-10} | 10.5 |
| 21113 | 02-309 05:50:50 | 2 | 2 | 4 | 32 | 30 | 57 | 27 | 13 | 15 | 0 | 1 | 1 | 26 | 6 | 5 | 0 | 1 | 1 | 1 | 6 | 125.2 | 0.6 | 2.975 | 45 | 183 | 35 | 2.0 | 1.9 | 2.4×10^{-07} | 10.5 |
| 21114 | 02-309 05:51:49 | 2 | 2 | 3 | 45 | 23 | 25 | 18 | 15 | 15 | 0 | 1 | 1 | 46 | 9 | 5 | 0 | 1 | 1 | 1 | 6 | 125.2 | 0.6 | 2.958 | 27 | 170 | 47 | 2.5 | 1.6 | 2.2×10^{-09} | 6.0 |
| 21116 | 02-309 05:53:46 | 2 | 2 | 3 | 40 | 21 | 24 | 13 | 13 | 12 | 6 | 0 | 1 | 17 | 19 | 5 | 0 | 1 | 1 | 1 | 6 | 125.2 | 0.6 | 2.926 | 34 | 176 | 43 | 2.5 | 1.6 | 1.3×10^{-09} | 6.0 |
| 21117 | 02-309 05:53:46 | 2 | 1 | 2 | 22 | 8 | 18 | 18 | 15 | 1 | 0 | 1 | 0 | 41 | 8 | 5 | 0 | 1 | 1 | 1 | 6 | 125.2 | 0.6 | 2.926 | 59 | 188 | 25 | 2.0 | 1.9 | 2.3×10^{-10} | 10.5 |
| 21118 | 02-309 05:54:45 | 2 | 2 | 3 | 24 | 21 | 24 | 19 | 13 | 15 | 0 | 1 | 1 | 23 | 15 | 5 | 0 | 1 | 1 | 1 | 6 | 125.2 | 0.6 | 2.910 | 56 | 187 | 27 | 2.5 | 1.6 | 1.3×10^{-09} | 6.0 |
| 21119 | 02-309 05:56:43 | 2 | 2 | 3 | 71 | 23 | 21 | 11 | 14 | 15 | 15 | 0 | 1 | 23 | 2 | 5 | 0 | 1 | 1 | 1 | 6 | 125.2 | 0.6 | 2.878 | 350 | 124 | 54 | 2.0 | 1.9 | 3.0×10^{-09} | 10.5 |
| 21120 | 02-309 05:56:43 | 2 | 1 | 2 | 221 | 9 | 7 | 3 | 15 | 15 | 0 | 1 | 0 | 11 | 31 | 5 | 0 | 1 | 1 | 1 | 6 | 125.2 | 0.6 | 2.878 | 139 | 181 | -38 | 2.0 | 1.9 | 6.5×10^{-11} | 10.5 |
| 21121 | 02-309 05:57:40 | 2 | 3 | 4 | 224 | 26 | 9 | 26 | 9 | 1 | 10 | 0 | 1 | 17 | 1 | 5 | 0 | 1 | 1 | 1 | 6 | 125.2 | 0.6 | 2.862 | 135 | 183 | -35 | 7.2 | 1.9 | 1.2×10^{-11} | 10.5 |
| 21122 | 02-309 05:59:38 | 2 | 2 | 3 | 148 | 20 | 21 | 8 | 14 | 15 | 0 | 1 | 1 | 46 | 31 | 5 | 0 | 1 | 1 | 1 | 6 | 125.2 | 0.6 | 2.831 | 242 | 86 | -22 | 2.0 | 1.9 | 1.8×10^{-09} | 10.5 |
| 21123 | 02-309 05:59:38 | 2 | 2 | 2 | 36 | 12 | 7 | 3 | 15 | 3 | 13 | 0 | 0 | 19 | 3 | 5 | 0 | 1 | 1 | 1 | 6 | 125.2 | 0.6 | 2.831 | 39 | 179 | 39 | 2.0 | 1.9 | 1.1×10^{-10} | 10.5 |
| 21124 | 02-309 06:00:36 | 2 | 2 | 4 | 229 | 26 | 30 | 26 | 12 | 12 | 0 | 1 | 1 | 18 | 9 | 5 | 0 | 1 | 1 | 1 | 6 | 125.2 | 0.6 | 2.815 | 128 | 186 | -29 | 2.5 | 1.6 | 7.3×10^{-09} | 6.0 |
| 21127 | 02-309 06:03:06 | 2 | 2 | 2 | 196 | 9 | 15 | 6 | 11 | 0 | 15 | 0 | 1 | 18 | 4 | 5 | 0 | 1 | 1 | 1 | 6 | 125.2 | 0.6 | 2.775 | 174 | 145 | -54 | 7.2 | 1.9 | 2.6×10^{-12} | 10.5 |
| 21128 | 02-309 06:05:04 | 2 | 1 | 2 | 12 | 13 | 11 | 25 | 15 | 3 | 0 | 1 | 0 | 41 | 28 | 5 | 0 | 1 | 1 | 1 | 6 | 125.2 | 0.6 | 2.744 | 73 | 191 | 14 | 2.0 | 1.9 | 2.4×10^{-10} | 10.5 |
| 21130 | 02-309 06:08:01 | 2 | 2 | 4 | 42 | 24 | 28 | 28 | 12 | 14 | 0 | 1 | 1 | 20 | 10 | 5 | 0 | 1 | 1 | 1 | 6 | 125.2 | 0.6 | 2.698 | 31 | 174 | 44 | 2.5 | 1.6 | 4.1×10^{-09} | 6.0 |
| 21131 | 02-309 06:09:00 | 2 | 2 | 3 | 29 | 23 | 26 | 25 | 15 | 10 | 6 | 0 | 1 | 9 | 7 | 5 | 0 | 1 | 1 | 1 | 6 | 125.2 | 0.6 | 2.683 | 49 | 185 | 32 | 4.9 | 2.1 | 2.9×10^{-10} | 14.3 |
| 21133 | 02-309 06:09:58 | 2 | 2 | 4 | 30 | 27 | 27 | 25 | 11 | 11 | 0 | 1 | 1 | 21 | 12 | 5 | 0 | 1 | 1 | 1 | 6 | 125.2 | 0.6 | 2.668 | 48 | 184 | 33 | 2.3 | 1.9 | 8.1×10^{-09} | 10.5 |
| 21135 | 02-309 06:16:48 | 2 | 2 | 3 | 226 | 20 | 22 | 12 | 13 | 12 | 8 | 0 | 1 | 12 | 7 | 5 | 0 | 1 | 1 | 1 | 6 | 125.2 | 0.6 | 2.565 | 132 | 184 | -33 | 2.5 | 1.6 | 7.8×10^{-10} | 6.0 |
| 21137 | 02-309 06:16:48 | 2 | 2 | 2 | 38 | 8 | 12 | 13 | 15 | 14 | 0 | 1 | 1 | 44 | 20 | 5 | 0 | 1 | 1 | 1 | 6 | 125.2 | 0.6 | 2.565 | 37 | 178 | 41 | 2.5 | 1.6 | 4.5×10^{-11} | 6.0 |
| 21138 | 02-309 06:17:47 | 2 | 2 | 4 | 43 | 28 | 28 | 25 | 12 | 12 | 0 | 1 | 1 | 62 | 15 | 5 | 0 | 1 | 1 | 1 | 6 | 125.2 | 0.6 | 2.551 | 30 | 172 | 45 | 2.0 | 1.9 | 2.0×10^{-08} | 10.5 |
| 21139 | 02-309 06:17:47 | 2 | 2 | 3 | 226 | 20 | 21 | 19 | 14 | 13 | 0 | 1 | 1 | 25 | 20 | 5 | 0 | 1 | 1 | 1 | 6 | 125.2 | 0.6 | 2.551 | 132 | 184 | -33 | 2.0 | 1.9 | 1.8×10^{-09} | 10.5 |
| 21140 | 02-309 06:17:47 | 2 | 2 | 2 | 213 | 12 | 11 | 14 | 15 | 12 | 0 | 1 | 1 | 46 | 22 | 5 | 0 | 1 | 1 | 1 | 6 | 125.2 | 0.6 | 2.551 | 150 | 173 | -45 | 2.0 | 1.9 | 2.0×10^{-10} | 10.5 |
| 21141 | 02-309 06:18:44 | 2 | 2 | 3 | 31 | 22 | 8 | 10 | 13 | 3 | 9 | 0 | 1 | 5 | 5 | 5 | 0 | 1 | 1 | 1 | 6 | 125.2 | 0.6 | 2.537 | 46 | 183 | 34 | 2.0 | 1.9 | 4.5×10^{-10} | 10.5 |
| 21143 | 02-309 06:18:44 | 2 | 2 | 2 | 230 | 12 | 20 | 3 | 14 | 14 | 13 | 0 | 0 | 37 | 6 | 5 | 0 | 1 | 1 | 1 | 6 | 125.2 | 0.6 | 2.537 | 127 | 186 | -28 | 2.0 | 1.9 | 5.7×10^{-10} | 10.5 |
| 21144 | 02-309 06:19:43 | 2 | 2 | 2 | 198 | 13 | 21 | 3 | 15 | 14 | 14 | 0 | 0 | 4 | 15 | 5 | 0 | 1 | 1 | 1 | 6 | 125.2 | 0.6 | 2.523 | 172 | 149 | -53 | 2.0 | 1.9 | 8.1×10^{-10} | 10.5 |
| 21145 | 02-309 06:20:42 | 2 | 1 | 2 | 32 | 9 | 11 | 4 | 13 | 12 | 15 | 0 | 0 | 20 | 3 | 5 | 0 | 1 | 1 | 1 | 6 | 125.2 | 0.6 | 2.508 | 45 | 183 | 35 | 5.2 | 1.9 | 4.1×10^{-12} | 10.3 |
| 21146 | 02-309 06:20:42 | 2 | 2 | 4 | 44 | 30 | 56 | 26 | 13 | 15 | 0 | 1 | 1 | 26 | 6 | 5 | 0 | 1 | 1 | 1 | 6 | 125.2 | 0.6 | 2.508 | 28 | 171 | 46 | 2.0 | 1.9 | 2.0×10^{-07} | 10.5 |
| 21147 | 02-309 06:20:42 | 2 | 3 | 3 | 173 | 21 | 5 | 7 | 14 | 1 | 10 | 0 | 1 | 13 | 5 | 5 | 0 | 1 | 1 | 1 | 6 | 125.2 | 0.6 | 2.508 | 207 | 105 | -46 | 2.0 | 1.9 | 2.2×10^{-10} | 10.5 |
| 21148 | 02-309 06:21:40 | 2 | 2 | 4 | 51 | 26 | 27 | 15 | 14 | 15 | 3 | 1 | 1 | 52 | 5 | 5 | 0 | 1 | 1 | 1 | 6 | 125.2 | 0.6 | 2.495 | 18 | 161 | 51 | 2.0 | 1.9 | 1.3×10^{-08} | 10.5 |
| 21149 | 02-309 06:22:20 | 2 | 3 | 2 | 207 | 9 | 20 | 20 | 14 | 15 | 14 | 0 | 1 | 8 | 4 | 5 | 0 | 1 | 1 | 1 | 6 | 125.2 | 0.6 | 2.485 | 159 | 165 | -49 | 2.0 | 1.9 | 3.5×10^{-10} | 10.5 |
| 21150 | 02-309 06:22:20 | 2 | 2 | 3 | 163 | 23 | 14 | 7 | 15 | 15 | 0 | 1 | 1 | 46 | 31 | 5 | 0 | 1 | 1 | 1 | 6 | 125.2 | 0.6 | 2.485 | 221 | 94 | -38 | 2.0 | 1.9 | 1.4×10^{-09} | 10.5 |
| 21151 | 02-309 06:23:19 | 2 | 2 | 2 | 30 | 9 | 13 | 5 | 15 | 15 | 10 | 0 | 1 | 6 | 5 | 5 | 0 | 1 | 1 | 1 | 6 | 125.2 | 0.6 | 2.471 | 48 | 184 | 33 | 2.1 | 1.6 | 1.3×10^{-10} | 6.0 |
| 21152 | 02-309 06:24:20 | 2 | 2 | 3 | 67 | 23 | 6 | 28 | 14 | 3 | 15 | 0 | 1 | 17 | 5 | 5 | 0 | 1 | 1 | 1 | 6 | 125.2 | 0.6 | 2.457 | 356 | 132 | 55 | 2.0 | 1.9 | 3.9×10^{-10} | 10.5 |
| 21153 | 02-309 06:25:19 | 2 | 2 | 4 | 245 | 26 | 14 | 5 | 15 | 10 | 14 | 0 | 1 | 27 | 1 | 5 | 0 | 1 | 1 | 1 | 6 | 125.2 | 0.6 | 2.444 | 105 | 191 | -12 | 2.0 | 1.9 | 2.3×10^{-09} | 10.5 |
| 21154 | 02-309 06:25:19 | 2 | 1 | 2 | 209 | 8 | 9 | 12 | 15 | 15 | 0 | 1 | 0 | 43 | 31 | 5 | 0 | 1 | 1 | 1 | 6 | 125.2 | 0.6 | 2.444 | 156 | 168 | -48 | 2.0 | 1.9 | 7.5×10^{-11} | 10.5 |
| 21155 | 02-309 06:26:25 | 2 | 2 | 2 | 185 | 13 | 0 | 13 | 15 | 15 | 0 | 1 | 1 | 0 | 31 | 5 | 0 | 1 | 1 | 1 | 6 | 125.2 | 0.6 | 2.429 | 190 | 124 | -53 | 2.0 | 1.9 | 7.4×10^{-10} | 10.5 |
| 21156 | 02-309 06:27:46 | 2 | 2 | 4 | 206 | 27 | 28 | 21 | 14 | 14 | 0 | 1 | 1 | 62 | 18 | 5 | 0 | 1 | 1 | 1 | 6 | 125.2 | 0.6 | 2.410 | 160 | 163 | -50 | 2.0 | 1.9 | 1.8×10^{-08} | 10.5 |
| 21157 | 02-309 06:28:25 | 2 | 2 | 2 | 181 | 12 | 7 | 15 | 15 | 0 | 0 | 1 | 1 | 43 | 28 | 5 | 0 | 1 | 1 | 1 | 6 | 125.2 | 0.6 | 2.402 | 195 | 117 | -51 | 2.0 | 1.9 | 1.1×10^{-10} | 10.5 |
| 21158 | 02-309 06:28:40 | 2 | 2 | 4 | 242 | 25 | 26 | 19 | 11 | 12 | 0 | 1 | 1 | 58 | 10 | 5 | 0 | 1 | 1 | 1 | 6 | 125.2 | 0.6 | 2.398 | 110 | 191 | -15 | 2.3 | 1.9 | 5.1×10^{-09} | 10.5 |
| 21159 | 02-309 06:29:27 | 2 | 1 | 2 | 237 | 8 | 10 | 18 | 15 | 14 | 0 | 1 | 0 | 43 | 31 | 5 | 0 | 1 | 1 | 1 | 6 | 125.2 | 0.6 | 2.388 | 117 | 189 | -21 | 2.5 | 1.6 | 3.3×10^{-11} | 6.0 |
| 21160 | 02-309 06:29:27 | 2 | 2 | 3 | 0 | 21 | 11 | 11 | 14 | 15 | 0 | 1 | 1 | 18 | 29 | 5 | 0 | 1 | 1 | 1 | 6 | 125.2 | 0.6 | 2.388 | 999 | 999 | 999 | 2.0 | 1.9 | 5.9×10^{-10} | 10.5 |

Table 7 (continued)

| No. | IMP. DATE | TEV | CLN | AR | SEC | IA | EA | CA | IT | ET | EIT | EIC | ICC | PA | PET | EVD | ICP | ECP | CCP | PCP | HV | LON | LAT | D _{Jup} | ROT | S _{LON} | S _{LAT} | V | VEF | M | MEF |
|-------|-----------------|-------|-----|----|-----|----|----|----|----|----|-----|-----|-----|----|-----|-----|-----|-----|-----|-----|----|-------|-----|------------------|-----|------------------|------------------|-----|-----|-------------------------|-------|
| 21161 | 02-309 06:29:41 | 2 | 2 | 4 | 183 | 25 | 21 | 13 | 15 | 14 | 0 | 1 | 1 | 24 | 31 | 5 | 0 | 1 | 1 | 1 | 6 | 125.2 | 0.6 | 2.385 | 193 | 120 | -52 | 2.0 | 1.9 | 4.0 × 10 ⁻⁰⁹ | 10.5 |
| 21162 | 02-309 06:30:30 | 2 | 2 | 2 | 162 | 11 | 6 | 4 | 12 | 11 | 10 | 0 | 0 | 10 | 28 | 5 | 0 | 1 | 1 | 1 | 6 | 125.2 | 0.6 | 2.374 | 222 | 94 | -37 | 4.5 | 1.9 | 3.9 × 10 ⁻¹² | 10.5 |
| 21163 | 02-309 06:30:38 | 2 | 2 | 3 | 211 | 22 | 23 | 18 | 12 | 12 | 0 | 0 | 0 | 61 | 14 | 5 | 0 | 1 | 1 | 1 | 6 | 125.2 | 0.6 | 2.372 | 153 | 170 | -46 | 2.0 | 1.9 | 3.5 × 10 ⁻⁰⁹ | 10.5 |
| 21164 | 02-309 06:31:12 | 2 | 1 | 2 | 223 | 9 | 4 | 4 | 15 | 15 | 0 | 1 | 0 | 7 | 29 | 5 | 0 | 1 | 1 | 1 | 6 | 125.2 | 0.6 | 2.365 | 136 | 182 | -36 | 2.0 | 1.9 | 3.9 × 10 ⁻¹¹ | 10.5 |
| 21165 | 02-309 06:31:43 | 5 | 3 | 4 | 218 | 30 | 12 | 22 | 14 | 4 | 10 | 0 | 1 | 11 | 1 | 5 | 0 | 1 | 1 | 1 | 6 | 125.2 | 0.6 | 2.358 | 143 | 178 | -40 | 2.0 | 1.9 | 3.0 × 10 ⁻⁰⁹ | 10.5 |
| 21166 | 02-309 06:32:28 | 2 | 2 | 2 | 159 | 10 | 6 | 3 | 15 | 15 | 0 | 1 | 1 | 5 | 31 | 5 | 0 | 1 | 1 | 1 | 6 | 125.2 | 0.6 | 2.349 | 226 | 91 | -34 | 2.0 | 1.9 | 6.4 × 10 ⁻¹¹ | 10.5 |
| 21167 | 02-309 06:32:41 | 2 | 2 | 3 | 246 | 22 | 23 | 10 | 12 | 12 | 0 | 1 | 1 | 27 | 15 | 5 | 0 | 1 | 1 | 1 | 6 | 125.2 | 0.6 | 2.346 | 104 | 192 | -11 | 2.0 | 1.9 | 3.5 × 10 ⁻⁰⁹ | 10.5 |
| 21169 | 02-309 06:33:45 | 2 | 3 | 4 | 212 | 30 | 49 | 27 | 14 | 15 | 12 | 0 | 1 | 25 | 1 | 5 | 0 | 1 | 1 | 1 | 6 | 125.2 | 0.6 | 2.333 | 152 | 172 | -45 | 2.0 | 1.9 | 6.1 × 10 ⁻⁰⁸ | 10.5 |
| 21171 | 02-309 06:34:38 | 2 | 2 | 3 | 48 | 21 | 20 | 14 | 14 | 13 | 0 | 1 | 1 | 18 | 18 | 5 | 0 | 1 | 1 | 1 | 6 | 125.2 | 0.6 | 2.322 | 23 | 166 | 49 | 2.0 | 1.9 | 1.7 × 10 ⁻⁰⁹ | 10.5 |
| 21172 | 02-309 06:34:46 | 2 | 2 | 4 | 21 | 30 | 14 | 20 | 14 | 13 | 15 | 0 | 1 | 28 | 4 | 5 | 0 | 1 | 1 | 1 | 6 | 125.2 | 0.6 | 2.320 | 60 | 189 | 24 | 2.0 | 1.9 | 4.2 × 10 ⁻⁰⁹ | 10.5 |
| 21174 | 02-309 07:30:05 | 259 | 2 | 2 | 217 | 11 | 29 | 11 | 11 | 10 | 15 | 0 | 1 | 26 | 1 | 5 | 0 | 1 | 1 | 1 | 6 | 125.2 | 0.6 | 1.992 | 145 | 177 | -41 | 7.2 | 1.9 | 2.5 × 10 ⁻¹¹ | 10.5 |
| 21175 | 02-309 07:30:23 | 259 | 2 | 3 | 31 | 20 | 15 | 19 | 14 | 0 | 14 | 0 | 1 | 25 | 3 | 5 | 0 | 1 | 1 | 1 | 6 | 125.2 | 0.6 | 1.992 | 46 | 183 | 34 | 2.0 | 1.9 | 9.5 × 10 ⁻¹⁰ | 10.5 |
| 21176 | 02-309 07:30:23 | 259 | 3 | 2 | 43 | 11 | 20 | 8 | 15 | 15 | 14 | 0 | 1 | 27 | 5 | 5 | 0 | 1 | 1 | 1 | 6 | 125.2 | 0.6 | 1.992 | 30 | 172 | 45 | 2.0 | 1.9 | 4.8 × 10 ⁻¹⁰ | 10.5 |
| 21178 | 02-309 07:30:23 | 259 | 3 | 4 | 57 | 27 | 12 | 24 | 14 | 6 | 13 | 0 | 1 | 27 | 5 | 5 | 0 | 1 | 1 | 1 | 6 | 125.2 | 0.6 | 1.992 | 10 | 151 | 54 | 2.0 | 1.9 | 1.9 × 10 ⁻⁰⁹ | 10.5 |
| 21179 | 02-309 07:30:31 | 259 | 2 | 3 | 168 | 20 | 15 | 13 | 14 | 15 | 0 | 1 | 1 | 10 | 29 | 5 | 0 | 1 | 1 | 1 | 6 | 125.2 | 0.6 | 1.993 | 214 | 99 | -42 | 2.0 | 1.9 | 9.5 × 10 ⁻¹⁰ | 10.5 |
| 21180 | 02-309 07:30:40 | 259 | 3 | 4 | 212 | 24 | 25 | 11 | 11 | 14 | 12 | 0 | 1 | 60 | 3 | 5 | 0 | 1 | 1 | 1 | 6 | 125.2 | 0.6 | 1.993 | 152 | 172 | -45 | 2.3 | 1.9 | 3.7 × 10 ⁻⁰⁹ | 10.5 |
| 21181 | 02-309 07:30:40 | 259 | 2 | 3 | 254 | 23 | 28 | 20 | 15 | 8 | 7 | 0 | 1 | 46 | 0 | 5 | 0 | 1 | 1 | 1 | 6 | 125.2 | 0.6 | 1.993 | 93 | 192 | -1 | 7.3 | 3.9 | 1.1 × 10 ⁻¹⁰ | 128.4 |
| 21183 | 02-310 00:44:19 | 259 | 3 | 2 | 90 | 8 | 50 | 14 | 14 | 14 | 8 | 0 | 1 | 25 | 1 | 5 | 0 | 1 | 1 | 1 | 6 | 125.3 | 0.6 | 16.303 | 323 | 97 | 41 | 2.0 | 1.9 | 3.4 × 10 ⁻⁰⁹ | 10.5 |
| 21202 | 02-329 06:20:41 | 259 | 3 | 4 | 235 | 24 | 28 | 26 | 15 | 12 | 11 | 0 | 1 | 44 | 0 | 5 | 0 | 1 | 1 | 1 | 6 | 126.7 | 0.6 | 148.699 | 120 | 189 | -23 | 2.5 | 1.6 | 4.1 × 10 ⁻⁰⁹ | 6.0 |
| 21207 | 03-030 00:00:00 | 95000 | 3 | 4 | 239 | 28 | 30 | 20 | 12 | 13 | 5 | 0 | 1 | 46 | 1 | 5 | 0 | 1 | 1 | 1 | 6 | 131.7 | 0.7 | 318.493 | 114 | 207 | -16 | 2.5 | 1.6 | 9.7 × 10 ⁻⁰⁹ | 6.0 |
| 21208 | 03-030 00:14:23 | 95000 | 3 | 4 | 6 | 25 | 30 | 24 | 15 | 12 | 5 | 0 | 1 | 35 | 31 | 5 | 0 | 1 | 1 | 1 | 6 | 131.7 | 0.7 | 318.508 | 82 | 210 | 9 | 2.5 | 1.6 | 6.2 × 10 ⁻⁰⁹ | 6.0 |
| 21210 | 03-066 18:14:23 | 1020 | 3 | 4 | 17 | 24 | 29 | 13 | 15 | 12 | 6 | 0 | 1 | 46 | 1 | 5 | 0 | 1 | 1 | 1 | 6 | 134.6 | 0.8 | 357.009 | 66 | 209 | 22 | 2.5 | 1.6 | 4.8 × 10 ⁻⁰⁹ | 6.0 |
| 21211 | 03-066 18:14:23 | 1020 | 2 | 2 | 41 | 11 | 23 | 7 | 13 | 15 | 7 | 0 | 0 | 43 | 1 | 5 | 0 | 1 | 1 | 1 | 6 | 134.6 | 0.8 | 357.009 | 32 | 195 | 47 | 2.3 | 1.9 | 4.4 × 10 ⁻¹⁰ | 10.5 |
| 21212 | 03-066 18:15:50 | 1020 | 3 | 2 | 234 | 13 | 24 | 10 | 13 | 15 | 6 | 0 | 1 | 44 | 1 | 5 | 0 | 1 | 1 | 1 | 6 | 134.6 | 0.8 | 357.010 | 121 | 205 | -22 | 2.3 | 1.9 | 7.3 × 10 ⁻¹⁰ | 10.5 |
| 21213 | 03-067 15:07:11 | 1560 | 3 | 2 | 13 | 10 | 21 | 18 | 13 | 13 | 11 | 0 | 1 | 37 | 0 | 5 | 0 | 1 | 1 | 1 | 6 | 134.6 | 0.8 | 357.592 | 72 | 210 | 17 | 2.3 | 1.9 | 2.7 × 10 ⁻¹⁰ | 10.5 |
| 21214 | 03-067 15:08:38 | 1560 | 3 | 2 | 240 | 15 | 23 | 23 | 14 | 12 | 11 | 0 | 1 | 41 | 1 | 5 | 0 | 1 | 1 | 1 | 6 | 134.6 | 0.8 | 357.593 | 113 | 207 | -15 | 2.0 | 1.9 | 1.5 × 10 ⁻⁰⁹ | 10.5 |
| 21215 | 03-069 15:00:00 | 260 | 2 | 3 | 32 | 22 | 22 | 22 | 11 | 8 | 0 | 1 | 1 | 46 | 23 | 5 | 0 | 1 | 1 | 1 | 6 | 134.8 | 0.8 | 358.875 | 45 | 202 | 38 | 2.3 | 1.9 | 1.6 × 10 ⁻⁰⁹ | 10.5 |
| 21216 | 03-069 15:00:00 | 260 | 3 | 2 | 4 | 15 | 26 | 14 | 13 | 15 | 6 | 0 | 1 | 3 | 31 | 5 | 0 | 1 | 1 | 1 | 6 | 134.8 | 0.8 | 358.875 | 84 | 210 | 7 | 2.3 | 1.9 | 1.4 × 10 ⁻⁰⁹ | 10.5 |
| 21218 | 03-264 02:12:38 | 259 | 3 | 2 | 16 | 10 | 21 | 18 | 14 | 13 | 9 | 0 | 1 | 42 | 0 | 5 | 0 | 1 | 1 | 1 | 6 | 150.4 | 1.0 | 17.003 | 68 | 209 | 21 | 2.0 | 1.9 | 4.9 × 10 ⁻¹⁰ | 10.5 |
| 21219 | 03-264 10:49:32 | 259 | 2 | 2 | 11 | 10 | 4 | 3 | 12 | 1 | 10 | 0 | 0 | 37 | 31 | 5 | 0 | 1 | 1 | 1 | 6 | 150.5 | 1.0 | 10.372 | 75 | 210 | 15 | 4.5 | 1.9 | 2.4 × 10 ⁻¹² | 10.5 |
| 21220 | 03-264 12:24:22 | 259 | 3 | 4 | 205 | 24 | 27 | 20 | 15 | 10 | 9 | 0 | 1 | 46 | 0 | 5 | 0 | 1 | 1 | 1 | 6 | 150.5 | 1.0 | 8.938 | 162 | 177 | -46 | 4.9 | 2.1 | 3.9 × 10 ⁻¹⁰ | 14.3 |
| 21222 | 03-264 14:54:04 | 8 | 2 | 3 | 188 | 20 | 23 | 6 | 15 | 15 | 15 | 0 | 1 | 20 | 4 | 5 | 0 | 1 | 1 | 1 | 6 | 150.5 | 1.0 | 6.424 | 186 | 148 | -50 | 2.5 | 1.6 | 9.3 × 10 ⁻¹⁰ | 6.0 |
| 21224 | 03-264 15:01:08 | 8 | 3 | 4 | 137 | 28 | 30 | 25 | 12 | 13 | 7 | 0 | 1 | 6 | 1 | 5 | 0 | 1 | 1 | 1 | 6 | 150.5 | 1.0 | 6.295 | 257 | 101 | -7 | 2.5 | 1.6 | 9.7 × 10 ⁻⁰⁹ | 6.0 |
| 21225 | 03-264 15:15:18 | 8 | 3 | 3 | 33 | 21 | 26 | 25 | 15 | 8 | 7 | 0 | 1 | 46 | 1 | 5 | 0 | 1 | 1 | 1 | 6 | 150.5 | 1.0 | 6.033 | 44 | 202 | 39 | 7.3 | 3.9 | 5.3 × 10 ⁻¹¹ | 128.4 |
| 21226 | 03-264 15:29:27 | 8 | 3 | 3 | 229 | 21 | 24 | 26 | 15 | 15 | 8 | 0 | 1 | 43 | 0 | 5 | 0 | 1 | 1 | 1 | 6 | 150.5 | 1.0 | 5.767 | 128 | 202 | -27 | 2.5 | 1.6 | 1.3 × 10 ⁻⁰⁹ | 6.0 |
| 21229 | 03-264 15:43:36 | 8 | 3 | 2 | 16 | 11 | 22 | 21 | 13 | 15 | 8 | 0 | 1 | 41 | 1 | 5 | 0 | 1 | 1 | 1 | 6 | 150.5 | 1.0 | 5.495 | 68 | 209 | 21 | 2.3 | 1.9 | 3.7 × 10 ⁻¹⁰ | 10.5 |
| 21230 | 03-264 16:40:13 | 8 | 1 | 2 | 254 | 10 | 10 | 3 | 13 | 15 | 15 | 0 | 0 | 13 | 6 | 5 | 0 | 1 | 1 | 1 | 6 | 150.5 | 1.0 | 4.346 | 93 | 210 | 0 | 2.3 | 1.9 | 6.7 × 10 ⁻¹¹ | 10.5 |
| 21231 | 03-264 17:01:27 | 8 | 2 | 2 | 31 | 8 | 13 | 11 | 15 | 13 | 15 | 0 | 1 | 13 | 5 | 5 | 0 | 1 | 1 | 1 | 6 | 150.5 | 1.0 | 3.884 | 46 | 203 | 37 | 3.9 | 1.6 | 1.1 × 10 ⁻¹¹ | 6.0 |
| 21232 | 03-264 17:15:36 | 8 | 2 | 4 | 135 | 29 | 15 | 25 | 13 | 0 | 7 | 0 | 1 | 17 | 1 | 5 | 0 | 1 | 1 | 1 | 6 | 150.5 | 1.0 | 3.565 | 260 | 101 | -5 | 2.0 | 1.9 | 4.0 × 10 ⁻⁰⁹ | 10.5 |
| 21233 | 03-264 17:15:36 | 8 | 3 | 3 | 191 | 22 | 28 | 6 | 15 | 8 | 13 | 0 | 1 | 26 | 1 | 5 | 0 | 1 | 1 | 1 | 6 | 150.5 | 1.0 | 3.565 | 181 | 153 | -51 | 7.3 | 3.9 | 9.1 × 10 ⁻¹¹ | 128.4 |

| | | | | | | | | | | | | | | | | | | | | | | | | | | | | | | | | | | |
|-------|-----------------|----|---|---|-----|----|----|----|----|----|----|---|---|----|----|---|---|---|---|---|---|---|---|---|---|---|-------|-----|-----|-----|-----|-----|-----------------------|------|
| 21234 | 03-264 17:22:41 | 8 | 3 | 2 | 210 | 13 | 14 | 6 | 15 | 9 | 14 | 0 | 1 | 24 | 2 | 5 | 0 | 1 | 1 | 1 | 1 | 1 | 1 | 1 | 1 | 1 | 3,401 | 155 | 185 | -44 | 2.0 | 1.9 | 3.9×10^{-10} | 10.5 |
| 21235 | 03-264 17:29:46 | 8 | 2 | 3 | 250 | 21 | 12 | 5 | 13 | 7 | 13 | 0 | 0 | 46 | 2 | 5 | 0 | 1 | 1 | 1 | 1 | 1 | 1 | 1 | 1 | 1 | 3,235 | 98 | 210 | -4 | 2.0 | 1.9 | 7.0×10^{-10} | 10.5 |
| 21236 | 03-264 17:29:46 | 8 | 3 | 2 | 224 | 14 | 14 | 4 | 13 | 14 | 8 | 0 | 1 | 24 | 2 | 5 | 0 | 1 | 1 | 1 | 1 | 1 | 1 | 1 | 1 | 1 | 3,235 | 135 | 199 | -32 | 2.3 | 1.9 | 2.5×10^{-10} | 10.5 |
| 21238 | 03-264 17:36:50 | 8 | 3 | 4 | 195 | 30 | 57 | 26 | 14 | 15 | 5 | 0 | 1 | 26 | 2 | 5 | 0 | 1 | 1 | 1 | 1 | 1 | 1 | 1 | 1 | 1 | 3,066 | 176 | 161 | -50 | 2.0 | 1.9 | 2.4×10^{-07} | 10.5 |
| 21239 | 03-264 17:36:50 | 8 | 3 | 3 | 237 | 21 | 25 | 12 | 13 | 15 | 12 | 0 | 1 | 26 | 1 | 5 | 0 | 1 | 1 | 1 | 1 | 1 | 1 | 1 | 1 | 1 | 3,066 | 117 | 206 | -19 | 2.5 | 1.6 | 1.5×10^{-09} | 6.0 |
| 21240 | 03-264 17:36:50 | 8 | 3 | 2 | 166 | 14 | 26 | 5 | 15 | 15 | 14 | 0 | 1 | 25 | 1 | 5 | 0 | 1 | 1 | 1 | 1 | 1 | 1 | 1 | 1 | 1 | 3,066 | 217 | 117 | -38 | 2.0 | 1.9 | 2.2×10^{-09} | 10.5 |
| 21241 | 03-264 17:43:55 | 8 | 3 | 4 | 241 | 24 | 12 | 12 | 14 | 6 | 6 | 0 | 1 | 49 | 1 | 5 | 0 | 1 | 1 | 1 | 1 | 1 | 1 | 1 | 1 | 1 | 2,894 | 111 | 208 | -14 | 2.0 | 1.9 | 1.2×10^{-09} | 10.5 |
| 21242 | 03-264 17:43:55 | 8 | 2 | 2 | 246 | 12 | 22 | 5 | 15 | 14 | 15 | 0 | 1 | 18 | 5 | 5 | 0 | 1 | 1 | 1 | 1 | 1 | 1 | 1 | 1 | 1 | 2,894 | 104 | 209 | -8 | 2.0 | 1.9 | 8.0×10^{-10} | 10.5 |
| 21243 | 03-264 17:50:59 | 8 | 3 | 4 | 186 | 30 | 56 | 25 | 14 | 14 | 7 | 0 | 1 | 26 | 1 | 5 | 0 | 1 | 1 | 1 | 1 | 1 | 1 | 1 | 1 | 1 | 2,720 | 188 | 144 | -50 | 2.0 | 1.9 | 2.0×10^{-07} | 10.5 |
| 21244 | 03-264 17:50:59 | 8 | 3 | 2 | 33 | 14 | 24 | 8 | 14 | 12 | 13 | 0 | 1 | 13 | 10 | 5 | 0 | 1 | 1 | 1 | 1 | 1 | 1 | 1 | 1 | 1 | 2,720 | 44 | 202 | 39 | 2.0 | 1.9 | 1.6×10^{-09} | 10.5 |
| 21246 | 03-264 17:59:01 | 22 | 3 | 2 | 239 | 9 | 22 | 5 | 14 | 12 | 13 | 0 | 1 | 37 | 8 | 5 | 0 | 1 | 1 | 1 | 1 | 1 | 1 | 1 | 1 | 1 | 2,518 | 114 | 207 | -16 | 2.0 | 1.9 | 4.9×10^{-10} | 10.5 |
| 21248 | 03-264 17:59:01 | 22 | 3 | 4 | 4 | 24 | 28 | 25 | 15 | 10 | 5 | 0 | 1 | 46 | 14 | 5 | 0 | 1 | 1 | 1 | 1 | 1 | 1 | 1 | 1 | 1 | 2,518 | 84 | 210 | 7 | 4.9 | 2.1 | 4.6×10^{-10} | 14.3 |
| 21249 | 03-264 17:59:01 | 22 | 3 | 3 | 44 | 21 | 22 | 5 | 13 | 14 | 8 | 0 | 1 | 49 | 6 | 5 | 0 | 1 | 1 | 1 | 1 | 1 | 1 | 1 | 1 | 1 | 2,518 | 28 | 191 | 49 | 2.0 | 1.9 | 2.4×10^{-09} | 10.5 |
| 21250 | 03-264 17:59:01 | 22 | 3 | 4 | 172 | 27 | 11 | 18 | 9 | 3 | 10 | 0 | 1 | 27 | 2 | 5 | 0 | 1 | 1 | 1 | 1 | 1 | 1 | 1 | 1 | 1 | 2,518 | 208 | 123 | -42 | 7.2 | 1.9 | 1.9×10^{-11} | 10.5 |

be larger in the jovian magnetosphere than in interplanetary space the charge measured on the entrance grid of the dust instrument did not give any convincing results yet. Reliable charge measurements for interplanetary dust grains and for dust in Saturn's E ring were recently reported for the Cassini dust detector (Kempf et al., 2004, 2006). These measurements may lead to an improved understanding of the charge measurements of Ulysses and Galileo in the future.

Entries for the parameter PA in Table 7 sometimes have values between 49 and 63 although the highest possible value allowed by the instrument electronics is 48 (Paper I). This is also inherent in all Galileo and Ulysses data sets published earlier (Papers II to IX) and it is due to a bit flip. According to our present understanding the correct PA values are obtained by subtracting 32 from all entries which have values between 49 and 63. Values of 48 and lower should remain unchanged.

4. Analysis

The positive charge measured on the ion collector, Q_i , is the most important impact parameter determined by the dust instrument because it is rather insensitive to noise. Fig. 5 shows the distribution of Q_i for the full 2000–2003 data set (small and big particles together). Ion impact charges were only detected over four orders of magnitude instead of the entire range of six orders of magnitude the instrument could measure. Note that the saturation limit of the instrument was at about $\sim 10^{-8}$ C but the maximum measured charge was $Q_i = 9.7 \times 10^{-11}$ C, well below the saturation limit. This is most likely due to instrument degradation (Section 2.5 and Krüger et al., 2005).

The impact charge distribution of the big particles ($Q_i > 10^{-13}$ C) follows a power law with index -0.15 and is shown as a dashed line in Fig. 5. This slope is flatter than the values of approximately $-1/3$ derived for the jovian system from the 1996–1999 Galileo data set (Papers VI and VIII). Whether this flattening is due to changes in the particle properties or due to electronics degradation remains unclear. Note that the jovian stream particles (AR1) were excluded from the power law fit.

In Fig. 5 the small stream particles ($Q_i < 10^{-13}$ C) are squeezed into the two leftmost histogram bins. In order to investigate their behaviour in more detail we show their number per individual digital step separately in Fig. 6. The distribution flattens for impact charges below 2×10^{-14} C. Such a flattening was also evident in the earlier data sets (Papers II, IV, VI and VIII), indicating the sensitivity threshold of the dust instrument may

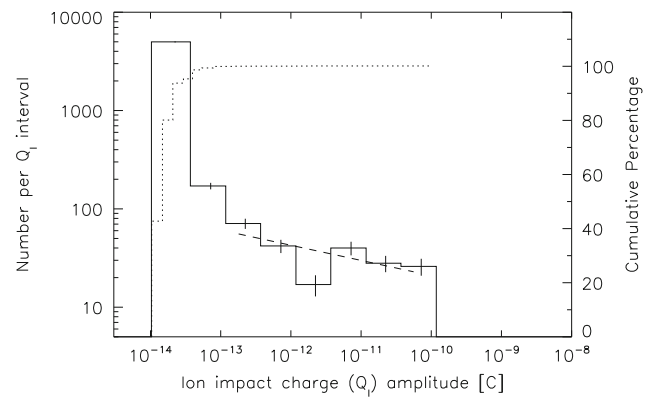


Fig. 5. Amplitude distribution of the impact charge Q_i for the 5389 dust particles detected in 2000–2003. The solid line indicates the number of impacts per charge interval, whereas the dotted line shows the cumulative distribution. Vertical bars indicate the \sqrt{n} statistical fluctuation. A power law fit to the data with $Q_i > 10^{-13}$ C (big particles, AR2–4) is shown as a dashed line (Number $N \sim Q_i^{-0.15}$).

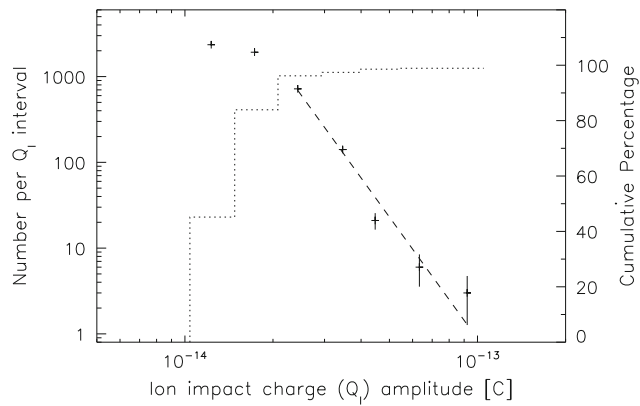


Fig. 6. Same as Fig. 5 but for the 5165 small particles in the lowest amplitude range (AR1) only. A power law fit to the data with $2 \times 10^{-14} \text{ C} < Q_i < 10^{-13} \text{ C}$ is shown as a dashed line (Number $N \sim Q_i^{-4.72}$).

not be sharp. The impact charge distribution for small particles with $Q_i > 2 \times 10^{-14} \text{ C}$ follows a power law with index -4.7 . It is very close to the slope found from the 1996 Galileo data set (-4.5 , Paper VI) and somewhat steeper than the value measured in 1997–1999 (-3.6 , Paper VIII). The charge distribution strongly increases towards smaller impact charges. Note that the distribution of the stream particles is much steeper than that of the big particles shown in Fig. 5. Interestingly, if we restrict the time interval to the period between 00-220 and 00-250 when Galileo was outside the jovian magnetosphere in orbit G28 the stream particles show a somewhat steeper slope of -5.9 (not shown here).

The ratio of the channeltron charge Q_C and the ion collector charge Q_i is a measure of the channeltron amplification A which is an important parameter for dust impact identification (Paper I). The in-flight channeltron amplification was monitored in Papers II, IV, VI and VIII for the initial ten years of the Galileo mission to identify possible degrading of the channeltron. In the earlier mission the amplification $A = Q_C/Q_i$ for a channeltron high voltage setting of 1020 V (HV=2) determined from impacts with $10^{-12} \text{ C} \leq Q_i \leq 10^{-10} \text{ C}$ was in the range $1.4 \leq A \leq 1.8$. No significant channeltron degradation was evident until the end of 1996. In the 1997–1999 interval (Paper VIII) a value of $A \approx 0.7$ was found which indicated serious channeltron degradation. As a consequence, the channeltron high voltage was raised two times (on days 99-305 and 99-345) to return to the original amplification factor.

Here we repeat the same analysis for the 2000–2003 interval. Fig. 7 shows the charge ratio Q_C/Q_i as a function of Q_i for a constant high voltage, HV, as in the previous papers. Here we show data for HV=6. The charge ratio Q_C/Q_i determined for $10^{-12} \text{ C} \leq Q_i \leq 10^{-10} \text{ C}$ is $A \approx 1.6$ and is obtained from 65 impacts. The data for HV=4 and 5 (time intervals 00-001 to 00-209 and 00-209 to 01-352) give $A \approx 1.3$ and 0.5, respectively. These values, however, are derived from only 9 and 15 impacts, respectively, and therefore have a much lower statistical significance. The amplification for HV=6 is close to the value from the interplanetary cruise and the early Jupiter mission, showing that the original channeltron amplification could be roughly reestablished. Details of the dust instrument degradation due to the harsh radiation environment in the jovian magnetosphere are described by Krüger et al. (2005, see also Section 2.5). It should be noted that the ratio Q_C/Q_i is entirely determined by the instrument performance. It does not depend upon the properties of the detected particles.

Fig. 8 displays the calibrated masses and speeds of all 5389 dust grains detected in the 2000–2003 interval. Although the

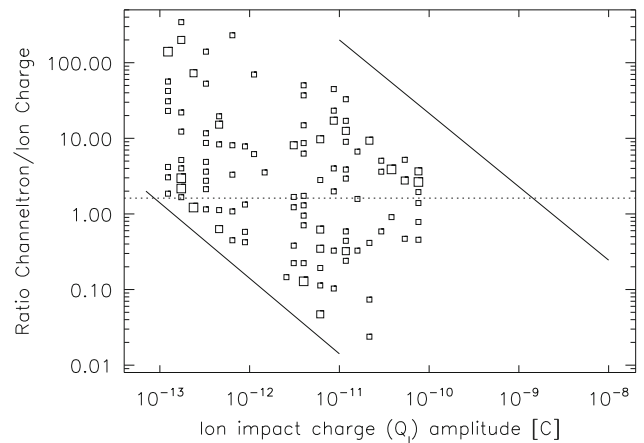


Fig. 7. Channeltron amplification factor $A = Q_C/Q_i$ as a function of impact charge Q_i for big particles (AR2-4) detected in 2000–2003. No impacts were measured in AR5 and AR6. Only impacts measured with a channeltron high voltage setting HV=6 are shown. The solid lines indicate the sensitivity threshold (lower left) and the saturation limit (upper right) of the channeltron. Squares indicate dust particle impacts, and the area of the squares is proportional to the number of events (the scaling of the squares is the same as in Papers VI and VIII). The dotted horizontal line shows the mean value of the channeltron amplification $A = 1.62$ calculated from 65 impacts in the ion impact charge range $10^{-12} \text{ C} < Q_i < 10^{-10} \text{ C}$.

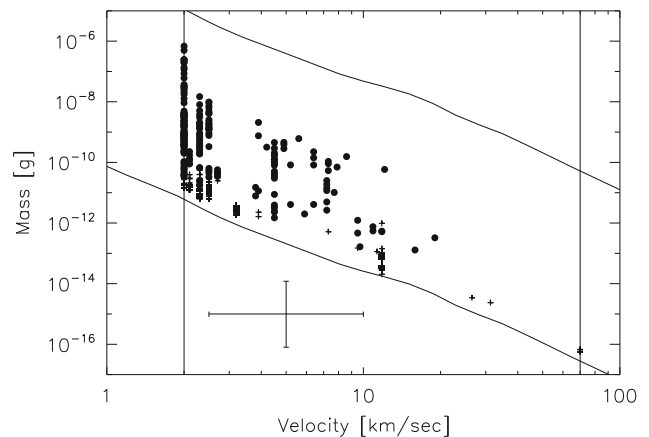


Fig. 8. Masses and impact speeds of all 5389 impacts recorded in 2000–2003. The lower and upper solid lines indicate the threshold and saturation limits of the detector, respectively, and the vertical lines indicate the calibrated velocity range. A sample error bar is shown that indicates a factor of two error for the velocity and a factor of 10 for the mass determination. Note that all particles are most likely much faster and smaller than implied by this diagram (see text for details). Plus signs show particles in AR1 while filled circles refer to particles in AR2-4. No impacts were measured in AR5 or AR6.

range of impact speeds calibrated in the laboratory extends from 2 to 70 km s^{-1} , the measured impact speeds range only up to about 20 km s^{-1} . This is caused by the degradation of the dust instrument electronics which lead to extended rise time measurements and, hence, impact speeds which are artificially too low, and calibrated grain masses artificially too large. This becomes apparent when comparing Fig. 8 with the corresponding figures in the earlier Papers II, IV, VI and VIII where the measured range of impact speeds extends up to 70 km s^{-1} . Therefore, due to the strong electronics degradation, all calibrated impact speeds and masses in the time interval considered in this paper should be considered as lower and upper limits, respectively. Any clustering of the speed values is due to discrete steps in the rise time measurement but this quantization is much smaller than the speed uncertainty. For further details of the mass and speed

calibration the reader is referred to the description of the mass-segment diagrams in our earlier papers.

The impact direction of the dust particles detected in the 2000–2003 interval is shown in Figs. 9 and 10. Before 2000 the detection geometry of the small dust stream (AR1) particles was such that the grains could only be detected during a very limited period of time around perijove passage (cf. Paper VIII, Table 4 therein, which lists the times of onset, 180° shift in impact direction and cessation of the dust streams observed by the Galileo dust detector). This changed in 2000 when the streams became detectable from rotation angles $90 \pm 70^\circ$ during almost the entire orbit of Galileo. This is best seen in orbits G28 to C30 in 2000 and 2001. Big particles (AR2–4) were, as in the earlier periods, mostly detected in the inner jovian system when Galileo was close to Jupiter with the exception of several impacts recorded in March 2003 at about $350 R_J$ from Jupiter (Section 5.4). Note that an error occurred in our earlier rotation angle plots in Paper VIII (Fig. 9 in that paper). The corrected figure is shown in the Appendix.

5. Discussion

The dust data set from Galileo's entire Jupiter mission is a unique set of dust measurements from the jovian system for

many years to come. Various jovian dust populations were investigated during the last 15 years which we have summarised in Section 1.1. The present paper finalises our series of Galileo dust data papers and we discuss some particular aspects of the 2000–2003 data set.

5.1. Variability of Io's dust emission

Imaging observations of Io with Voyager, Galileo, Cassini and New Horizons detected at least 17 volcanic centres with related plumes (Porco et al., 2003; McEwen et al., 2004; Spencer et al., 2007; Geissler and McMillan, 2008). Most of the plumes were sensed through the scattering of sunlight by dust particles entrained within the plumes, and ring-shaped surface deposits on Io suggest that other plumes have been recently active as well. The dust data from the entire Galileo Jupiter mission are a unique record of the dust ejected from Io. In particular, as the plumes are the most plausible sources of the grains (Graps et al., 2000), the dust measurements monitor plume activity (Krüger et al., 2003a).

The Galileo dust data show a large orbit-to-orbit variation due to both systematic and stochastic changes. Systematic effects include Io's orbital motion, changes in the geometry of Galileo's orbit and in the magnetic field configuration due to the rotation of Jupiter. Stochastic variations include fluctuations of Io's volcanic activity, changes of the particle charging in the Io torus, variations

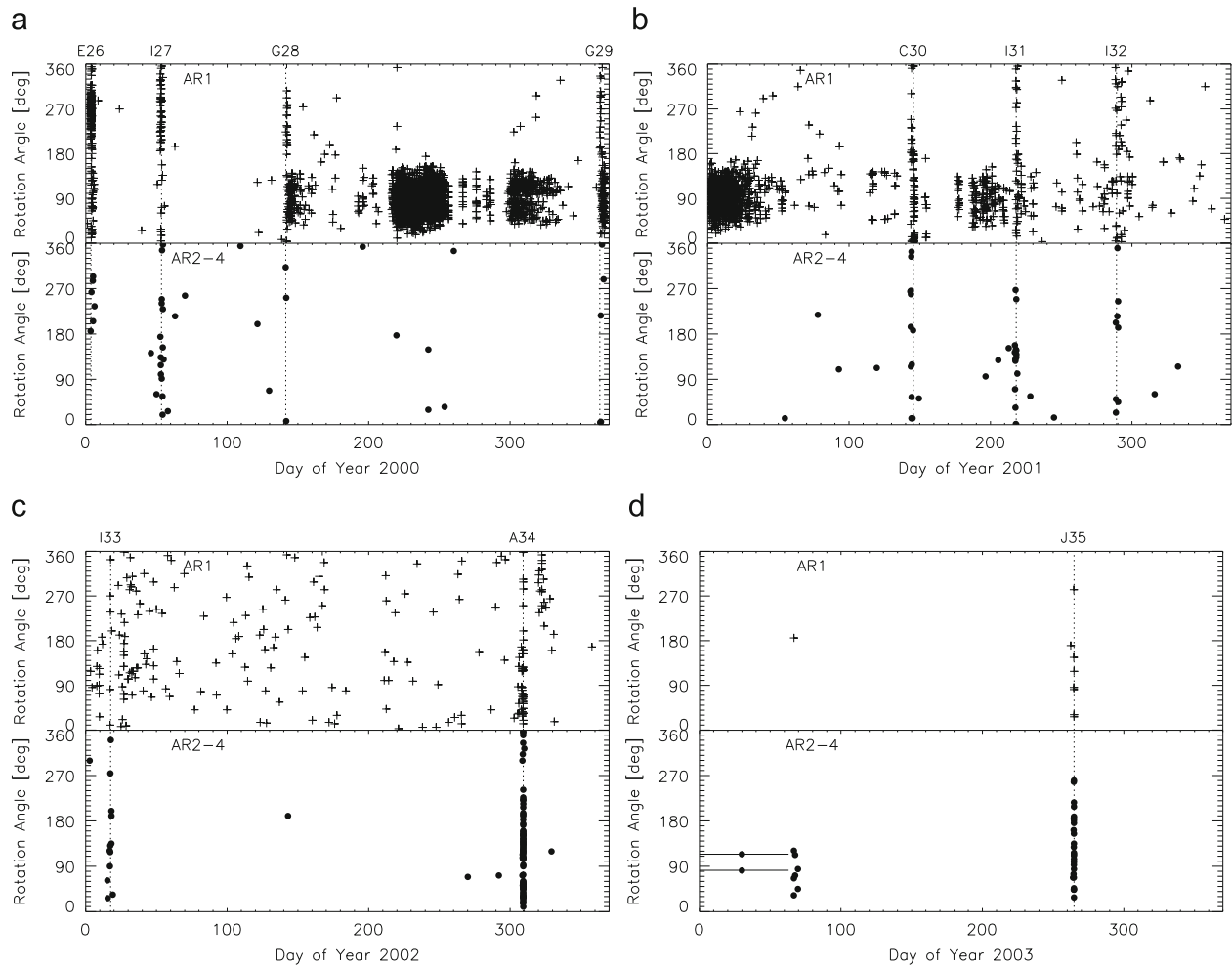


Fig. 9. Rotation angle vs. time for two different mass ranges. Upper panel: small particles, AR1; lower panel: big particles, AR2–4 (no impacts were detected in AR5 and AR6 in the time interval considered in this paper). See Section 2 for an explanation of the rotation angle. Vertical dotted lines indicate Galileo's satellite encounters (E26–A34) or the spacecraft impact into Jupiter (J35). The uncertainty in the determination of the impact time is usually much smaller than the symbol sizes, except for two impacts in 2003 (panel d) which have a very large uncertainty (indicated by two horizontal bars).

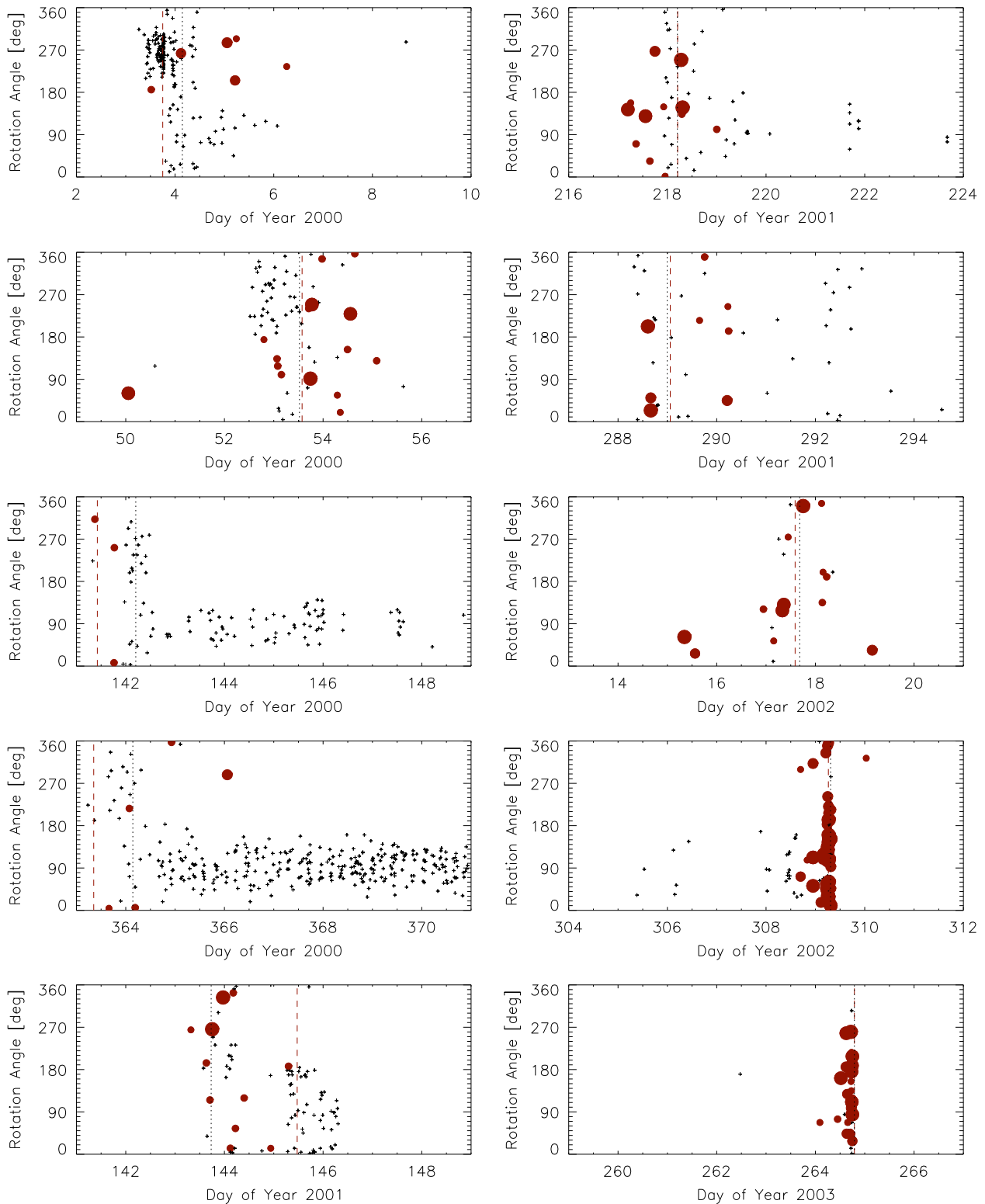


Fig. 10. Rotation angle detected by the dust instrument in the inner jovian system in higher time resolution. Only dust data for classes 2 and 3 are shown. Crosses denote impacts in AR1, filled circles those in AR2–4, with the circle size indicating the amplitude range. Dotted lines indicate perijove passages of Galileo, dashed lines satellite closest approaches (E26–A34) or Jupiter impact (J35).

in grain release from the torus, and the deformation of the outer magnetosphere in response to the variable solar wind conditions. It should be emphasized that the mechanisms acting on the grains in the Io torus and in particular the connected temporal variability are presently not well understood. By combining the entire Galileo dust data set, the variability due to stochastic processes

could be averaged out and a strong flux variation with jovian local time showed up (Krüger et al., 2003b), confirming earlier predictions (Horányi et al., 1997).

Dust emission rates of Io were derived by Krüger et al. (2003a). After removal of the systematic variations, the total dust emission rate of Io turned out to be between 10^{-3} and 10 kg s^{-1} , with

typical values in the range $0.1\text{--}1\text{ kg s}^{-1}$. Exceptionally high dust emission rates occurred during orbits E4 (1996), C21 (1999), G28, and, to a lesser extent, also during G29 and C30. Some of these peaks in the dust emission could be related to specific plume sightings or other markers of volcanic activity on Io: the Pele plume is one of the most powerful plumes and the most steady high-temperature volcanic centre on Io. Surface changes at the Pele site were detected frequently, whereas detections of the Pele plume are relatively rare. Two detections of the Pele plume are coincident with our measurements of high dust fluxes in E4 and G29, while a low dust flux in E6 may be explained by the absence of the Pele plume (McEwen et al., 1998; Porco et al., 2003). In August/September 2000 (orbit G28; Section 5.2) when Galileo was far away from Jupiter, a large dust flux was observed which is likely connected with surface changes observed at the site of the Tvashtar plume (Krüger et al., 2003a).

Here we investigate the orbit-to-orbit variability of the dust emission pattern on much shorter timescales of days to weeks. As in earlier works (Krüger et al., 2003a) we assume a particle radius $s=10\text{ nm}$, grain density $\rho=1.5\text{ g cm}^{-3}$, dust grain charging to $+5\text{ V}$ in the Io torus, and calculate the effective dust sensor area from the particle dynamics based on the model of Horányi et al. (1997). We divide the measured dust impact rate by the effective sensor area to obtain the dust flux $f\text{ (m}^{-2}\text{ s}^{-1}\text{)}$ as a function of distance d from Jupiter. If we assume that Io's dust emission, the dust charging, ejection conditions from the plasma torus and the grain speed remain constant over the time interval considered, we expect a "dilution" of the dust with d^{-2} . Dynamical modelling implies that—after the grains are released from the Io torus—the major acceleration occurs within approximately $10 R_J$ from Jupiter so that their speed remains basically unchanged further away from the planet. Finally, the variation of the dust flux with jovian local time is usually below a factor of five (Krüger et al., 2003b) and thus of minor significance compared to the orbit-to-orbit variability considered here. With all these assumptions, we expect a variation of the dust flux with d^{-2} . It should be emphasized that here we use exactly the same assumptions for calculating dust emission rates as Krüger et al. (2003a).

Contrary to our assumption made above that the dust stream particles are dispersed in space into three dimensions, based on the model of Horányi et al. (1993) one might consider that the dust gets dispersed in space into a two-dimensional warped dust sheet. In this case one expects a dilution with d^{-1} instead of d^{-2} . Such a configuration seems unlikely because dynamical modelling has shown that the grains also experience a significant acceleration away from Jupiter's equatorial plane and reach jovian latitudes up to 20° (Horányi et al., 1997) while some grains can be accelerated to even higher latitudes (Graps, 2001). This is supported by the dust streams measurements from Ulysses' second Jupiter flyby in 2004 when the dust streams were detected at high jovian latitudes up to 70° (Krüger et al., 2006c). Furthermore, the picture of the warped dust sheet assumes particles with a constant charge and a single size. Graps (2001) has shown, however, that the grain charge quickly responds to the ambient plasma conditions and that different sized particles have a different phase with respect to Jupiter's magnetic field, leading to a wide distribution of dust in space. Thus, particle emission in a three-dimensional configuration appears to reflect the real situation much better than a two-dimensional structure.

In Table 8 we list the slopes of power law fits $f \propto d^\alpha$ to the derived dust flux profiles. We only considered Galileo orbits where sufficiently long data sets for at least two days are available so that meaningful flux profiles could be obtained. Large variations in the flux profiles are obvious from Table 8. Given the overall uncertainties we believe that slopes in the range $-3 \lesssim \alpha \lesssim -1$ are still compatible with a rather constant dust

ejection rate from Io and the Io torus ($\alpha = -2$). Fig. 11 shows the dust flux during the G29 orbit as an example. Here the power law fit to the data gives a slope $\alpha \approx -2$. It implies that the dust release from the Io torus stayed remarkably constant for a rather long period of more than two months. For comparison we also show power law curves with slopes -1 and -3 . A flux profile following a power law with slope -1 would imply that within the approximately two-months period when Galileo moved from 20 to $200 R_J$ from Jupiter, the dust ejection had increased by a factor of ten. Similarly, with a slope of -3 the dust ejection would have dropped by the same factor in this time interval.

Large deviations from this simple and ideal case with constant dust ejection are also obvious in the table. For example, orbits E4, E19, I32 and A34 show very flat profiles in the range $-1 \lesssim \alpha \lesssim 0$, implying that during these orbits stronger dust emissions occurred when Galileo was far away from Jupiter than when the spacecraft was closer to the planet. On the other hand, during orbits G2, G8, E14, E16, E18 and E26 Galileo experienced a stronger dust ejection when the spacecraft was in the inner jovian system (power law slopes $-4 \lesssim \alpha \lesssim -7$). Note that the time coverage of these data sets usually ranges from days to a few weeks, indicating that Io's plume activity or the dust charging and

Table 8

Slopes α of power law fits to the measured dust flux profiles and Io's dust production.

| Orbit | Distance (R_J) | Time interval | α | Dust production (kg s^{-1}) |
|-------|--------------------|------------------|----------|--|
| G1 | 48-15 | 96-175 to 96-179 | -1.9 | 0.1-2 |
| G2 | 128-20 | 96-214 to 96-250 | -4.3 | 0.2-5 |
| C3 | 113-20 | 96-284 to 96-310 | -1.9 | 0.2-10 |
| E4 | 49-20 | 96-349 to 96-352 | -0.7 | 3-20 |
| E6 | 38-15 | 97-048 to 97-051 | -1.6 | 0.01-0.07 |
| G7 | 59-20 | 97-087 to 97-093 | -3.5 | 0.1-5 |
| G8 | 48-20 | 97-123 to 97-127 | -5.4 | 0.2-3 |
| C9 | 50-20 | 97-173 to 97-177 | -2.0 | 0.07-1 |
| C10 | 55-20 | 97-256 to 97-260 | -1.7 | 0.1-5 |
| E11 | 57-20 | 97-304 to 97-309 | -3.7 | 0.1-1 |
| E12 | 50-20 | 97-344 to 97-348 | -2.1 | 0.05-0.7 |
| E14 | 48-20 | 98-083 to 98-087 | -6.1 | 0.05-0.3 |
| E16 | 39-20 | 98-198 to 98-200 | -7.3 | 0.01-0.5 |
| E17 | 44-20 | 98-265 to 98-268 | -1.4 | 0.05-0.5 |
| E18 | 47-33 | 98-321 to 98-323 | -5.6 | 0.05-0.5 |
| E19 | 48-20 | 99-027 to 99-030 | -0.6 | 0.05-0.5 |
| E26 | 15-30 | 00-005 to 00-006 | -5.3 | 0.01-0.05 |
| G28 | 22-167 | 00-143 to 00-168 | -1.8 | 0.1-3 |
| G28 | 270-290 | 00-227 to 00-252 | - | 10-1000 |
| G29 | 290-172 | 00-253 to 00-335 | +10.4 | 0.1-500 |
| G29 | 20-216 | 01-365 to 01-070 | -2.1 | 0.01-1 |
| I32 | 22-93 | 01-290 to 01-300 | +0.2 | 0.005-0.5 |
| I33 | 61-348 | 02-023 to 02-164 | -1.1 | 0.05-5 |
| A34 | 348-22 | 02-164 to 02-308 | -0.4 | 0.05-1 |

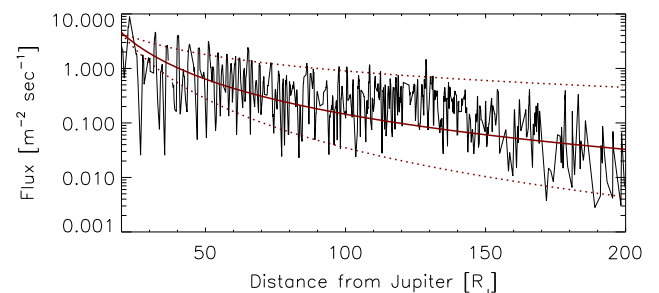


Fig. 11. Dust flux measured during Galileo's G29 orbit. The data were smoothed with a 2-h boxcar average. A power law fit with slope -2.1 is shown as a solid line. Dotted lines show curves with slopes -1 and -3 for comparison.

release from the Io torus, or both frequently changed on such rather short timescales.

Dust production rates of Io calculated with the method described above are also listed in Table 8. It should be emphasized that within less than a week the dust release frequently changed by approximately a factor of 10, and the absolute levels of the dust emission may have been vastly different from one Galileo orbit to the next. For a detailed discussion of the total dust ejection rates from Io and correlations with individual plume sightings the reader is referred to Krüger et al. (2003a) who showed that all intervals with elevated dust emission exceeding $\sim 1 \text{ kg s}^{-1}$ (six intervals in total) can be connected with giant plume eruptions or large area surface changes on Io or both. See also Section 5.2.

5.2. Io's dust emission in August/September 2000

In summer 2000 (orbit G28) Galileo left the jovian magnetosphere for the first time since it was injected into the jovian system in 1995 and reached a joviocentric distance of $\sim 280 R_J$ (0.13 AU). In August/September 2000, around Galileo's apoJove, the dust instrument measured a surprisingly large dust impact rate exceeding 10 min^{-1} for about two months (Fig. 12). Similarly high fluxes were also recorded with the Cassini dust instrument at $\sim 0.3 \text{ AU}$ from Jupiter when the spacecraft was approaching the planet in September 2000 (Hsu et al., 2009). The dust emission from Io derived from the Galileo measurements by Krüger et al. (2003a) in this time period exceeds $\sim 100 \text{ kg s}^{-1}$. Later, when Galileo approached Jupiter again, the dust flux profile showed a surprisingly steep drop (slope $\alpha \approx 10$), implying a huge decrease in Io's dust emission.

Frequency analysis of the Galileo dust data from the first three years of the Galileo Jupiter mission (1996–1998) revealed strong 5 and 10 h periodicities which were due to Jupiter's rotation (Graps et al., 2000). A weak "Io footprint" with approximately 42 h frequency caused by this moon's orbital motion about Jupiter and harmonics with Jupiter's rotation frequencies were also revealed. These data were collected mostly in the inner jovian magnetosphere between 10 and $60 R_J$. In the data obtained during the later Galileo orbits in 1999 and 2000 the Io footprint became more prominent and was evident during most Galileo orbits from E19 to G29 (Graps, 2001).

In the data from a total of 26 Galileo orbits measured between 1996 and 2000, 11 orbits showed a clear modulation with Io's frequency, three showed a weak Io modulation, while the remaining 12 orbits showed no Io signature at all (Graps, 2001). In many, but not all, cases the missing Io signature coincided with time periods when a rather weak dust flux was measured.

In the data set from August/September 2000, collected between days 00–220 and 00–250 at much larger joviocentric distances, Io's signature dominated all other frequency signatures

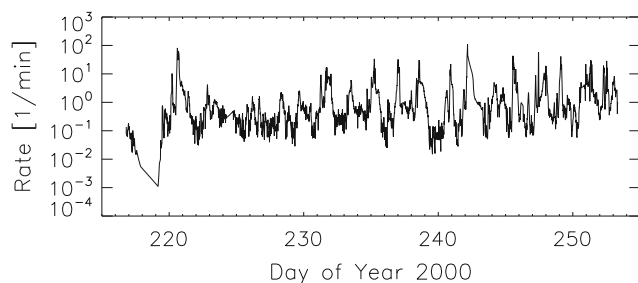


Fig. 12. Impact rate of jovian dust stream particles (AC21 and AC31) measured during Galileo's G28 orbit at approximately $280 R_J$ from Jupiter (no smoothing applied).

including the 5 and 10 h periods caused by Jupiter's rotation (Graps et al., 2001). These data provide direct evidence for Io being the source for the majority of the jovian dust stream particles during this time period. The presence of Io's orbital frequency implies that Io is a localised source of charged dust particles because charged dust from diffuse sources would couple to Jupiter's magnetic field and appear in frequency space with Jupiter's rotation frequency and its harmonics.

The period of strong dust emission seen in August/September 2000 coincided with enhanced neutral gas production from the Io torus, suggesting a coupling mechanism between gas and dust ejection, although the relation between the dust emissions and the production of neutral gas is not known (Delamere et al., 2004). Furthermore, there was a significant reduction in the neutral source beginning in October 2000, again coinciding with the strong drop in the dust emission as derived from our Galileo dust data.

5.3. Galileo–Cassini joint dust stream measurements

On 30 December 2000 the Cassini spacecraft flew by Jupiter, providing a unique opportunity for a two-spacecraft time-of-flight measurement (Cassini–Galileo) of particles from one collimated stream from the jovian dust streams. The goal was to detect particles in a stream first with Galileo when the spacecraft was inside the jovian magnetosphere close to the orbit of Europa (about $12 R_J$), and particles in potentially the same stream later by Cassini outside the magnetosphere (at $140 R_J$) (see Graps et al., 2001, for a preliminary analysis).

The Cassini data from the Jupiter flyby imply that particles of different sizes have different phases with respect to Jupiter's rotation (Sascha Kempf, personal communication), a result which is also seen in earlier Galileo data (Grün et al., 1998). Comparison of the measurements from both dust instruments, however, is hampered by the lower detection sensitivity of the Galileo detector with respect to the Cassini sensor. Both instruments have detected stream particles with different sizes and, hence likely different phases. The analysis is ongoing, and more detailed modelling to describe the phase relation of different-sized particles taking into account the three-dimensional structure of the dust emission pattern from the jovian system is necessary. Our present preliminary analysis indicates particle speeds of about 400 km s^{-1} . This value is in agreement with speeds for 10 nm particles as derived from dynamical modelling (Hamilton and Burns, 1993; Horányi et al., 1993), and earlier studies of the jovian dust stream dynamics (Zook et al., 1996).

5.4. Large dust grains far from Jupiter

On 29 December 2002 (day 02–363) the last MRO of the dust instrument memory occurred for the remainder of the Galileo mission. The next time we received dust data was during the time interval 4–11 March 2003 (days 03–063 to 03–070). These data were obtained as RTS data. We identified a total number of nine large dust impacts in amplitude ranges AR2–4 which occurred between 29 December 2002 and 11 March 2003. Due to corruption of the readings from the instrument's internal clock and one clock reset in this time interval, two of these impacts have an exceptionally large uncertainty in the impact time of 66 days. We could reconstruct the impact time of the remaining seven impacts with a higher accuracy from accumulator readings obtained with test pulses which were routinely performed by the dust instrument (see Krüger et al., 2005, for more details). This gave impact times for five impacts with about one day uncertainty and for two impacts with 4.3 h uncertainty (Table 7).

The reconstruction of these partially corrupted data implies that at least seven impacts occurred during a period of only four days when Galileo was outside Jupiter's magnetosphere in interplanetary space at approximately $350 R_J$ from Jupiter. This is a surprisingly large number of impacts at such a large distance from Jupiter given the Galileo measurements from the earlier Jupiter mission (Papers VI and VIII) and from Galileo's interplanetary cruise. Potential sources for these grains are, for example, collisional ejecta from an (unknown) small jovian satellite or a cometary trail crossed by the spacecraft. Judging from the impact charge distribution of the measured grains, jovian stream particles (Fig. 6) can be most likely ruled out because a much larger number of impacts should have occurred in the lower amplitude range AR1. In fact, only few impacts were recognized in AR1 during this time. A more detailed analysis of these impacts has to be postponed to a future investigation.

5.5. Galileo's gossamer ring passages

On 5 November 2002 (orbit A34, day 02-309) Galileo traversed Jupiter's gossamer rings for the first time and approached the planet to $2 R_J$. During this ring passage the spacecraft had a close flyby at Amalthea at 244 km distance from the moon's centre, well outside Amalthea's Hill sphere. During approach to Jupiter dust data were collected with the highest possible rate (record mode; Section 2.3) while Galileo was within Io's orbit (i.e. within $\sim 5.9 R_J$). Shortly after Amalthea flyby a spacecraft anomaly at $2.33 R_J$ joviocentric distance prevented the collection of further Galileo dust data. Although the dust instrument continued to measure dust impacts after the anomaly, the data were not written to the tape recorder on board and, hence, the majority of them were lost. Only the data sets of a few dust impacts were received from an MRO on day 02-322. These events could be located to have happened during the gossamer ring passage but their impact time is uncertain by a few hours (Table 7). The traverse of the optically visible ring from its outer edge at $\sim 3.75 R_J$ until the spacecraft anomaly occurred lasted about 100 min, and the total gossamer ring traverse from $\sim 3.75 R_J$ inbound to $\sim 3.75 R_J$ outbound took approximately 6 h.

During the A34 ring passage the lowest amplitude range in class 2 (AC21) was strongly contaminated with noise, while the higher amplitude ranges showed little or no noise contamination. In addition, many class 1 events recognized within Io's orbit showed signatures of being true dust impacts as well. The noise identification scheme applied to the dust data from both Galileo gossamer ring passages is described in Section 3.1 and given in Table 5.

With the new noise identification scheme, complete data sets of 90 dust impacts were identified in the Galileo recorded data from the gossamer ring region. Several hundred more events were counted only and their data sets were lost, in particular in AR1. The completeness of the transmitted ring data varied between 100% in the highest amplitude ranges (AR2-4) in the faint ring extension beyond Thebe's orbit down to only 4% for the lowest amplitude range (AR1) in the more populated Amalthea ring.

In record mode, the dust instrument memory was read out once per minute, and this readout frequency determined the spatial resolution of the measurements: within 1 min Galileo moved about 1800 km through the ring which corresponds to about 1100 km (or $0.015 R_J$) in radial direction. This is the highest spatial resolution achievable in the ring with the Galileo in-situ measurements.

Dust measurements in the gossamer rings were also obtained during Galileo's second ring traverse on 21 September 2003 (orbit J35) a few hours before Galileo impacted Jupiter. The data sets of about 20 dust impacts were successfully transmitted to Earth as

RTS data. This time the spatial resolution was only about 14,000 km (or $0.2 R_J$).

The data from both gossamer ring traverses allowed for the first actual comparison of in-situ measurements with the properties inferred from inverting optical images. A detailed analysis of this data was published by Krüger et al. (2009). Below we summarise the most important results.

Images of the rings imply inclinations of the grain orbits of $i \approx 1^\circ$ for the visible 5–10 μm grains (Showalter et al., 2008). The expected rotation angle for ring particles on circular prograde uninclined joviocentric orbits was $\approx 90^\circ$. The rotation angles measured within Io's orbit and in particular during the ring passages were—to a first approximation—consistent with these expectations. However, the width of the rotation angle distribution was much wider than the expected width for the geometry conditions during both gossamer ring passages.

What was the reason for such a broad distribution in impact directions? One possibility was the sensor side wall which was very sensitive to dust impacts (Altobelli et al., 2004; Willis et al., 2005). Taking the sensor side wall into account (Table 3), the expected width in rotation angle was still significantly smaller than the observed width. Another potential explanation was impacts onto nearby spacecraft structures like the magnetometer boom, the EPD and PLS instruments which masquerade as particles with high inclinations. We are convinced that such an explanation can be ruled out for two reasons (Moissl, 2005): First, the impact parameters (charge rise times, charge signal coincidences, etc.) of grains measured with rotation angles outside the nominal field-of-view for low-inclination particles do not show significant differences compared to grains inside the nominal field-of-view. Second, the data from both Galileo ring traverses show similarly broad rotation angle patterns although they had different detection geometries. During the first flyby the magnetometer boom obscured the field-of-view while during the second flyby this was not the case (Krüger et al., 2009).

The most likely explanation for the observed structure in the rotation angle pattern is the particle dynamics: The wide range in impact directions as well as a drop measured in the impact rate profile immediately interior to Thebe's orbit and a gradual increase in the relative abundance of small particles closer to Jupiter can best be explained by a shadow resonance caused by varying particle charge on the day and night side of Jupiter, driving particles onto high inclination orbits (Hamilton and Krüger, 2008). In fact, inclinations up to 20° nicely explain the measured impact directions for most grains.

Comparison of our in-situ measurements with imaging observations showed that the in-situ measurements preferentially probe the large population of small sub-micron particles while the images are sensitive to larger grains with radii of at least several microns. The grains form a halo of material faint enough to be invisible to imaging, but populated enough to be detectable with the Galileo sensor. The faint gossamer ring extension previously imaged to about $3.75 R_J$ was detected out to at least $5 R_J$, indicating that ejecta from Thebe spread much further and particle orbits get higher eccentricities than previously known. Both the gap in the ring and the faint ring extension indicate that the grain dynamics is strongly influenced by electromagnetic forces. For a more detailed discussion of the ring particle dynamics the reader is referred to Hamilton and Krüger (2008).

6. Conclusions

In this paper, which is the tenth in a series of Galileo and Ulysses dust data papers, we present data from the Galileo dust

instrument for the period January 2000 to September 2003. In this time interval the spacecraft completed nine revolutions about Jupiter in the jovicentric distance range between 2 and 370 R_J (Jupiter radius, $R_J=71,492$ km). On 21 September 2003 Galileo was destroyed in a planned impact with Jupiter.

The data sets of a total of 5389 (or 2% of the total) recorded dust impacts were transmitted to Earth in this period. Many more impacts (98%) were counted with the accumulators of the instrument but their complete information was lost because of the low data transmission capability of the Galileo spacecraft. Together with 15,861 impacts recorded in interplanetary space and in the Jupiter system between Galileo's launch in October 1989 and December 1999 published earlier (Grün et al., 1995a; Krüger et al., 1999a, 2001a, 2006b), the complete data set of dust impacts measured with the dust detector during Galileo's entire mission contains 21,250 impacts.

The Galileo dust detector has been extremely successful, measuring dust streams flowing away from Jupiter, a tenuous dust ring throughout the jovian magnetosphere and Jupiter's gossamer rings over the almost four year timespan of data considered in this paper.

Most of the time the jovian dust streams dominated the overall impact rate, reaching maxima of more than 10 min^{-1} in the inner jovian system. A surprisingly large impact rate up to 100 min^{-1} was measured in August/September 2000 (G28 orbit) when the spacecraft was at about 280 R_J distance from Jupiter. This strong

dust emission was most likely connected with a heavy volcanic eruption on Io (Krüger et al., 2003a; Geissler, 2003; Geissler et al., 2004). A strong variation in the release of neutral gas from the Io torus in this time interval was also reported by Delamere et al. (2004).

Io's dust emission as derived from the measured dust fluxes varied by many orders of magnitude, with typical values ranging between 0.1 and 1 kg s^{-1} of dust ejected. In August/September 2000 the derived dust emission exceeded 100 kg s^{-1} . The investigation of the dust impact rate profiles measured for the jovian stream particles as a function of radial distance from Jupiter revealed large orbit-to-orbit variations and variability by a factor of 10 or more on timescales of days to a few weeks. This implies variability of the dust release into circumjovian space from Io or the Io torus or variability of the jovian magnetosphere on such short timescales.

A surprisingly large number of impacts of bigger micron-sized dust grains was detected within a four-day time interval far away from Jupiter in March 2003 when Galileo was in interplanetary space. The source of these grains remains unclear.

Finally, in November 2002 and September 2003 Galileo traversed Jupiter's gossamer rings twice, providing the first actual opportunity to compare in-situ dust measurements with the results obtained from remote imaging. These flybys revealed previously unknown structures in the gossamer rings (Krüger et al., 2009): a drop in the dust density between the moons Amalthea and Thebe, grains orbiting Jupiter on highly inclined

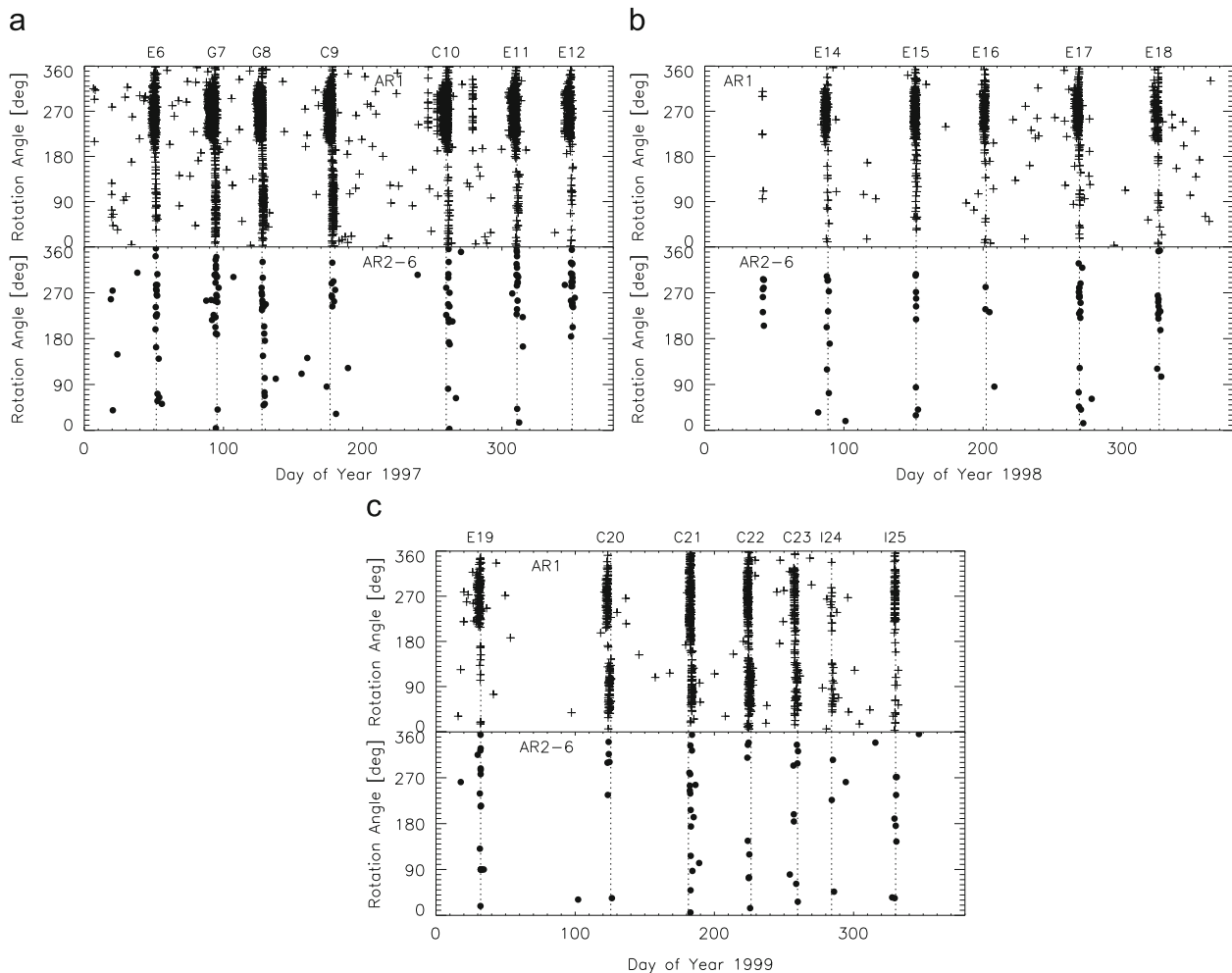


Fig. 13. Correction for Paper VIII: rotation angle vs. time for two different mass ranges for the time interval 1997–1999. Upper panel: small particles, AR1 (Io dust stream particles); lower panel: big particles, AR2-6. Vertical dotted lines indicate Galileo's satellite encounters.

orbits and an increase in the number of small grains in the inner regions of the rings as compared to the regions further away from the planet. All these features can nicely be explained by electromagnetic forces on the grains that shape the gossamer rings (Hamilton and Krüger, 2008).

Strong degradation of the dust instrument electronics was recognised in the Galileo dust data (Krüger et al., 2005). It was most likely caused by the harsh radiation environment in the jovian magnetosphere and lead to a degradation of the instrument sensitivity for noise and dust detection during the Galileo mission. The Galileo data set obtained until the end of 1999 (Papers VI and VIII) was not seriously affected by this degradation. In the time interval 2000–2003 which is the subject of this paper, however, the electronics degradation became so severe that the instrument calibration does not give reliable impact speeds and masses of the dust particles anymore. Instead, only lower limits for the impact speed and upper limits for the grain mass, respectively, can be given. The only exception are dust impacts for which their impact speeds can be derived from other means (e.g. impacts in the gossamer rings; Krüger et al., 2009). On the other hand, a reduction of the channeltron amplification was counterbalanced by four increases of the channeltron high voltage during the entire Jupiter mission (two in 1999, one each in 2000 and 2001) to maintain stable instrument operation.

Even though this is the final paper in our series of Galileo dust data papers published during the last 15 years, the evaluation of this unique data set is continuing. A list of specific open questions raised in this and earlier data papers includes:

- *Electromagnetic interaction and phase relation of different sized stream particles:* dust grains with different sizes have a different susceptibility to electromagnetic interaction with the jovian magnetosphere. Different-sized grains released from a source in the inner jovian system at the same time are expected to arrive at Galileo at a different phase of Jupiter's rotation (Grün et al., 1998). This rather simple picture is further complicated by the grains' charging history. Studies of the phase relation may lead to better constraints of the grain size distribution and may give new insights into the grains' electromagnetic interaction. The phase relation may turn out to be essential to understand the Galileo–Cassini joint dust streams measurements.
- *Galileo–Cassini joint dust streams measurements:* being originally designed as a two-spacecraft time-of-flight measurement of one collimated stream from the jovian dust streams, the analysis of this data set turned out to be more complicated than anticipated. More detailed modelling of the three-dimensional structure of the dust stream emission pattern from the jovian system is necessary to describe the phase relation of different-sized particles and to understand these unique measurements.
- *“Big” micron-sized particles:* impacts of micron-sized dust grains were preferentially detected in the inner jovian system between the Galilean moons. Two sub-populations—one orbiting Jupiter on prograde and one on retrograde orbits—were identified in earlier analyses (Thiessenhusen et al., 2000). The derived ratio in number density was approximately 4:1 with the majority of grains being on prograde orbits. At the time, however, only about half of the entire Galileo dust data set from Jupiter was available. Given that the detection geometry of the dust instrument changed with time during the mission, re-evaluation of the full data set from the entire Galileo Jupiter mission would be worthwhile to verify the abundance of grains on retrograde orbits.
- *Dust–plasma interaction:* very preliminary comparison of the Galileo dust measurements from the gossamer ring passages with energetic particle data from the same period has revealed

some interesting correlations between both data sets (Norbert Krupp, personal communication). New insights into the dust–plasma interaction and particle dynamics can be expected from combined studies of the dust data and other Galileo particles and fields data.

Acknowledgements

We dedicate this work to the memory of Dietmar Linkert who passed away in spring 2009. He was Principal Engineer for space instruments at MPI für Kernphysik including the dust instruments flown on the HEOS-2, Helios, Galileo, Ulysses and Cassini missions. His friends and colleagues around the world appreciated his experience and sought his professional advice. The authors wish to thank the Galileo project at NASA/JPL for effective and successful mission operations. This research was supported by the German Bundesministerium für Bildung und Forschung through Deutsches Zentrum für Luft- und Raumfahrt e.V. (DLR, grant 50 QJ 9503 3). Support by MPI für Kernphysik and MPI für Sonnensystemforschung is also gratefully acknowledged. The authors also wish to thank two anonymous referees for their valuable comments for the manuscript.

ERRATUM: Due to an error in Paper VIII, all panels of Fig. 9 in that paper have wrong labels on the vertical axis. Furthermore, the third panel (data of 1999) erroneously shows the dataset of 1997. We apologize for this error and show the corrected plots in Fig. 13.

References

- Altobelli, N., Moissl, R., Krüger, H., Landgraf, M., Grün, E., 2004. Influence of wall impacts on the Ulysses dust detector in modelling the interstellar dust flux. *Planetary and Space Science* 52, 1287–1295.
- Anderson, J.D., Johnson, T.V., Schubert, G., Asmar, S., Jacobson, R.A., Johnston, D., Lau, E.L., Lewis, G., Moore, W.B., Taylor, A., Thomas, P.C., Weinwurm, G., 2005. Amalthea's density is less than that of water. *Science* 308, 1291–1293.
- Colwell, J.E., Horányi, M., Grün, E., 1998. Capture of interplanetary and interstellar dust by the Jovian magnetosphere. *Science* 280, 88–91.
- D'Amario, L.A., Bright, L.E., Wolf, A.A., 1992. Galileo trajectory design. *Space Science Reviews* 60, 23–78.
- Delamere, P.A., Steffl, A., Bagenal, F., 2004. Modeling temporal variability of plasma conditions in the Io torus during the Cassini era. *Journal of Geophysical Research (Space Physics)* 109, 10216–10224.
- Flandes, A., 2005. Dust dynamics in the jovian system. Ph.D. Thesis, Universidad Nacional Autónoma de México.
- Flandes, A., Krüger, H., 2007. Solar wind modulation of Jupiter dust stream detection. In: Krüger, H., Graps, A.L. (Eds.), *Dust in Planetary Systems*, ESA Publications Division, ESTEC Noordwijk, The Netherlands, pp. 87–90, ESA SP-643.
- Geissler, P.E., 2003. Volcanic activity on Io during the Galileo Era. *Annual Reviews of Earth and Planetary Sciences* 31, 175–211.
- Geissler, P.E., McEwen, A., Phillips, C., Kesthelyi, L., Spencer, J., 2004. Surface changes on Io during the Galileo mission. *Icarus* 169, 29–64.
- Geissler, P.E., McMillan, M.T., 2008. Galileo observations of volcanic plumes on Io. *Icarus* 197, 505–518.
- Graps, A.L., 2001. Io revealed in the Jovian dust streams. Ph.D. Thesis, Ruprecht-Karls-Universität Heidelberg.
- Graps, A.L., 2006. Characterization of Jovian plasma-embedded dust particles. *Planetary and Space Science* 54, 911–918.
- Graps, A.L., Grün, E., Krüger, H., Horányi, M., Svedhem, H., 2001. Io revealed in the jovian dust streams. In: *Proceedings of the Meteoroids 2001 Conference*, pp. 601–608, ESA SP-495.
- Graps, A.L., Gruñ, E., Svedhem, H., Krugeř, H., Horányi, M., Heck, A., Lammers, S., 2000. Io as a source of the Jovian dust streams. *Nature* 405, 48–50.
- Grün, E., Baguhl, M., Divine, N., Fechtig, H., Hamilton, D.P., Hanner, M.S., Kissel, J., Lindblad, B.A., Linkert, D., Linkert, G., Mann, I., McDonnell, J.A.M., Morfill, G.E., Polansky, C., Riemann, R., Schwehm, G.H., Siddique, N., Staubach, P., Zook, H.A., 1995a. Three years of Galileo dust data. *Planetary and Space Science* 43, 953–969, Paper II.
- Grün, E., Baguhl, M., Divine, N., Fechtig, H., Hamilton, D.P., Hanner, M.S., Kissel, J., Lindblad, B.A., Linkert, D., Linkert, G., Mann, I., McDonnell, J.A.M., Morfill, G.E., Polansky, C., Riemann, R., Schwehm, G.H., Siddique, N., Staubach, P., Zook, H.A., 1995b. Two years of Ulysses dust data. *Planetary and Space Science* 43, 971–999, Paper III.
- Grün, E., Baguhl, M., Hamilton, D.P., Kissel, J., Linkert, D., Linkert, G., Riemann, R., 1995c. Reduction of Galileo and Ulysses dust data. *Planetary and Space Science* 43, 941–951, Paper I.

- Grün, E., Baguhl, M., Hamilton, D.P., Riemann, R., Zook, H.A., Dermott, S.F., Fechtig, H., Gustafson, B.A., Hanner, M.S., Horányi, M., Khurana, K.K., Kissel, J., Kivelson, M., Lindblad, B.A., Linkert, D., Linkert, G., Mann, I., McDonnell, J.A.M., Morfill, G.E., Polansky, C., Schwehm, G.H., Srama, R., 1996a. Constraints from Galileo observations on the origin of Jovian dust streams. *Nature* 381, 395–398.
- Grün, E., Fechtig, H., Hanner, M.S., Kissel, J., Lindblad, B.A., Linkert, D., Maas, D., Morfill, G.E., Zook, H.A., 1992a. The Galileo dust detector. *Space Science Reviews* 60, 317–340.
- Grün, E., Fechtig, H., Kissel, J., Linkert, D., Maas, D., McDonnell, J.A.M., Morfill, G.E., Schwehm, G.H., Zook, H.A., Giese, R.H., 1992b. The Ulysses dust experiment. *Astronomy and Astrophysics*, (Suppl. 92), 411–423.
- Grün, E., Hamilton, D.P., Riemann, R., Dermott, S.F., Fechtig, H., Gustafson, B.A., Hanner, M.S., Heck, A., Horányi, M., Kissel, J., Kivelson, M., Krüger, H., Lindblad, B.A., Linkert, D., Linkert, G., Mann, I., McDonnell, J.A.M., Morfill, G.E., Polansky, C., Schwehm, G.H., Srama, R., Zook, H.A., 1996b. Dust measurements during Galileo's approach to Jupiter and Io encounter. *Science* 274, 399–401.
- Grün, E., Krüger, H., Graps, A., Hamilton, D.P., Heck, A., Linkert, G., Zook, H., Dermott, S.F., Fechtig, H., Gustafson, B., Hanner, M., Horányi, M., Kissel, J., Lindblad, B., Linkert, G., Mann, I., McDonnell, J.A.M., Morfill, G.E., Polansky, C., Schwehm, G.H., Srama, R., 1998. Galileo observes electromagnetically coupled dust in the Jovian magnetosphere. *Journal of Geophysical Research* 103, 20011–20022.
- Grün, E., Krüger, P., Dermott, S.F., Fechtig, H., Graps, A.L., Gustafson, B.A., Hamilton, D.P., Heck, A., Horányi, M., Kissel, J., Lindblad, B.A., Linkert, D., Linkert, G., Mann, I., McDonnell, J.A.M., Morfill, G.E., Polansky, C., Schwehm, G.H., Srama, R., Zook, H.A., 1997a. Dust measurements in the Jovian magnetosphere. *Geophysical Research Letters* 24, 2171–2174.
- Grün, E., Staubach, P., Baguhl, M., Hamilton, D.P., Zook, H.A., Dermott, S.F., Gustafson, B.A., Fechtig, H., Kissel, J., Linkert, D., Linkert, G., Srama, R., Hanner, M.S., Polansky, C., Horányi, M., Lindblad, B.A., Mann, I., McDonnell, J.A.M., Morfill, G.E., Schwehm, G.H., 1997b. South-north and radial traverses through the interplanetary dust cloud. *Icarus* 129, 270–288.
- Grün, E., Zook, H.A., Baguhl, M., Balogh, A., Bame, S.J., Fechtig, H., Forsyth, R., Hanner, M.S., Horányi, M., Kissel, J., Lindblad, B.A., Linkert, D., Linkert, G., Mann, I., McDonnell, J.A.M., Morfill, G.E., Polansky, C., Schwehm, G.H., Siddique, N., Staubach, P., Svestka, J., Taylor, A., 1993. Discovery of Jovian dust streams and interstellar grains by the Ulysses spacecraft. *Nature* 362, 428–430.
- Hamilton, D.P., Burns, J.A., 1993. Ejection of dust from Jupiter's gossamer ring. *Nature* 364, 695–699.
- Hamilton, D.P., Krüger, H., 2008. Jupiter's shadow sculpts its gossamer rings. *Nature* 453, 72–75.
- Heck, A., 1998. Modellierung und Analyse der Raumsonde Galileo im Jupitersystem vorgefundener Mikrometeoroiden-Populationen. Ph.D. Thesis, Ruprecht-Karls-Universität Heidelberg.
- Horányi, M., Grün, E., Heck, A., 1997. Modeling the Galileo dust measurements at Jupiter. *Geophysical Research Letters* 24, 2175–2178.
- Horányi, M., Morfill, G.E., Grün, E., 1993. Mechanism for the acceleration and ejection of dust grains from Jupiter's magnetosphere. *Nature* 363, 144–146.
- Hsu, H.W., Kempf, S., Postberg, F., Srama, R., Jackman, C.M., Moragas-Klostermeyer, G., Helfert, S., Grün, E., 2009. Interaction of the solar wind and stream particles, results from the cassini dust detector. In: AIP Conference Proceedings; Solar Wind, vol. 12, in press.
- Johnson, T.V., Yeates, C., Young, R., 1992. Galileo mission overview. *Space Science Reviews* 60, 3–21.
- Kempf, S., Beckmann, U., Srama, R., Horányi, M., Auer, S., Grün, E., 2006. The electrostatic potential of E ring particles. *Planetary and Space Science* 54, 999–1006.
- Kempf, S., Srama, R., Altobelli, N., Auer, S., Tschernjawski, V., Bradley, J., Burton, M.E., Helfert, S., Johnson, T.V., Krüger, H., Moragas-Klostermeyer, G., Grün, E., 2004. Cassini between earth and asteroid belt: first in-situ charge measurements of interplanetary grains. *Icarus* 171, 317–335.
- Krivov, A.V., Krüger, H., Grün, E., Thiessenhusen, K.-U., Hamilton, D.P., 2002a. A tenuous dust ring of Jupiter formed by escaping ejecta from the Galilean satellites. *Journal of Geophysical Research* 107, E1, doi:10.1029/2000JE001434.
- Krivov, A.V., Sremčević, M., Spahn, F., Dikarev, V.V., Kholshevnikov, K.V., 2003. Impact-generated dust clouds around planetary satellites: spherically-symmetric case. *Planetary and Space Science* 51, 251–269.
- Krivov, A.V., Wardinski, I., Spahn, F., Krüger, H., Grün, E., 2002b. Dust on the outskirts of the Jovian system. *Icarus* 157, 436–455.
- Krüger, H., Hamilton, D.P., Moissl, R., Grün, E., 2009. Galileo in-situ dust measurements in Jupiter's gossamer rings. *Icarus* 203, 198–213.
- Krüger, H., 2003. Jupiter's Dust Disc, An Astrophysical Laboratory. Shaker Verlag Aachen, Habilitation Thesis Ruprecht-Karls-Universität Heidelberg, ISBN 3-8322-2224-3.
- Krüger, H., Altobelli, N., Anweiler, B., Dermott, S.F., Dikarev, V., Graps, A.L., Grün, E., Gustafson, B.A., Hamilton, D.P., Hanner, M.S., Horányi, M., Kissel, J., Landgraf, M., Lindblad, B., Linkert, D., Linkert, G., Mann, I., McDonnell, J.A.M., Morfill, G.E., Polansky, C., Schwehm, G.H., Srama, R., Zook, H.A., 2006a. Five years of Ulysses dust data: 2000 to 2004. *Planetary and Space Science* 54, 932–956, Paper IX.
- Krüger, H., Bindschadler, D., Dermott, S.F., Graps, A.L., Grün, E., Gustafson, B.A., Hamilton, D.P., Hanner, M.S., Horányi, M., Kissel, J., Lindblad, B., Linkert, D., Linkert, G., Mann, I., McDonnell, J.A.M., Moissl, R., Morfill, G.E., Polansky, C., Schwehm, G.H., Srama, R., Zook, H.A., 2006b. Galileo dust data from the Jovian system: 1997 to 1999. *Planetary and Space Science* 54, 879–910, Paper VIII.
- Krüger, H., Dikarev, V., Anweiler, B., Dermott, S.F., Graps, A.L., Grün, E., Gustafson, B.A., Hamilton, D.P., Hanner, M.S., Horányi, M., Kissel, J., Linkert, D., Linkert, G., Mann, I., McDonnell, J.A.M., Morfill, G.E., Polansky, C., Schwehm, G.H., Srama, R., 2010. Three years of Ulysses dust data: 2005 to 2007. *Planetary and Space Science*, Paper XI, this issue, doi:10.1016/j.pss.2009.11.002.
- Krüger, H., Geissler, P., Horányi, M., Graps, A.L., Kempf, S., Srama, R., Moragas-Klostermeyer, G., Moissl, R., Johnson, T.V., Grün, E., 2003a. Jovian dust streams: a monitor of Io's volcanic plume activity. *Geophysical Research Letters* 30, 2101–2105.
- Krüger, H., Graps, A.L., Hamilton, D.P., Flandes, A., Forsyth, R.J., Horányi, M., Grün, E., 2006c. Ulysses jovian latitude scan of high-velocity dust streams originating from the Jovian system. *Planetary and Space Science* 54, 919–931.
- Krüger, H., Grün, E., Graps, A.L., Bindschadler, D.L., Dermott, S.F., Fechtig, H., Gustafson, B.A., Hamilton, D.P., Hanner, M.S., Horányi, M., Kissel, J., Lindblad, B., Linkert, D., Linkert, G., Mann, I., McDonnell, J.A.M., Morfill, G.E., Polansky, C., Schwehm, G.H., Srama, R., Zook, H.A., 2001a. One year of Galileo dust data from the Jovian system: 1996. *Planetary and Space Science* 49, 1285–1301, Paper VI.
- Krüger, H., Grün, E., Hamilton, D.P., Baguhl, M., Dermott, S.F., Fechtig, H., Gustafson, B.A., Hanner, M.S., Horányi, M., Kissel, J., Lindblad, B.A., Linkert, D., Linkert, G., Mann, I., McDonnell, J.A.M., Morfill, G.E., Polansky, C., Riemann, R., Schwehm, G.H., Srama, R., Zook, H.A., 1999a. Three years of Galileo dust data: II. 1993 to 1995. *Planetary and Space Science* 47, 85–106, Paper IV.
- Krüger, H., Grün, E., Heck, A., Lammers, S., 1999b. Analysis of the sensor characteristics of the Galileo dust detector with collimated Jovian dust stream particles. *Planetary and Space Science* 47, 1015–1028.
- Krüger, H., Grün, E., Landgraf, M., Baguhl, M., Dermott, S.F., Fechtig, H., Gustafson, B.A., Hamilton, D.P., Hanner, M.S., Horányi, M., Kissel, J., Lindblad, B., Linkert, D., Linkert, G., Mann, I., McDonnell, J.A.M., Morfill, G.E., Polansky, C., Schwehm, G.H., Srama, R., Zook, H.A., 1999c. Three years of Ulysses dust data: 1993 to 1995. *Planetary and Space Science* 47, 363–383, Paper V.
- Krüger, H., Grün, E., Landgraf, M., Dermott, S.F., Fechtig, H., Gustafson, B.A., Hamilton, D.P., Hanner, M.S., Horányi, M., Kissel, J., Lindblad, B., Linkert, D., Linkert, G., Mann, I., McDonnell, J.A.M., Morfill, G.E., Polansky, C., Schwehm, G.H., Srama, R., Zook, H.A., 2001b. Four years of Ulysses dust data: 1996 to 1999. *Planetary and Space Science* 49, 1303–1324, Paper VII.
- Krüger, H., Grün, E., Linkert, D., Linkert, G., Moissl, R., 2005. Galileo long-term dust monitoring in the Jovian magnetosphere. *Planetary and Space Science* 53, 1109–1120.
- Krüger, H., Horányi, M., Grün, E., 2003b. Jovian dust streams: probes of the Io plasma torus. *Geophysical Research Letters* 30, 1058–1061.
- Krüger, H., Horányi, M., Krivov, A.V., Graps, A.L., 2004. Jovian dust: streams clouds and rings. In: Bagenal, F., Dowling, T.E., McKinnon, W.B. (Eds.), *Jupiter. The Planet, Satellites and Magnetosphere*, Cambridge Planetary Science, vol. 1. Cambridge University Press, Cambridge, UK, ISBN: 0-521-81808-7, pp. 219–240.
- Krüger, H., Krivov, A.V., Grün, E., 2000. A dust cloud of Ganymede maintained by hypervelocity impacts of interplanetary micrometeoroids. *Planetary and Space Science* 48, 1457–1471.
- Krüger, H., Krivov, A.V., Hamilton, D.P., Grün, E., 1999d. Detection of an impact-generated dust cloud around Ganymede. *Nature* 399, 558–560.
- Krüger, H., Krivov, A.V., Sremčević, M., Grün, E., 2003c. Galileo measurements of impact-generated dust clouds surrounding the Galilean satellites. *Icarus* 164, 170–187.
- McEwen, A., Keszthelyi, L., Lopes, R., Schenk, P., Spencer, J., 2004. The lithosphere and surface of Io. In: Bagenal, F., McKinnon, B., Dowling, T. (Eds.), *Jupiter: Planet, Satellites & Magnetosphere*, Cambridge University Press, pp. 307–328.
- McEwen, A.S., Keszthelyi, L., Geissler, P., Simonelli, D.P., Carr, M.H., Johnson, T.V., Klaasen, K.P., Breneman, H.H., Jones, T.J., Kaufman, J.M., Magee, K.P., Senske, D.A., Belton, M.J.S., Schubert, G., 1998. Active volcanism on Io as seen by Galileo SSI. *Icarus* 135, 181–219.
- Moissl, R., 2005. Galileos Staubmessungen in Jupiters Gossamer-Ringen. Ruprecht-Karls-Universität Heidelberg, Diploma Thesis.
- Porco, C.C., West, R.A., McEwen, A., DelGenio, A.D., Ingersoll, A.P., Thomas, P., Squyres, S., Dones, L., Murray, C.D., Johnson, T.V., Burns, J.A., Brahic, A., Neukum, G., Veverka, J., Barbara, J.M., Denk, T., Evans, M., Ferrier, J.J., Geissler, P., Helfenstein, P., Roatsch, T., Throop, H., Tiscareno, M., Vasavada, A.R., 2003. Cassini imaging of Jupiter's atmosphere, satellites, and rings. *Science* 299, 1541–1547.
- Postberg, F., Kempf, S., Green, S.F., Hillier, J.K., McBride, N., Grün, E., 2006. Composition of Jovian dust stream particles. *Icarus* 183, 122–134.
- Showalter, M.R., de Pater, I., Verbanac, G., Hamilton, D.P., Burns, J.A., 2008. Properties and dynamics of Jupiter's gossamer rings from Galileo, Voyager, Hubble and Keck Images. *Icarus* 195, 361–377.
- Spencer, J.R., Stern, S.A., Cheng, A.F., Weaver, H.A., Reuter, D.C., Retherford, K., Lunsford, A., Moore, J.M., Abramov, O., Lopes, R.M.C., Perry, J.E., Kamp, L., Showalter, M., Jessup, K.L., Marchis, F., Schenk, P.M., Dumas, C., 2007. Io volcanism seen by new horizons: a major eruption of the Tvashtar volcano. *Science* 318, 240–243.
- Sremčević, M., Krivov, A.V., Krüger, H., Spahn, F., 2005. Impact-generated dust clouds around planetary satellites: model versus Galileo data. *Planetary and Space Science* 53, 625–641.
- Sremčević, M., Krivov, A.V., Spahn, F., 2003. Impact-generated dust clouds around planetary satellites: asymmetry effects. *Planetary and Space Science* 51, 455–471.
- Svestka, J., Auer, S., Baguhl, M., Grün, E., 1996. Measurements of dust electric charges by the Ulysses and Galileo dust detectors. In: Gustafson, B.A., Hanner, M.S. (Eds.), *Physics, Chemistry and Dynamics of Interplanetary Dust*, ASP

- Conference Series, vol. 104, Astronomical Society of the Pacific Conference Series, 1996, pp. 481–484.
- Thiessenhusen, K.-U., Krüger, H., Spahn, F., Grün, E., 2000. Dust grains around Jupiter—the observations of the Galileo Dust Detector. *Icarus* 144, 89–98.
- Willis, M.J., Burchell, M., Ahrens, T.J., Krüger, H., Grün, E., 2005. Decreased values of cosmic dust number density estimates in the solar system. *Icarus* 176, 440–452.
- Willis, M.J., Burchell, M., Cole, M., McDonnell, J.A.M., 2004. Influence of impact ionization detection methods on determination of dust particle flux in space. *Planetary and Space Science* 52, 711–725.
- Zook, H.A., Grün, E., Baguhl, M., Hamilton, D.P., Linkert, G., Linkert, D., Liou, J.-C., Forsyth, R., Phillips, J.L., 1996. Solar wind magnetic field bending of Jovian dust trajectories. *Science* 274, 1501–1503.